University of Alberta

Understanding the alteration of the Tagish Lake meteorite through mineralogy, geochemistry and oxygen isotopes.

by

Alexandra I. Blinova

A thesis submitted to the Faculty of Graduate Studies and Research
in partial fulfillment of the requirements for the degree of

Doctor of Philosophy

Department of Earth and Atmospheric Sciences

Fall 2013
Edmonton, Alberta

This thesis is dedicated to my daughter, Sophia,
who was born in the last year of my writing this work.

Sophia, may you grow up to be curious about the world
around you as it holds so many mysteries.

ABSTRACT

Our understanding of the origin and formation of the various components of meteorites, and ultimately understanding the formation of the early Solar System, comes from our knowledge of the asteroidal alteration processes and modifications that such processes induce on these components. The majority of our knowledge in this area comes from the meteorites that have been subjected to some kind of terrestrial modification which has partly or completely erased any prior history of its components. Meteorites unaffected by terrestrial modification are rare but invaluable. Tagish Lake is one such meteorite; due to its fall history it is considered to be the best candidate for studying the alteration history of the asteroidal parent body.

Four samples (TL5b, TL11h, TL11i, and TL11v) from the pristine collection of the Tagish Lake meteorite were studied to characterize and understand its alteration history. Based on petrological and mineralogical observations I conclude that the Tagish Lake parent body was a heterogeneous mixture of anhydrous precursors of nebular origin, which were brecciated and aqueously altered to various degree. The degree to which the studied samples experienced aqueous alteration is in the order TL5b < TL11h < TL11i. Specimen TL11v, which consists of disaggregated material, is heterogeneous on the microscale and encompasses the petrologic characteristics of other three specimens as seen through EPMA observation. The whole-rock geochemistry confirms the inferred alteration sequence observed through mineralogy. There is a positive correlation with aqueously mobile trace elements, such as K, Ba, and Br, which appear to be controlled by an increase of phyllosilicates from least to most altered samples. Yet, the homogeneity of other elements suggests that elemental mass transfer occurred on a localized scale and aqueous alteration was isochemical for these elements. Oxygen isotopic results from my study corroborate the conclusion that the range of variations observed in the Tagish Lake meteorite covers the oxygen isotopic composition seen in all other carbonaceous

chondrites. Such variation found in one meteorite suggests that the Tagish Lake parent asteroid sampled the material from different oxygen isotope reservoirs, perhaps ^{16}O-rich and ^{17}O-rich gaseous reservoirs.

ACKNOWLEDGEMENTS

First and foremost, I would like to acknowledge my supervisor, Chris Herd. I have been fortunate to work with Chris for the past 7 years both on my Master's and Ph.D. projects. I am grateful for his guidance in this project and insightful discussions. His style of supervision has been the most comfortable for me, which also helped me to finish this project at my own pace and on time.

I would also like to acknowledge all the people who helped me one way or another during this project. These people are from the Department of Earth and Atmospheric Sciences and from other departments in the university, and also from the organizations down in the States. They are Sergei Matveev, who helped with the EPMA; Andrew Leacock, who helped with the XRD: Diane Caird, who helped with the XRD; Larry Heaman, who helped with the whole-rock digestion protocol; Richard Stern, who helped with the oxygen isotope measurements; Rob Creaser, who helped with the whole-rock digestion protocol; Guangcheng Chen, who helped with the ICP-MS; Andy DuFrane, who lended me his Parr bombs; John Duke, who helped me with INAA; Aaron Skelhorne, who helped me with ICP-AES; Tom Zega and Rhonda Stroud, both of whom helped with the TEM; Conel Alexander, who helped with Mn-Cr measurements; Fred Wicks, Barbara and Gordon Cressey, all of whom helped me with understanding the serpentine morphology; Emma Bullock, who helped with EPMA; and Larry Nittler, who helped with financially supporting travel to the Carnegie Institution of Washington.

Also I would like to mention my friends who have been the big support during all the years at the U of A: Erin Walton, Karen Smit, Britta Jensen and Lucy Hunt-Ramsden.

This project was generously supported by the Natural Sciences and Engineering Research Council (NSERC) CGS D3 scholarship, the Alberta Ingenuity Doctoral scholarship and the Dissertation Fellowship from the University of Alberta.

At the last, BUT not the least, I would like to thank my family. My husband, Alexei, has been there for me throughout the whole process. Thank you for everything you've done for me. And my little daughter Sophia, to whom I dedicate this work, was born in the last year of this project. She has been an inspiration and the drive for me to finish my thesis as soon as possible. Also I thank my mom and dad for giving me the chance to do what I do.

TABLE OF CONTENT **pages**

LIST OF TABLES **pages**

LIST OF FIGURES **pages**

LIST OF SYMBOLS AND ABBREVIATIONS

°C	- degrees Celsius
^{16}O, ^{17}O, ^{18}O	- isotopes of oxygen
a	- activity
AOAs	- amoeboid olivine aggregates
B('00)	- Brown et al. (2000)
BSE	- back-scattered electron
C2	- carbonaceous chondrite, Type 2 alteration
CAIs	- calcium aluminum inclusions
CCAM	- carbonaceous chondrite anhydrous mineral line
CI	- Ivuna-type carbonaceous chondrite
CL	- cathodoluminesces
CM	- Mighei-type carbonaceous chondrite
CO	- Ornans-type carbonaceous chondrite
CR	- Renazzo-type carbonaceous chondrite
CV	- Vigarano-type carbonaceous chondrite
EDS	- energy-dispersive X-ray spectrometer
Eh	- oxidation potential
En	- enstatite
EPMA	- electron probe microanalysis
eV	- electron volts
f	- fugacity
F('02)	- Friedrich et al. (2002)
Fa	- fayalite
FIB-SEM	- focused-ion-beam scanning-electron microscope
Fo	- forsterite
Fs	- ferrosilite
g	- grams
GEMS	- glass with embedded metal and sulfides
HAADF	- high-angle annular-dark-field detectors
HF	- hydrofluoric acid
HNO_3	- nitric acid

HRTEM	- high-resolution transmission electron microscope
ICDD-PD	- the International Centre for Diffraction Data - Powder Diffraction File database
ICP-AES	- inductively coupled plasma atomic emission spectroscopy
IDPs	- interstellar dust particles
IMF	- instrumental mass fractionation
INAA	- instrumental neutron activation analysis
IOM	- insoluble organic matter
keV	- kilo electron volts
kg	- kilograms
Kv	- kilovolts
MC-ICP-MS	- multi-collector inductively coupled plasma mass spectrometre
MAI	- mineral alteration index
MSS	- monosulfide solid solution
nA	- nanoampere
NRL	- National Research Laboratory
pH	- hydrogen potential
ppm	- parts per million,
REE	- rare earth elements
RIF	- Radiogenic Isotope Facility
RM	- reference material
RNAA	- radiochemical neutron activation analysis
SAED	- selected-area electron-diffraction
SIMS	- secondary ion mass spectrometre
STEM	- scanning transmission electron microscope
stdev	- standard deviation
T	- temperature
TEM	- transmission electron microscope
TL11h	- Tagish Lake meteorite sample “11h”
TL11i	- Tagish Lake meteorite sample “11i”
TL11v	- Tagish Lake meteorite sample “11v”
TL5b	- Tagish Lake meteorite sample “5b”

VSMOW	- Vienna Standard Mean Ocean Water
USGS	- Unites States Geological Survey
vol%	- volume percent
Wo	- wollastonite
wt%	- weight percent
XRD	- X-Ray diffraction
$\Delta^{17}O$	- "Big delta" notation, $\Delta^{17}O = \delta^{17}O - 0.5 \times \delta^{18}O$
$\delta^{18}O_{VSMOW}$	- $\delta\ ^{18}O_{VSMOW} = 1000\ [(^{18}O/^{16}O_{sample})/\ ^{18}O/^{16}O_{VSMOW} - 1]$
σ	- sigma or standard deviation
μm	- micrometer, 1×10^{-6}

INTRODUCTION

On January 18th, 2000, an unusual carbonaceous meteorite fell on the frozen surface of the Tagish Lake in British Columbia. Among the unique characteristics of the Tagish Lake meteorite are a low bulk density of 1.6 g/cm^3 and extreme porosity of 40% (Brown et al. 2002). The circumstances of the fall, such as the time of the year (subzero ambient temperature) and location (frozen surface of a northern lake), were favorable for recovery of several hundred grams of uncontaminated, so-called 'pristine', extraterrestrial material, by local resident Jim Brook. Such unique fall conditions are also favorable for preserving the most volatile organics in the 'pristine' samples. The Tagish Lake meteorite contains a high amount of organic carbon (~2.6 wt%; Grady et al. 2002), the characteristics of which correlate with mineralogy and petrology, providing insights into parent body alteration (Herd et al. 2011).

Another set of samples that are referred to as 'degraded' or 'non-pristine' was collected by a team from the University of Calgary and the University of Western Ontario in the spring of 2000. These samples were immersed in the lake meltwater and bear evidence of terrestrial contamination. A total of ~10 kg were recovered during that expedition (Brown et al. 2000). The present study utilizes four pristine specimens available from the University of Alberta Meteorite Collection to study in-depth mineralogy, petrology, whole-rock geochemistry and oxygen isotopes of the Tagish Lake meteorite and its components. This is a first time such a broad and comprehensive study has been carried out on the pristine Tagish Lake material.

The Tagish Lake meteorite is an ungrouped, type 2 carbonaceous chondrite that represents some of the most primitive, organic-rich extraterrestrial material available for study. Four pristine Tagish Lake specimens (TL5b = 0.1739 g; TL11h = 0.272 g; TL11v = two pieces total 0.0746 g; TL11i = 0.3082 g) were chosen on the basis of macroscopic differences seen in a hand-sample with the naked eye, such as presence/lack of chondrules and grain size (Fig. 1). Macroscopically specimen TL5b is a compact, coherent lithology with relatively abundant chondrules or light-colored clasts evident in hand sample. Specimen TL11i is friable, tends to shed a residue of a very fine black dust when handling it, and has been referred to as an example of a "dark, dusty" lithology (Blinova *et al.* 2009). Sample TL11v is disaggregated pristine material that was collected by the finder after the fall and stored in a Ziploc® bag. Macroscopically, sample TL11h is similar to TL11i, and was chosen as a possible second specimen of the "dark, dusty" lithology

Preliminary mineralogical work identified the Tagish Lake meteorite as an accretionary breccia exhibiting petrological and chemical similarities to CM (Mighei-type) and CI (Ivuna-type) carbonaceous chondrites albeit distinct from these groups. Zolensky et al. (2002) identified two main lithologies (carbonate-poor and carbonate-rich) and a CM1 clast similar to the Kaidun meteorite in the samples that they studied, which included both pristine and degraded specimens. The two main lithologies of Zolensky et al. (2002) consist of a matrix-supported mixture of olivine-rich aggregates, rare chondrules, sparse altered calcium-aluminum inclusions (CAIs), magnetite and olivine grains, Ca-Fe-Mg-Mn carbonates, and Fe-Ni sulphides (Zolensky et al. 2002). Izawa et al. (2010) later determined that the Tagish Lake is more heterogeneous than previously thought and observed three additional lithologies (magnetite-rich, sulfide-rich, and siderite-dominated).

Oxygen isotopes on Tagish Lake mineral separates, in-situ minerals and matrix have been sparsely studied. Leshin et al. (2001) presented oxygen isotopic compositions for olivine and carbonate separates from 'degraded' Tagish Lake samples. These authors found that chondrules in the Tagish Lake meteorite are the most ^{16}O-enriched relative to typical chondrules and isolated olivines from other carbonaceous chondrites. Engrand et al. (2001) studied minerals and matrix in-situ, and found two of the most ^{16}O-enriched olivine aggregates thus far found in this meteorite. These authors concluded that the Tagish Lake meteorite covers the whole range of oxygen variations in the anhydrous silicates found in other carbonaceous chondrites. Russell et al. (2010) studied oxygen isotopic compositions of anhydrous mineral fractions from the 'degraded' Tagish Lake specimens, which describe a line similar to the CCAM (Carbonaceous Chondrite Anhydrous Mineral) line.

Regardless of the previous work outlined above, little systematic research has been conducted on pristine samples of Tagish Lake meteorite (Herd and Herd 2007). As a result many questions about this meteorite have yet to be answered (Herd and Herd 2007). As an example, the most recent mineralogical research by Izawa et al. (2010) identified the presence of gypsum and talc in several 'degraded' samples, but was unable to confirm whether the presence of these mineral phases was due to terrestrial contamination or indicates a new lithology not previously described. Likewise, the two studies of oxygen isotopes in Tagish Lake mineral separates (Leshin et al. 2001; Engrand et al. 2001) give contradictory results: Leshin et al. (2001) found that the more forsteritic

olivines tend to be more ^{16}O-rich, consistent with observations in other carbonaceous chondrites, whereas Engrand et al. (2001) did not observe such relationship.

The opportunity to assess the pristine Tagish Lake samples through in-depth mineralogy and petrology will help to establish a framework for lithological differences in this meteorite. Such framework might help to solve the problems such as of Izawa et al. (2010) by serving as a foundation for any future mineralogical and petrological comparison, as well as to help to unravel the alteration history of this meteorite and its parent body. The identification of the primitive anhydrous components (i.e., chondrules) in Tagish Lake meteorite and application of oxygen isotopic analysis to the study of these objects could add information about the events and conditions that shaped them. In addition, oxygen data from this study, completed using secondary ion mass-spectrometry (SIMS), will also assist in comparing and understanding contradictory oxygen results of previous studies (Leshin et al. 2001; Engrand et al. 2001; Russell et al. 2010).

Therefore, the focus of the project is two-fold: (1) to describe mineralogy, petrology and whole-rock geochemistry of the four pristine Tagish Lake specimens, and (2) to investigate primitive Tagish Lake objects, such as chondrules, identified through the mineralogical work, and to carry out measurements of oxygen isotope composition of various components in these objects. The first part of this project sets the stage for initial mineralogical and chemical distinction of the studied Tagish Lake lithologies. Identification of the least altered lithology will aid in recognizing the least altered components such as chondrules, which are used in the second part of the project.

Here I present three co-authored manuscripts, which describe in detail the two main foci outlined above. The first co-authored paper is on the mineralogy and petrology of the four pristine samples determined using electron microprobe, X-Ray diffraction and transmission electron microscopy (TEM). I was the main investigator in this part of the project performing the analyses and, in the majority of cases, operating the above instruments. Tom Zega and Rhonda Stroud were in charge of the TEM. Chris Herd helped with the electron microprobe analyses and preparation of the samples for the TEM. The second co-authored paper is on the whole-rock geochemistry of the four specimens determined using neutron activation analyses and a Parr bomb digestion method. In this part of the project I designed the digestion protocol for extracting the elements of interest and was the person who carried out the digestion method. John Duke managed the neutron activation analyses. The last co-authored manuscript is on the oxygen isotopes of two chondrules found in two studied Tagish Lake specimens.

Secondary ion mass spectrometry was conducted at the Canadian Centre for Isotopic Microanalysis (CCIM), under the guidance of Richard Stern. I assisted in preparing the samples, conducting EMPA on olivine reference materials, and measuring oxygen isotopes, and Richard Stern developed the methodology and was the principal analyst. Throughout the whole project Chris Herd gave guidance and supported this undertaking. In all three parts of this project I evaluated all the results and wrote the manuscripts.

FIGURE CAPTION INTRODUCTION:

Figure 1: Photos of specimens used in this study: a) 5b. b) 11h. c) 11v. d) 11i. Scale bar is 1 cm.

Figure 1:

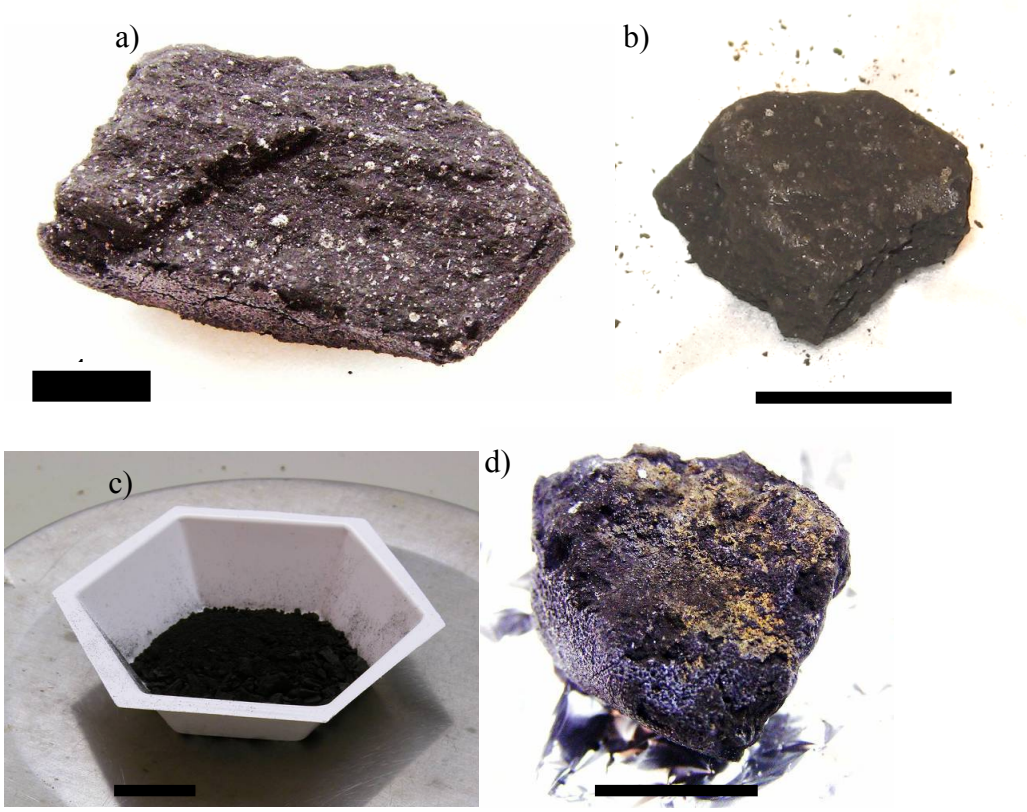

REFERENCES

Blinova, A., Herd, C.D.K., Zega, T., De Gregorio, B., and Stroud, R. 2009. Preliminary SEM and TEM study of pristine samples of Tagish Lake Meteorite (abstract #2039). 40th Lunar and Planetary Science Conference. CD-ROM.

Brown, P.G., Hildebrand, A.R., Zolensky, M.E., Grady, M., Clayton, R.N., Mayeda, T.K., Tagliaferri, E., Spalding, R., MacRae, N.D., Hoffman, E.L., Mittlefehldt, D.W., Wacker, J.F., Bird, J.A., Campbell, M.D., Carpenter, R., Gingerich, H., Glatiotis, M., Greiner, E., Mazur, M.J., and McCausland, P.J.A. 2000. The fall, recovery, orbit, and composition of the Tagish Lake Meteorite: a new type of carbonaceous chondrite. Science 290:320-325.

Brown, P.G., ReVelle, D.O., Tagliaferri, E., and Hildebrand, A.R. 2002. An entry model for the Tagish Lake fireball using seismic, satellite and infrasound records. Meteoritics and Planetary Science 37:661-675.

Engrand, C., Gounelle, M., Duprat, J., and Zolensky, M.E. 2001. In-situ oxygen isotopic composition of individual minerals in Tagish Lake, a unique type 2 carboneceous chondrite (abstract #1568). 32nd Lunar and Planetary Science Conference. CD-ROM.

Grady, M. M., Verchovsky, A. B., Franchi, I. A., Wright, I. P., and Pillinger, C. T. 2002. Light element geochemistry of the Tagish Lake CI2 chondrite; comparison with CI1 and CM2 meteorites. Meteoritics & Planetary Science **37**(5): 713-735.

Herd, R.K., and Herd, C.D.K. 2007. Towards systematic study of the Tagish Lake meteorite (abstract #2347). 38th Lunar and Planetary Science Conference. CD-ROM.

Herd, C.D.K., Blinova, A., Simkus, D.N., Huang, Y., Tarozo, R., Alexander, C.M.O'D., Gyngard, F., Nittler, L.R., Cody, G.D., Fogel, M.L., Kebukawa, Y., Kilcoyne, A.L.D., Hilts, R.W., Slater, G.F., Glavin, D.P., Dworkin, J.P., Callahan, M.P., Elsila, J.E., De Gregorio, B.T., and Stroud, R.M. 2011. Origin and evolution of prebiotic organic matter as inferred from the Tagish Lake Meteorite. Science 332:1304-1307.

Izawa, M.R.M., Flemming, R.L., King, P.L., Peterson, R.C., and McCausland, P.J.A. 2010. Mineralogical and spectroscopic investigation of the Tagish Lake carbonaceous chondrite by X-ray diffraction and infrared reflectance spectroscopy. Meteoritics and Planetary Science 45:675-698.

Leshin, L.A., Farquhar, J., Guan, Y., Pizzarello, S., Jackson, T. and Thiemens, M.H. 2001. Oxygen isotopic anatomy of Tagish Lake: Relationship to primary and secondary minerals in CI and CM chondrites (abstract #1843). 32nd Lunar and Planetary Science Conference. CD-ROM.

Russell, S.D.J., Longstaffe, F.J., King, P.L. and Larson, T.E. 2010. The oxygen-isotope cxsomposition of chondrules and isolated forsterite and olivine grains from the Tagish Lake carbonaceous chondrite. Geochimica et Cosmochimica Acta 74:2484-2499.

Zolensky, M.E., Nakamura, K., Gounelle, M., Mikouchi, T., Kasama, T., Tachikawa, O. and Tonui, E. 2002. Mineralogy of Tagish Lake: An ungrouped type 2 carbonaceous chondrite. Meteoritics and Planetary Science 37:737-761.

CHAPTER 1

TESTING VARIATIONS WITHIN THE TAGISH LAKE METEORITE - I: MINERALOGY AND PETROLOGY OF PRISTINE SAMPLES[1]

Alexandra I. Blinova[1*], Thomas J. Zega[2^], Christopher D. K. Herd[1], and Rhonda M. Stroud[2]

[1]Dept. Earth and Atmospheric Sciences, 1-23 Earth Sciences Building, University of Alberta, Edmonton, Alberta, T6G 2E3, Canada

[2]Materials Science and Technology Division, Naval Research Laboratory, 4555 Overlook Ave. SW, Washington DC 20375, USA

^Present address: Dept. of Planetary Sciences, Lunar and Planetary Laboratory, University of Arizona, 1629 E. University Blvd., Tucson AZ, 85721-0092, USA

1.1 INTRODUCTION

On January 18th, 2000, an extremely bright fireball was observed over northern Canada, in the Yukon, Northwest Territories and British Columbia. This fireball was tracked to an unusual carbonaceous meteorite that fell on the frozen surface of the Tagish Lake in British Columbia. The fall was recorded by three local seismic stations, three distant infrasound stations, a U.S. Department of Defense satellite, which observed the entry from the Earth's orbit, and over 90 eyewitnesses (Brown *et al.* 2002; Hildebrand *et al.* 2006). Based on all available data from these recordings, it was possible to reconstruct the atmospheric entry model, fragmentation behavior, and size of the fallen body (Hildebrand *et al.* 2006). It has been estimated that the initial 56 tons of material entered the Earth's atmosphere but only 1300 kg reached the ground, with 97% of the meteorite lost to ablation (Brown *et al.* 2002). This disparity is in part due to the unique characteristics of this meteorite, such as high porosity (Brown *et al.* 2002).

The circumstances of the fall, including the time of the year (subzero ambient temperature) and location (frozen surface of the northern lake), were favorable for recovering several hundred grams of uncontaminated, so-called 'pristine', material. Local

[1] A version of this chapter has been submitted for publication to the Meteoritics and Planetary Science journal.

resident Jim Brook was the first person to discover fragments of the meteorite on the Taku Arm of the Tagish Lake on the 25th of January. He was aware of the importance of the meteoritic samples as he was involved with the Geological Survey of Canada collecting snow samples for possible meteoritic dust, so he retrieved the samples with little contamination using plastic bags and stored them frozen, wrapped in aluminum foil, and placed in Ziploc® bags (Hildebrand *et al.* 2006). Approximately 0.85 kg of pristine samples were collected (Brown *et al.* 2000). The pristine nature of this material was confirmed by the stepped pyrolysis of 'waters' extracted from the bulk sample that bear little terrestrial signature (Baker *et al.* 2002). Prior to 2006, the pristine samples were on loan to NASA Johnson Space Center, where they were kept under cold, clean conditions. In 2006, a consortium purchase of the pristine samples was accomplished (Herd and Herd 2007) yielding approximately 643 gram of pristine samples that are currently housed in the Meteorite Collection at the Dept. of Earth and Atmospheric Sciences, University of Alberta, and 200 g in the Meteorite Collection of the Royal Ontario Museum.

Another set of samples, which are usually referred to as 'degraded', was collected by a team in the spring of 2000. These samples were immersed in the lake meltwater and contain evidence of terrestrial contamination confirmed by oxygen isotopes (Russell *et al.* 2008) and amino acids (Kminek *et al.* 2002). A total of ~5 to 10 kg were recovered during that expedition (Brown *et al.* 2000). The majority of these samples are now located at the University of Calgary and the University of Western Ontario.

The Tagish Lake meteorite, henceforth referred to as Tagish Lake, is the most friable and unusual meteorite fallen to date. It has a low bulk density of 1.6 g/cm^3, extreme porosity of 40%, and it does not fit into the present meteorite taxonomy (Brown *et al.* 2002). Zolensky et al. (2002) identified two main lithologies (carbonate-poor and carbonate-rich) and a CM1 clast similar to the Kaidun meteorite in the samples that they studied, which included both pristine and degraded specimens. These authors concluded that it is a brecciated meteorite with a matrix-supported mixture of olivine-rich aggregates, rare chondrules, sparse altered CAIs, magnetite, individual grains of olivine, Ca-Fe-Mg-Mn carbonates, and Fe-Ni sulfides. Rare chondrules range in diameter from 0.1 to 1 mm, and rarer CAIs average 2 mm in diameter (Zolensky *et al.* 2002). Most chondrules and CAIs found by Zolensky *et al.* (2002) show evidence of aqueous alteration. Olivine and pyroxene compositions are $Fa_{0\text{-}29}$ and $Fs_{1\text{-}7}$, respectively. Matrix consists mostly of intergrown serpentine and saponite.

The latest quantitative bulk mineralogy study of degraded samples (collected in the spring of 2000) by Izawa *et al.* (2010) determined, through identification of three 'new' lithologies (magnetite-, and sulfide-rich, and siderite-dominated), that Tagish Lake is much more varied in major mineralogy than previously thought. In addition, these authors found such minerals as gypsum and talc; however, they were unable to determine whether these minerals are original to the Tagish Lake mineralogy and thus represent a new lithology, or are related to the degraded nature of the examined samples as a result of their terrestrial modification. Izawa *et al.* (2010) also identified several samples with an increased amount of olivine and magnetite relative to previously characterized Tagish Lake material, but completely lacking in sulfates and have only a minor saponite and serpentine component. They hypothesised that this could be due to the nature of terrestrial melt-water interaction that dissolved sulfates and mechanically separated clay components, or preferentially preserved denser material with less clay components. Although these authors were able to identify new lithologies and noted more mineralogical variation in samples than Zolensky *et al.* (2002), they have admitted that the disaggregated Tagish Lake material may have undergone mechanical separation and mixing due to melt-water interaction, and may not be linked to any specific lithology. Nevertheless, Izawa *et al.* (2010) noted that simple mixing of just two lithologies (carbonate-poor and carbonate-rich) identified by Zolensky *et al.* (2002) cannot explain their newly identified lithologies.

At present Tagish Lake is classified as C2-ungrouped. There are, however, a few uncertainties and inconsistencies with this classification. The Tagish Lake CAIs found by Zolensky *et al.* (2002) have a sinuous texture typical of CM chondrites, but the alteration in the former is mostly Mg-rich serpentine whereas those in the latter tend to contain Fe-rich serpentine (Zolensky *et al.* 2002). Classification of Tagish Lake is not comprehensive because we know very little about the mineralogical, petrological, and textural variations. Regardless of the previous work outlined above, little systematic research has been conducted on pristine samples of Tagish Lake (Herd and Herd 2007).

A systematic study of Tagish Lake, most notably on pristine samples, is required in order to establish a mineralogical framework for determining the variation in the degree of alteration. This in turn will help to identify the least altered components (*e.g.*, chondrules, CAIs) as tools for understanding the formation conditions and events that shaped these primitive early solar system objects prior to their incorporation into the Tagish Lake parent body.

This paper is Part I of a project that encompasses the investigation of mineralogical, bulk chemical variations, and isotopic signatures of pristine samples of Tagish Lake available from the University of Alberta Meteorite Collection. Here we present the results of the detailed mineralogic, petrologic, and textural study of four such samples.

1.2 SPECIMENS AND ANALYTICAL METHODS

Four pristine Tagish Lake specimens (TL5b = 0.1739 g; TL11h = 0.272 g; TL11v = two pieces total 0.0746 g; TL11i = 0.3082 g) were chosen on the basis of macroscopic differences seen in a hand-sample with the naked eye (*e.g.*, presence/lack of chondrules, grain sizes). Specimen TL5b is a compact, coherent lithology with relatively abundant chondrules or light-colored clasts evident in hand sample. Specimen TL11i is friable, tends to shed a residue of a very fine black dust when handling it, and has been referred to as an example of a "dark, dusty" lithology (Blinova *et al.* 2009). Sample TL11v is disaggregated pristine material that was collected by Jim Brook and stored in a Ziploc® bag. Macroscopically, sample TL11h is similar to TL11i, and was chosen as a possible second specimen of the "dark, dusty" lithology

Instruments described below are housed in the Department of Earth and Atmospheric Sciences at the University of Alberta unless indicated otherwise. For microprobe analyses, chips of the above samples (two chips for 11v, referred as TL11v-1 and TL11v-2) were prepared into 1- inch diameter mounts using Buehler EPOKWICK two part epoxy, and polished on a Logitech WG2 polishing unit with Pellon polishing pads, diamond paste 6, 3, and 1 micron and Engis OS type 1V lubricant.

Major and minor element concentrations on all samples were obtained by electron probe microanalysis (EPMA) using either a JEOL 8900 Superprobe or a Cameca SX100. Both instruments were operated using a 1 to 2 μm diameter focused electron beam with a current of 20 nA and an accelerating voltage of 20 kV. Natural minerals such as chromite, albite, diopside, *etc.* were used as external standards (Jarosewich 2002) for both instruments. Phi-rho-Z correction algorithm was used to correct the electron microprobe data. The instrument calibration was deemed successful when the composition of standards was reproduced within the error margins defined by the counting statistics.

Mineral analyses and bulk rock mineralogy on powdered samples were determined using a Rigaku Ultima IV Powder Diffractometer. Each sample was ground

by hand under acetone in an agate mortar and pestle to produce a fine-grained powder. The instrument is equipped with a Co tube and a high-speed Si strip detector. We used Co Kα radiation (λ = 1.7903 Å), a step size of 0.02° 2θ over the range 5-80° 2θ, and 0.3 s count time per step. Samples were top loaded onto the round aluminum holders (or glass where necessary) and spun at 0.5 Hertz. The detection limit for mineral phases is estimated at 1 wt%. Phase identification and semi-quantitative phase abundances were determined by Rietveld refinement using the WPF module of JADE 9.0 software from MDI. Rietveld refinement uses nonlinear least-squares optimization to fit the data with a calculated model (calculated as ideal crystals) that is based on powder-diffraction patterns taken from the International Centre for Diffraction Data Powder Diffraction File database (ICDD-PDF). There is a 10% relative error on the calculations made by this method. Most of the samples were found to contain abundant clay minerals, for which no ideal structure model exists in this database, and an amorphous phase.

Three samples (TL5b, TL11i, and TL11h), which represent the range of macroscopic diversity within the pristine Tagish Lake suite, were examined for textural and mineralogical variations in their matrices. We used an FEI Nova 600 focused-ion-beam scanning-electron microscope (FIB-SEM) at the Naval Research Laboratory (NRL) in Washington, D.C., to make electron-transparent cross-sections (~10 μm wide) using previously described methods (Zega *et al.* 2007). A total of four FIB sections were made from polished probe mounts: one each from 5b and 11h, and two from 11i (one from the matrix and one from a lithic clast). All FIB sections were examined at the NRL with a 200 keV JEOL 2200FS transmission electron microscope (TEM) equipped with an energy-dispersive X-ray spectrometer (EDS) and scanning-TEM (STEM) based bright- and high-angle annular-dark-field detectors (HAADF). Phase identification was based on mineral structure and chemistry, the former via measurements of high-resolution TEM (HRTEM) images and selected-area electron-diffraction (SAED) patterns; the latter via qualitative EDS.

Geochemist Workbench Essentials 8.0 (Act2) was used for geochemical modeling. We used the major minerals from our mineralogical Rietveld refinement method and from the thermal IR study by Izawa et al. (2010) in this modeling, including forsterite, magnetite, siderite, calcite, pyrrhotite, pentlandite, and saponite as a proxy for phyllosilicates.

1.3 BULK MINERALOGY

1.3.1 Composition of major minerals in the Tagish Lake meteorite

Minerals such as olivine, pyroxene, carbonate, magnetite and sulfides represent major minerals and are present in all four samples. Table 1.1 presents average compositions of these minerals.

Olivine grains are found both in the chondrules and in the matrix. The majority of olivine compositions in both groups vary between Fo_{99} and Fo_{95}. Isolated olivines in the matrix, which range in size from a few microns up to 400 μm, have compositions of $Fo_{99.4\text{-}99.6}$. Some appear to be fragments. Rare zoned and oscillatory-zoned olivines were identified in one chondrule in specimen TL11i only. The compositions of the olivines in this chondrule range from Mg-rich cores ($Fo_{98.6\text{-}89.4}$) to Fe-rich rims ($Fo_{66.7\text{-}70.2}$) (Fig. 1.1a). The majority of olivines, either in chondrules or isolated in the matrix, have well preserve faceting and appear to have been minimally affected by hydrous alteration.

Similar to olivine grains, pyroxenes are found both in the chondrules and in the matrix. However, unlike olivines, the majority of pyroxenes show a higher degree of hydrous processing. The most common pyroxene composition encountered within the Tagish Lake chondrules is $En_{96}Fs_{3.6}Wo_{0.5}$ and accounts for up to 85% of all pyroxene compositions in these objects. Rare, isolated grains of this composition can also be found in the matrix. The other 15% of pyroxenes in the chondrules are high in Ca, typically $En_{56}Fs_{6.4}Wo_{37.3}$. The majority of the low-Ca pyroxenes in the matrix have the average composition of $En_{76.2}Fs_{23.5}Wo_{0.32}$ (Fig. 1.1b).

The predominant sulfide composition is pyrrhotite with average Ni content of 2.60 wt%. Some intermediate compositions with average Ni content of 10.64 wt% are also found. Pentlandite contains up to average of 34 wt% Ni and occurs as exsolutions in pyrrhotite as well as occasional isolated grains (Table 1.1 and Fig. 1.2; with data from Zolensky *et al.*, 2002, for comparison).

Magnetite occurs in all Tagish Lake specimens but its abundance varies. Our calculations of magnetite based on 32 O atoms showed that its composition is close to the pure magnetite end-member composition with total metal ions of 24 and with Fe^{3+}/Fe^{2+} of 1.988 ± 0.001 (using Droop, 1987, for calculation of Fe^{3+} in these and all further analyses). Magnetite morphology ranges from platelets to framboids consisting of even smaller framboids. Such similar morphologies have been observed both CI and CR chondrites (*e.g.*, Weisberg *et al.* 1993).

Carbonates fall into three groups (formulae calculated based on 2 positive charges following Brandelik (2009) CALCMIN calculations). One group is Ca-rich containing small amounts of Fe and can be expressed as $[Ca_{0.97-0.98}Fe_{0.01-0.02}]CO_3$. Another group is also Ca-rich but contains small amounts of both Fe, Mg and small amounts of Si, Al or Na and expressed as $[Ca_{0.75-0.97}Mg_{0.01-0.07}Fe_{0.01-0.05}Si_{0.01-0.03}Al_{0.01}Na_{0.01}]CO_3$. A third group is Mg- and Fe-rich with small amounts of Ca, Na and Mn with a formula $[Mg_{0.45-0.47}Fe_{0.36-0.43}Ca_{0.04-0.06}Na_{0.02-0.03}Mn_{0.02-0.03}][C_{0.99-1.00}P_{0.00-0.01}]O_3$ (Fig. 1.3). Specimen TL5b contains all three compositional groups of carbonates. Three carbonates reported by Zolensky *et al.* (2002) have compositions similar to those we report here (Fig.1. 3). Zega *et al.* (2010) observed in their Tagish Lake sample a mixed-cation carbonate enriched in Fe and Mg with minor Ca and Mn, consistent with the third group of carbonates found in our studied samples. Carbonates of similar composition were found in CM2 chondrites (*e.g.*, Benedix *et al.* 2003).

Most of the carbonates range from 3 μm to 10 μm in diameter, with a rare grains reaching up to 30 μm. Only one large dolomite (100 x 200 μm) with an irregular, fine-grained rim (30 to 100 μm in thickness) that surrounds it was identified in specimen TL11h (Appendix 1; Blinova *et al.* 2012). The composition of the rim is dominated by sheet silicates rich in Mg and Si with small random pockets of Mn-Ca carbonates. The average composition (Table 1.1) of this large carbonate grain is dominated by Mg and Ca, but with up to 2 wt% Mn. The chemical formula of the grain based on 2 charges is $[Mg_{0.38-0.47}Ca_{0.41-0.48}Fe_{0.09-0.12}Mn_{0.01-0.04}Na_{0.00-0.01}]CO_3$. The composition of each analysis (normalized to 100%) is plotted on a ternary CaO-MgO-(FeO+MnO) diagram (Fig. 1.3), along with the approximate compositional ranges of dolomites from CI and CM chondrites. The composition of the TL11h dolomite grain falls in the Ivuna field and slightly overlaps the fields of other CI and CM dolomites.

1.3.2 Composition of other minerals and chondrule mesostasis

Minerals such as phosphates and chromites are minor in Tagish Lake specimens. Phosphates were identified in all samples and most of them are fine-grained (< 5 μm). Specimens TL11i and TL11h have the largest phosphate grains so far found in the studied specimens. One of them (in TL11h) is an irregular, large (~ 500 x 250 μm), fluffy grain with low analytical totals (85 wt%), enriched in Ca and Mg (Table 1.1) and contains a cracked lithic fragment enriched in sheet silicates on one side of the grain. A phosphate grain in specimen TL11i is more compact (~300 x 200 μm) and is situated outside of the

main specimen mount as if plucked out during the mounting procedure, precluding determination of the textural and mineralogical context of this grain relative to the matrix. This grain also has low analytical totals (~ 69 ± 7 wt%), possibly due to porosity and/or some volatile component, and is enriched in Mg only (Table 1.1).

We found that the majority of the Tagish Lake type IIA chondrules in our samples contain spinel grains, consistent with the observations of Simon and Grossman (2003). These grains are enriched in Cr_2O_3 (42.6 ± 3.5 wt%) and Al_2O_3 (28.5 ± 3.9 wt%) (Table 1.1). Their compositions vary from 47% to 53% Chromite [Chr = molar $Cr/(2Ti+Cr+Al+Fe^{3+})$], 44% to 50% Spinel [Sp = molar $Al/(2Ti+Cr+Al+Fe^{3+})$], up to 0.02% Magnetite [Mt = molar $Fe^{3+}/(2Ti+Cr+Al+Fe^{3+})$] and up to 0.02% Ulvöspinel [Usp = molar $2Ti/(2Ti+Cr+Al+Fe^{3+})$]. One grain has the composition 36% Chr (= molar $Cr/(2Ti+Cr+Al+Fe^{3+})$), 63% Sp (= molar $Al/(2Ti+Cr+Al+Fe^{3+})$) and 0.02% Usp (= molar $2Ti/(2Ti+Cr+Al+Fe^{3+})$) more consistent with Mg-Al spinel.

We have also found an unknown phase in the altered lithic fragment in the TL11v-1 specimen. All lithic fragments are extremely fine-grained and much denser than the matrix surrounding it and contain forsterite and numerous sulfide grains as well as unknown sub-rounded to rounded grains with low analytical totals (92-95 wt%). EDS identified these unknown grains as Mn-Ca silicate, enriched in MnO (24-25 wt%), CaO (28-30 wt%) and SiO_2 (34-35 wt%) with minor Al and Mg. The low analytical totals possibly point to a hydrous component (Table 1.1 in 'Mesostasis and other phases'). The morphology of these unknown grains is similar to the grains found in the outer rim of the broken chondrule in TL5b (see below).

The mesostasis was surveyed in detail in two areas in the largest chondrule (Fig.4a-d; and also see discussion below). Some areas of this chondrule contain microcrystallites (area 'a' in Fig. 1.4c). The compositions of these areas have high analytical totals (99.99 wt%; Table 1.1 in "Mesostasis and other phases") and are comparable to the measurements of mesostasis in chondrules of type 2-3 meteorites reported by Brearley and Jones (1998) (Table 1.1). In other areas (e.g., area 'b' on Fig. 1.4d) the mesostasis is hydrated, as indicated by low totals (~ 76 wt%; Table 1.1 in 'Mesostasis and other phases'). The majority of chondrules in the studied samples contain similar hydrated mesostasis.

1.3.3 Composition of the matrix and fine-grained rims around chondrules

Matrix is defined as any fine-grained material that is interstitial to the obvious inclusions and chondrules (*e.g.* Browning *et al.* 1996). In the Tagish Lake specimens this material is black and heterogeneous in macroscopic view. BSE imaging of matrix contains heterogeneous contrast due to numerous voids/pores, small (< 2-3 mm) oxides, carbonates, and silicate grains. We used defocused (10 mm) and focused (2 mm) EPMA beam setups to determine the compositional variations in the matrix. In Tables 2 (average of defocused and focused analyses) we present what we believe to be the analyses of the finest-grain fractions of the matrix. We acquired line scans on each sample with over 100 points for focused and over 50 points for defocused beam analyses. The majority of analyses have inconsistent results: some have low analytical totals (60-75 wt%), likely due to the presence of hydrous material and organics, or consistent with the highly porous nature of the measured samples; while others have higher analytical totals (90-93 wt%) possibly due to numerous small grains of oxides and silicates unevenly dispersed in the matrix, which are calculated as a part of the analyses. Therefore, we do not report average values based on totals from either line scans of focused and defocused beam analyses as it would not show the compositional variations of the sheet silicates found in the matrix of Tagish Lake, but rather a general composition of the matrix as a whole. We select only analyses that have totals to what is expected for the composition of sheet silicates (> 80 wt%) and present averages of these analyses (see number of analyses in Table 1.2). A lithic fragment (dense, light colored in BSE, irregular sheet silicate-rich area) from specimen TL11i was also measured. From this sample a higher number of analyses with totals of 82-87 wt% were obtained.

In Figure 5, we plot both focused and defocused analyses of matrix composition on an Fe-Si-Mg (wt% element) diagram. Similar to Zolensky *et al.* (1993) the focused beam analyses (Fig. 1.5b) show more scatter relative to the defocused analyses, although the overall area coverage is the same. Based on these analyses, no pure smectite end-members of sheet silicates are present in our samples. The majority of analyses fall between smectite and serpentine solid solutions but some plot near the Fe-rich sheet silicates. Based on these results, the Tagish Lake matrix is dominated by a mixture of smectite and other sheet silicates. The analyses of one sample overlap with the other samples and appear to have similar variations in FeO. For example, TL5b analyses (Fig. 1.5a) spread across the whole coverage area. All samples show more variation in FeO from a few wt% up to 60 wt% than in MgO or SiO_2 (Table 1.2). The same variation can

be seen in Tagish Lake data by Greshake *et al.* (2005) and Zolensky *et al.* (2002). One difference between our data and that of Zolensky *et al.* (2002) is in the S content as these authors disregarded the data with S > 1 wt% to avoid data points that were inconsistent with serpentine compositions (Zolensky *et al.* 2002). In our experience, by excluding analyses with S > 1 wt% more than 95% of the data we collected is eliminated.

Tomeoka and Buseck (1988) attributed large variations in Fe content in Orgueil to the presence of ferrihydrite. Greshake *et al.* (2005) explained the variations of Fe-rich compositions by invoking the heterogeneous spread of magnetite, sulfides and rare Fe-rich sheet silicates. As we have not observed any ferrihydrite in our sample through either EPMA or TEM, we conclude that the variations in FeO are attributable mainly to the presence of magnetite and Fe-rich sheet silicates. The composition of the lithic fragment matrix based on our TEM measurements (see below) was determined as a mixture of saponite and serpentine. This is consistent with the compositional range of this material measured by EPMA, which extends from the middle of the smectite-serpentine region up to and just above the serpentine solid solution line (green diamonds in Fig. 1.5). The analyses of the matrix in our Tagish Lake specimens cover a similar field as CM chondrites (Zolensky *et al.* 1993) and overlap the Ivuna field (Tomeoka and Buseck 1988) (Fig. 1.5).

Chondrules are the only objects in the Tagish Lake samples that have fine grained rims (FGRs) (*e.g.,* Zolensky *et al.* 1993) similar to the ones described previously in this meteorite (*e.g.* Greshake *et al.* 2005; Izawa *et al.* 2010; Takayama and Tomeoka 2012). The boundary between the rims and matrix is gradational, whereas that with the chondrule's surface is sharp. The overall composition of the FGRs is comparable to the Tagish Lake matrix except that they contain a lower abundance of Ca-carbonates and higher in S. Similar observations were noted by Greshake *et al.* (2005) and Takayama and Tomeoka (2012). Rims are extremely fine-grained (< 0.2 μm) and contain sulfides (Fe-Ni) and rare low-Ca pyroxene and forsterite. Some rims completely surround the chondrule, while others appear to be broken. In addition, the rims have numerous fractures that do not extend into the matrix. One large chondrule in TL5b has a rim of varied thickness (from 10 to 200 μm) and two different compositions (Fig. 1.4e). The outer part of the rim is enriched in Fe and S with prominent sub-rounded to rounded grains (possible carbonates), and the inner part is devoid of these grains and depleted in both Fe and S (Fig. 1.4e). The transition between the two parts of the rim is abrupt. The majority of chondrule rims were found to have similar compositional and textural characteristics

although thickness varies. Similar Fe-S gradational FGRs were noted in CM and CR chondrites (Metzler *et al.* 1992; Hanowski and Brearley 2000, 2001; Zega *et al.* 2003; Chizmadia and Brearley 2008).

1.3.4 EPMA observations: component abundances and textures in Tagish Lake specimens

We used BSE images (Fig. 1.6a-e) to observe and establish the quantitative abundance of components such as chondrules, matrix, lithic fragments, isolated silicates, sulfides, carbonates and magnetites to determine the mineralogical differences between the samples. We used these differences as a foundation for determining the alteration degree in each sample. We consider chondrules and istolated silicates, such as olivine and pyroxene grains, as primary components most likely of nebular origin (Brearley and Jones 1998). We used BSE images for calculating the modal abundance of these and fine-grained lithic fragments, which are composed entirely of sheet silicates with a mixture of fine-grained magnetite and sulfide. The abundances of sulfides, carbonates and magnetites, which are products of alteration and, hence, are secondary components, were visually estimated by comparing BSE images of samples. Matrix abundance was calculated as difference between 100% and the rest of the components.

We define chondrules as all objects that preserve rounded to semi-rounded exterior surface either partially altered or completely pseudomorphed and that look like chondrules as described by Brearley and Jones (1998). Because mesostasis in the studied samples is mostly replaced by hydrous phases (Table 1.1), except for the large TL5b chondrule (see below), the main key parameter that is used to distinguish different degrees of alteration in the Tagish Lake chondrules is the presence of olivine and pyroxene grains inside these objects that are visibly intact, non-hydrated and unaltered to sheet silicates. We consider a chondrule as slightly altered when it contains inside unhydrated silicate grains (e.g., Fig. 1.4). A chondrule is considered to be highly altered when the interior is completely replaced by sheet silicates (e.g., Fig. 1.7a-d). We have observed 'pseudomorphs of opaque nodules' in the majority of chondrules, similar to those described by Takayama and Tomeoka (2012), though their abundance is correlated with the degree of chondrule alteration.

Specimen TL5b (Fig. 1.6a) contains the highest number of chondrules (~ 30 vol%). The olivine grains in these chondrules show no evidence of alteration. Pyroxene grains, on the other hand, are altered to various degrees, similar to the observation of

Takayama and Tomeoka (2012) Therefore, we consider the chondrules in TL5b as slightly altered compared to chondrules in other studied samples. All observed chondrules in this sample are porphyritic Type I (Fe-poor, McSween 1977) with hydrated mesostasis. The TL5b specimen is also distinguished from the other samples by the size of chondrules, which varies from a few microns to a few millimeters. Most chondrules in TL5b are small (up to 500 μm) and have a deformed shape: either an hourglass or ellipsoidal. During processing of specimen TL5b a large (~ 2000 μm diameter) chondrule fell out of the porous matrix (Fig. 1.4a). This chondrule is nearly perfectly spherical and is only moderately altered on its exterior. It is a porphyritic Type I chondrule dominated by two types of pyroxene ($En_{96}Fs_{3.6}Wo_{0.4}$; and $En_{62.3}Fs_{4.2}Wo_{32.5}$) and olivine ($Fo_{95-96}$) with Mn enrichment in olivine rims. This chondrule is also distinguished from other chondrules in that some areas of mesostasis have high analytical totals (Table 1.1; Fig. 1.4). This suggests a glass with microcrystallites, either from quench or from the beginnings of devitrification. We believe that those high totals rule out significant hydration of this specific chondrule (Table 1.1).

Fine-grained matrix (~18-20 vol %) in TL5b, consisting a mixture of smectite and serpentine, occurs interstitially between the anhydrous components. In addition to the highest number of chondrules, specimen TL5b also contains the lowest proportion of lithic fragments (~ 2 vol%) and the most abundant isolated unaltered silicate grains. These grains are dominated by forsterite (Fo_{95-99}) (up to 5-8 vol %) with minor pyroxene (~ 2-3 vol %). Some of these Fo_{99} grains are large (400 x 500 μm) with thin fractured rims and rare sulfide inclusions. The specimen contains framboids of magnetites after sulfide crystals similar to the ones reported by Zolensky *et al.* (2002). Other sulfides (Fig. 1.8) can be found as solitary grains or in clusters (< 10 μm) with non-exsolved and exsolved morphologies. The exsolved morphologies in all studied samples are (1) pentlandite inside pyrrhotite grains with characteristic "flame" textures, (2) partially coarsened, en echelon blades of pentlandite in pyrrhotite, and (3) massive pentlandite intergrowths with pyrrhotite (Fig. 1.8). We have not observed any sulfide veins in either TL5b or other samples as was reported by Bullock *et al.* (2005).

Specimen TL11i (Fig. 1.6b) appears to be the opposite of TL5b as it is dominated by fine-grained matrix (up to 50 vol%). The majority of chondrules (~ 5 vol%) are pseudomorphed, containing mostly sheet silicates and are mostly devoid of any intact silicate grains (Fig. 1.7e). This sample, however, contains one porphyritic type IIA chondrule with unaltered zoned olivines, remnants of pyroxene grains altered by sheet

silicates, some sulfides and a hydrated mesostasis (Fig. 1.4f). Carbonates (~ 4 vol %) occur in lower abundance but larger size than in TL5b reaching up to 30 μm. Clusters of fine-grained (< 20 μm in diameter) framboidal and plaquette magnetites (~ 15 vol%) and isolated olivine grains (up to 5 vol%) are dispersed throughout the matrix. Some magnetite framboids and plaquettes are found in clusters with sulfides. Sulfides show similar morphologies (Fig. 1.8) to TL5b. The abundance of sulfides is similar to carbonates.

Specimen TL11h (Fig. 1.6c) has characteristics intermediate to TL5b and TL11i. The abundance of chondrules appears to be closer to TL5b (~ 25 vol%) but they are smaller in size (50 to 200 μm) and have more diverse morphologies than TL5b. The inside of one chondrule (Fig. 1.7a) surrounded by the FGR appears is extensively modified by alteration: silicate grains are partially altered by sheet silicates, with the latter growing into numerous voids as distinctive arrays (Fig. 1.7b). We also observe altered chondrules that have sulfide/magnetite rims of various thicknesses (~ 2-5 μm) with diverse interior textures: one (Fig. 1.7c) is similar to the coronal, 'flower-like', morphology described below in the focused-ion-beam (FIB) section of 11i-2, whereas another chondrule is fine-grained, dense and completely altered to sheet silicates with a sulfide rim around it (Fig. 1.7d). Greshake *et al.* (2005) found similar rims although with a larger thicknesses (up to 35 μm) and composed entirely of sulfides. Based on these morphologies, we infer that TL11h chondrules are more altered than TL5b but less altered than TL11i. The abundance of irregular lithic fragments (up to 10 vol%) in TL11h is similar to TL11i but they are much smaller (largest is ~ 100 μm), some contain cracks and are more fragmented. One of the lithic fragments is embedded in the lower right corner of the Ca-Mg phosphate grain (Fig. 1.7f). Fine-grained magnetite grains occur both isolated, in framboidal and plaquette clusters, or as pseudomorphs after sulfides (15 vol%). Most carbonates are fine-grained, with the exception of one large (100 x 200 μm) Mn-rich carbonate grain, and evenly distributed throughout the sample. Carbonate abundance is close to that of TL5b (up to 11 vol%). Sulfides are rare (1-2 vol%), but their microstructures are similar to TL5b and TL11i. Fine-grained matrix, rich in sheet silicates, is similar in abundance to TL11i (up to 40 vol%).

Specimen TL11v is a mixture of fragments as it was collected as a disaggregated sample. The two chips picked for this study (Fig. 1.6d, e) have different abundances of components. Chip one (TL11v-1; Fig. 1.6d) is similar in all respects to TL5b. This chip contains higher abundances (up to 10 vol%) of large (100-150 μm) isolated silicate grains

(the majority are forsteritic olivines) and higher abundance (up to 40 vol%) of chondrules. The majority of these chondrules have intact olivine and rare pyroxene grains with some sulfides and are therefore less altered compared to chondrules in the second chip. The abundance of components in the second chip (TL11v-2; Fig. 1.6e) is similar to TL11h although magnetite size differs. Large (up to 30 μm) framboidal magnetites are found in clusters (~ 17 vol%) along with sulfides (~ 15 vol%). Chondrules have been strongly altered by sheet silicates and comprise ≤ 10 vol% of the section. The isolated forsterite grains (~ 100 μm) reach up to 5 vol%. All components are embedded in fine-grained matrix (up to 50 vol%). Carbonates are rare (1-2 vol%). This chip also has a part of a fusion crust that takes up 20% of the chip.

In summary, we make two major observations from the EPMA results: (a) the samples differ from each other in abundances of both primary (nebular) components such as chondrules and isolated silicates, and secondary (alteration products) such as magnetites, carbonates and sheet silicates; and (b) these components have been altered to varied degrees in each sample. TL5b has the highest number of mildly altered chondrules compared to those in other samples. It also contains a large chondrule with devitrified mesostasis, which rules out substantial alteration of TL5b. Sample TL11i, on the other hand, contains the smallest volume percent of pseudomorphed chondrules. This sample, however, contains the highest volume percent of lithic fragments and sheet silicate-dominated matrix compared to other studied samples.

To substantiate the EPMA component estimations and the above conclusion, we used XRD to determine the abundance of minerals. This method determined that components such as forsterite, magnetite, pyrrhotite, enstatite, dolomite, calcite, clinochlore (representative of sheet silicates) and an amorphous phase occur in varied abundances (Fig. 1.9; Table 1.3). The refinement suggests that siderite also occurs in the specimens, but we have not analyzed any grains with this composition. Siderite, however, was reported by Zolensky *et al.* (2002). All samples were found to contain abundant clay minerals and an amorphous phase, but further identification was not possible because appropriate reference spectra/models for the Rietveld refinement are not available in the WPF module of JADE 9.0 software that we used. The results from this exercise showed that specimen TL11h and TL11i are very similar especially in the content of clay-like material (up to 55 vol%), while the bulk of specimen TL5b has a higher peak for an amorphous phase. The mixed specimen TL11v has up to 74 vol% of forsterite component, while specimen TL5b has the highest content of magnetite (up to 21 vol%) in bulk XRD.

Carbonate abundance varies dramatically in each specimen. According to XRD, siderite appears to be present in all samples whereas only calcite and dolomite occur in TL5b.

Results from EPMA-based abundance estimates (Fig. 1.9c) and those obtained by Rietveld analysis (Fig. 1.9b) are comparable within the error (10%). In both methods specimens TL11h and TL11i show a high percentage of sheet silicates (clinochlore in XRD and matrix in EPMA data). For specimen TL5b we identified up to 30 vol% of chondrule-like objects through EPMA observation. This observation is consistent, within error (10%), of the Rietveld calculations, which show up to 40% of 'forsterite' component, which could be represented as either chondrules or isolated silicates. Specimen TL11v is a mixture of various fragments (described above), and so it is not surprising that our EPMA observations are not reflected in XRD data.

The majority of the data from both methods support each other; however, there are some differences in sheet silicates, magnetite, carbonate and sulfide abundances. This could be related to the fact that Rietveld refinement is a semi-quantitative method that employs the least-squares analysis, which in turn is appropriate only if (a) the data points have an associated Gaussian error distribution and (ii) the proposed calculated model (*i.e.* an ideal crystal) taken from a database is a complete representation of the observed data (David 2004). Even though the first condition is usually satisfied, such heterogeneous planetary materials as Tagish Lake will inevitably have uncertainties with the second condition as no database will fit and/or fully cover its mineralogical heterogeneity (*e.g.* Howard *et al.* 2009, 2011). Other sources of errors such as preferred orientation, surface roughness, assumption of infinite samples thickness, *etc.*, could also contribute to observed differences (*e.g.* David 2004; Izawa *et al.* 2010).

1.4 TEM OBSERVATIONS OF THE MATRIX

We used TEM to gain further insights into mineralogical and textural variations among the specimens. We investigated whether the macroscopic variations are mirrored at the sub-micron level in the matrix of each sample.

1.4.1 Specimen TL5b matrix

The section contains large areas of amorphous groundmass and pores held together by epoxy (Fig. 1.10a, b). Porosity in Tagish Lake is high, and thought to be primary (Brown *et al.* 2002). Rare areas of the groundmass contain poorly ordered, fine-grained silicates with ribbon-like structures mixed in with abundant amorphous material.

The boundary between the two is usually gradational. Qualitative EDS analyses of the amorphous material show that it is rich in Si, Fe, Al, Ni and S. Large subhedral and anhedral sulfides (1 to 3 μm wide) occur in isolated domains. These domains contain nanosulfides of various shapes and sizes, *e.g.*, spheres and rods (~100-200 nm wide, respectively). The section contains a large grain (3 × 4 μm) with EDS-determined composition and *d*-spacings measured via SAED consistent with calcite. The carbonate grain is irregular in shape and consists of several sub-grains.

1.4.2 Specimen TL11i matrix

We made two FIB sections of specimen TL11i: 11i-1 and -2 (Fig. 1.11). Section 11i-1 was extracted from the part of the matrix that appears dark and porous on the macroscopic scale in SEM-BSE images, representative of typical matrix in TL11i and other samples (Fig. 1.11a, b). On the TEM scale, this section contains heterogeneously distributed sulfides (bands and patches), most of which have subhedral morphologies (up to 1.2 μm) but minor rods (up to 0.5 μm) also occur. Sheet silicates, exhibiting sinuous textures, occur interstitial to the sulfides, are enriched in Mg, and have varied degrees of order. Measurements of HRTEM images of ordered regions reveal lattice-fringe spacings of 0.10 to 0.11 nm, consistent with saponite, and up to 0.14 nm, a possible chlorite-type phase (Fig. 1.12), similar to observation made by Zolensky *et al.* (2002). The FIB section of 11i-1 also contains two large calcite grains (≤ 3 × 1.5 μm) and several euhedral rod-shaped olivine grains both identified by EDX. Overall, this matrix section is highly porous with large (1-2 x 3-4 μm), irregular cavities filled with epoxy and devoid of any minerals. Its porosity is similar to FIB section TL5b.

Section 11i-2 was extracted from a lithic fragment (Fig. 1.11c, d). The top part of FIB section of 11i-2 contains a compact area composed entirely of sheet silicates with a coronal, 'flower'-like, microstructure (Fig. 1.13). This morphology has a compact core (diameters range ~ 0.3 to 1 μm) composed of sulfides/oxides and fine-grained sheet silicates curled onto each other from which bundles of sheet silicates (0.05 × 0.4 μm) radiate. In some areas, sheet silicates in the core and those radiating from it have a 0.7 nm basal spacing, consistent with the serpentine structure. In comparison, other parts of the coronal, 'flower'-like, microstructure contain radial bundles with basal spacing of 0.9 nm, which more closely correspond to a smectite/saponite structure that tends to dehydrate under TEM vacuum causing a decrease in the layer spacing 1.2-0.9 nm (Klimentidis and Mackinnon 1986). The lower part of this FIB section is enriched in sulfides and has a

porous texture, similar to the FIB section of 11i-1. There is a large silicate grain on the boundary between the compact top and porous bottom areas of the section (white arrow on Fig. 1.11c). Part of the silicate grain (200 × 300 nm) is embayed on both sides by sheet silicates. A fractured nanoglobule, similar in appearance to the ones described by Nakamura *et al.* (2002), surrounded by fine-grained and ropy sheet silicates, occurs near the base of this FIB section (black arrow in Fig. 1.11c).

1.4.3 Specimen TL11h matrix

The bright-field and HAADF images (Fig. 1.10c, d) reveal an overall decrease in porosity across the 11h section. Some parts of it resemble the porosity of the TL5b matrix (top and bottom), whereas the middle is more compact. The sample contains abundant sulfides and carbonate grains. Some sulfides concentrate in large (2-3 μm × 0.5-1 μm) bands. The sulfide bands and carbonate grains are surrounded by sinuous sheet silicates. The middle part of the section is more compact and enriched in ribbon-like sheet silicates. Although this middle part is devoid of sulfide grains, a sulfide/oxide circular rim (possible highly altered chondrule) with a diameter of ~4 to 5 μm surrounds this more compact, sheet silicate-rich area. Within this area occurs a large (1 × 0.5 μm) grain identified through spectral imaging to be enriched in P, Ni and Fe, possibly schreibersite, but the thickness of the grain precluded SAED. This P-bearing grain is locally embayed by sheet silicates but otherwise completely surrounded by them. Several carbonate grains are present in this FIB section. Carbonate in the upper middle part of the section has a circular shape and HAADF imaging shows concentric contrast variations. EDS spectral imaging indicates that the outside of this carbonate grain is enriched in Mg, Ca and minor Mn, whereas the core is enriched Fe and sulfide grains (Fig. 1.14). Measurements from SAED patterns acquired from the core are consistent with a siderite structure.

1.5 MINERAL FORMATION MODELING

We performed a set of thermodynamic calculations to understand: (1) the redox and pH conditions, in which the minerals found in the Tagish Lake are stable; (2) what mineral(s) tell us the most about the alteration conditions it experienced; and (3) how do variations in CO_2 fugacity and activity of a particular element affect the stability of that mineral(s). To address point (1), the stabilities of each mineral were plotted on diagrams relating the oxidation potential (Eh) with hydrogen activity (pH), i.e., Eh-pH plots. We tested the following parameters: (1) a range of water temperatures were tested (T = 0 °C;

25 °C and 100 °C) based on prior estimates of aqueous alteration T on meteorite parent bodies (e.g., Clayton and Mayeda 2001; Zolnesky et al. 2002); and (2) a pressure range between 1 bar and 1 x 10^{-30} bars, which is the stability field of water at T = 0 °C.

Although we chose a pressure range likely beyond that encountered on the Tagish Lake parent body, we found that stability fields of the forsterite, siderite, calcite and pyrrhotite minerals follow the stability field of water regardless of total pressure. Therefore, these minerals do not help to constrain the alteration history of Tagish Lake. Pentlandite [$(Fe,Ni)_9S_8$] was also considered, but due to the fact that the data for this mineral does not exist in the version of the Geochemist Workbench's database used in this study, we tested several other nickel sulphides as proxies for it. All of them also follow the stability of water, so we presume that pentlandite behaves in an analogous manner. Similarly, we checked the behavior of clays using Al as the main element of consideration. Regardless of the end-member, e.g., Ca-saponite, Mg-saponite, and Na-saponite, these minerals follow the stability of water and, therefore, are not informative. We thus focus on magnetite, which is the only mineral among those tested that has a restricted stability field and which can, therefore, help to constrain formation conditions.

1.5.1 Stability of magnetite

At 0 °C and 1 bar magnetite is stable at 5.9<pH<14, and between -0.6<Eh<-0.1 (Fig. 1.15a). The minimum pressure and temperature at which magnetite is stable in the presence of water is 1 x 10^{-6} bar and 0 °C (Fig. 1.15a, b). At a higher pressure of 1 bar, magnetite can be stable at temperatures up to 100 °C, although its stability field is more restricted (Fig. 1.15c). However, at 1 x 10^{-6} bar magnetite can exist only up to 7 °C (Fig. 1.15d) and is replaced by hematite at this pressure and temperature conditions. Thus, magnetite can help constrain the minimum pressure, temperature, Eh and pH conditions at which this mineral could crystallize on the Tagish Lake parent body. Therefore, to address the point (3) only magnetite was considered as it has the most restricted stability field among other alteration minerals. We tested how CO_2 fugacity and the change in activity of different elements affect the stability of magnetite at minimum temperature of 0 °C.

The effect of CO_2 (Fig. 1.15e) was first tested by fixing Eh at -0.25 (the middle value of Eh from Fig. 1.15a), T = 0 °C, P = 0.001 bar (the middle-range pressure between 1 and 10^{-6} bar). On Fig. 1.15e both magnetite and siderite (iron carbonate) share a stability boundary. At fixed conditions (Eh, T and P), the boundary is slightly positive,

i.e., the log fCO_2 increases from 10^{-5} to 10^{-3} as pH increases from 6.1 to 7.4. If we change the Eh to -0.155V, i.e., the maximum Eh at which magnetite is stable at 0 °C and P=1 bar (Fig. 1.15a), the stability field of magnetite decreases tremendously and the boundary between it and siderite assumes a negative slope (Fig. 1.15f).

Next we tested the effect of changing element activity, specifically Fe^{2+} and Ca^{2+}, on the stability of magnetite (Fig. 1.15g, h). We also tested Mg^{2+}, but its change in activity has a similar effect as Fe^{2+}, and so we discuss only the latter here. We fixed fCO_2 at 10^{-4} because both magnetite and siderite share a stability boundary at this fugacity and pH = 7 (from Fig. 1.15e). Our calculations show that the minimum stability for both siderite and magnetite is defined by a point at log aFe^{2+}= -2 and pH = 6.9. Activities of Fe^{2+} <-2 and pH >6.9 result in the conversion of siderite to magnetite. In comparison, the siderite-magnetite stability boundary reaches a maximum at aCa^{2+}= 10.1. Increase in Ca^{2+} activities result in the conversion to calcium ferrite. The decrease in Ca^{2+} activity does not change the stability boundary as it stays at pH = 7.

From the above calculations and diagrams we conclude that for both siderite and magnetite to form in the Tagish Lake parent body at a temperature of 0°C and low pressure of 10^{-3} bar (the mid-range pressure of magnetite stability) the following conditions have to be met: minimum pH = 5.6, maximum Eh = -0.155 V and low fCO_2 = 10^{-4} with minimum activity of Fe^{2+} = -2 and maximum activity of Ca^{2+} = 10.1.

We note that in our calculations we tested alteration in the presence of water only, a single alteration event, and one end-member for each mineral. However, the alteration fluid on carbonaceous parent bodies likely contained various amounts of NH_3, CO_2, SO_2, and minor H_2S in addition to water (e.g., DuFresne and Anders 1962; Schulte and Shock 2004). Textural evidence from meteorites also suggests that there might have been multiple cycles or pulses of alteration fluids (e.g., Tomeoka and Buseck 1985; Zolensky et al. 1993; Benedix et al. 2003). In addition, compositional variations in phyllosilicates, carbonates, and sulfides found in the Tagish Lake meteorite (e.g. Zolensky et al. 2002; Blinova et al. 2009, 2010; Izawa et al. 2010) also indicate the conditions of alteration were more variable than modelled. Nonetheless, our calculations constrain the minimum conditions under which magnetite, an abundant mineral in Tagish Lake meteorite, could be stable and are in reasonable agreement with previous estimates of magnetite stability in carbonaceous chondrites (Schulete and Shock 2004)

1.6 DISCUSSION

1.6.1 Progressive alteration

Chondrites in general preserve a complex record of different processes that occurred during the earliest stages of the solar system evolution. Many presolar and nebular processes have been obscured by later secondary asteroidal processes (Brearley 2003) particularly within highly altered chondritic groups such as CI and CM. The Tagish Lake meteorite has been classified as an ungrouped petrologic type 2 carbonaceous chondrite with affinities to both CI and CM, and has a varied mineralogy dominated by hydrated minerals, which suggests different stages of parent-body alterations (Zolensky *et al.* 2002).

Our mineralogical and petrological observations indicate that there is a similarity in both primary (nebular-related) and secondary (alteration-related) components among the studied samples. This indicates that all four samples started off with similar anhydrous precursors. Zolensky *et al.* (2002) noted an analogous observation for the Tagish Lake samples. However, the variation in component abundance in the four samples we studied suggests an initial heterogeneity in the protolith material. Further, all samples experienced varied degrees of hydrous alteration. The alteration most likely occurred on the parent-body as all primary nebular components, e.g., chondrules, have been altered in all samples albeit to varied degrees. Based on our observations, we infer that sample TL5b experienced less alteration compared to other samples because it contains intact silicate grains and devitrified mesostasis inside moderately altered chondrules. In comparison, samples TL11v and TL11i both have pseudomorphed chondrules, which are entirely replaced by sheet silicates, implying a higher degree of alteration in these samples. Our observation of compact sheet-silicate-rich lithic fragments, which are highly abundant in TL11i, also suggests that this lithology sampled a part of the protolith that experienced a higher water/rock ratio and some kind of brecciation. Thus, based on petrological and mineralogical observations we conclude that the Tagish Lake parent body initially contained a heterogeneous mixture of anhydrous precursor minerals of nebular and presolar origin, which were later aqueously altered. The brecciation of components, which could have happened before the incorporation into the final the parent body (Takayama and Tomeoka 2012), and the alteration was not ubiquitous. The data suggest that the samples recorded increasing degrees of alteration in the order of TL5b < TL11h < TL11i. Specimen TL11v, which consists of disaggregated

material and is heterogeneous both on micro- and macro-scale, encompasses the petrologic characteristics of the other three specimens as seen through EPMA observation.

This order of alteration is also supported by variations in organic matter and whole rock oxygen data. Herd *et al.* (2011, 2012) showed that variations in organic matter, from the same four Tagish Lake samples studied here, correlate with variations in the inferred sequence of the parent body aqueous alteration. These authors found that sample TL5b has a higher amount of more primitive insoluble organic matter (IOM) than sample TL11i indicating more aqueous alteration effects on the latter sample. In addition, the IOM from the TL5b contains a higher fraction of nanoglobules than does the TL11v and TL11i IOM, indicating the latter two samples have undergone higher degrees of hydrothermal alteration to preferentially destroy the isotopically anomalous nanoglobules. In other words, the alteration sequence recorded by the IOM reflects the observations from mineralogy and petrology with the least altered TL5b to the more altered TL11v and TL11i.

This conclusion is also supported by the fact that the whole-rock oxygen-isotope analyses of the same four samples show that all fall on the same binary oxygen mixing isotopic trend (Herd *et al.* 2012). The least-altered TL5b sample is on one end of this trend closest to the CCAM (Carbonaceous Chondrite Anhydrous Mineral) line while TL11i is on the other end containing isotopically heavier sheet silicates, which are consistent with them being more extensively altered (Herd *et al.* 2012). Therefore, both organics and whole-rock oxygen isotopes argue that these samples started off from the same protolith, and then were gradually hydrated to different degrees, in agreement with our mineralogical and petrological results.

1.6.2 Formation of sheet silicates and the origin of the amorphous material in TL5b

Our petrographic observations (both XRD and TEM) indicate a high volume of amorphous material in TL5b, suggesting that it is indigenous rather than a product of terrestrial weathering. Amorphous material was found both in the FGRs and the matrices of CM and CR chondrites (*e.g.*, Chizmadia and Brearley 2008; Abreu and Brearley 2010). Detailed petrographic studies of the rims in CM chondrites (*e.g.*, Y-791198) indicate the presence of abundant amorphous material intermixed with nanocrystalline phyllosilicates consistent with limited thermally driven growth (Chizmadia and Brearley 2008). Matrices dominated by amorphous material were also found in two primitive, low metamorphic grade, CR chondrites (MET00426 and QUE99177), suggesting thermal metamorphism

and low-temperature parent-body alteration did not occur or was minimal (Abreu and Brearley 2010).

In our TEM observations of TL5b we see abundant amorphous material with rare bundles of fine-grained sheet silicates, comparable to the microstructure found in the FGRs and matrices of CM and CR chondrites. We conclude that TL5b underwent lower-T hydrothermal alteration than other studied samples (TL11i, TL11h) in order to preserve the observed amorphous material and produce fine-grained sheet silicates. Herd *et al.* (2011) inferred an upper limit for the Tagish Lake protolith alteration of ~150°C to preserve volatile organic compounds seen in these samples. This conclusion fits well our petrographic observations of the amorphous material in the TL5b. Progressive alteration of the metastable amorphous material results in the formation of increasingly coarse sheet silicates with continued alteration (Jones and Brearley 2006; Brearley and Burger 2007). The limited amount of amorphous material in the other studied Tagish Lake samples argues that they were affected by either longer alteration at higher T (>200°C) or higher water/rock ratio to preferentially destroy the amorphous material in favour of fine- and course-grained sheet silicates (Brearley and Burger 2007; Chizmadia and Brearley 2008). There are several hypotheses for the origins of amorphous material. Theories for its formation include: shock metamorphism, weathering of FeO-rich olivines, alteration of nebular material, or surviving non-equilibrium condensate from the solar nebula (Day and Donn 1978; Nuth and Donn 1983; Brearley 1993; Greshake 1997; Chizmadia and Brearley 2008; Abreu and Brearley 2010). The production of amorphous material by shock metamorphism does not fit with the observed petrography of TL5b. The shock-induced structures, such as high-density dislocations, planar fractures, and deformations (Greshake 1997), have not been observed in any Tagish Lake samples in this study. It was also noted that such shock processing would deplete the matrix in dissolved S and produce globules of sulfides (Ashworth 1985). In comparison, we find that the matrix in all four samples is highly enriched in S and Ni, and the morphology of sulfides is not globular (Fig. 1.8). The data are also not consistent with a formation via alteration of the FeO-rich olivines. The product of such alteration would be highly heterogeneous intergrowths or wispy grains of an Fe-oxide and silicate (Jones and Brearley 2006; Chizmadia and Brearley 2008), and we have not observed such morphologies in TL5b or the other samples studied herein.

We cannot completely rule out parent body hydrous alteration as a possible origin of some of the amorphous material because the studied samples do show modest

alteration in the mineralogy of TL5b chondrules (Fig. 1.4). However, the fact that we observed the highest amount of amorphous material in the least altered sample (TL5b) is a strong indicator that hydrous alteration is not the dominant formation mechanism. In addition, the sample TL11i, which showed the greatest levels of aqueous alteration, is dominated by sheet silicates, not amorphous silicates. Based on the above arguments we infer that amorphous material found in the Tagish Lake samples is of nebular origin similar to that in CM, CO, and CR chondrites (Brearley 1993; Chizmadia and Brearley 2008; Abreu and Brearley 2010).

Although most of the amorphous silicates likely are nebular in origin, some may be presolar (*e.g.*, Chizmadia and Brearley 2008). Brown *et al.* (2000) first indicated the presence of presolar grains in the Tagish Lake meteorite. This was later supported by Nakamura *et al.* (2003) who observed high levels of primordial noble gas indicative of high concentrations of presolar diamonds and SiC/graphite grains. Marhas and Hoppe (2005) reported 4 ppm presolar silicates within a Tagish Lake thin section of unknown alteration grade, an abundance which is small compared to primitive meteorites (up to 200 ppm) and the most primitive IDPs (> 400 ppm). We have not yet measured the presolar silicate abundance on our samples, but based on the variation in degree of alteration and abundance of amorphous material, we expect that if presolar silicates are preserved then TL5b should contain higher quantities than TL11h and TL11i.

1.6.3 Formation of sulfides

Exsolved pentlandite in pyrrhotite has been previously reported in other carbonaceous chondrites such as CI, CM and CR (*e.g.*, Fuchs *et al.* 1973; Ramdohr 1973; Schrader *et al.*, 2010; Brearley and Marinez 2010) and non-exsolved pentlandite along grain boundaries has been observed in several hydrated IDPs (Tomeoka and Buseck 1984; Zolensky and Thomas 1995). Our observations of exsolved pentlandite from pyrrhotite in the Tagish Lake meteorite (Fig. 1.8a, b, c, d) are contrary to Boctor *et al.* (2003) who did not observe any exsolution in Fe-Ni monosulfide. The studied specimens contain a large number of sulphides of intermediate composition and in BSE images we encounter a considerable amount of grains with both exsolved and non-exsolved morphologies (Fig. 1.8).

The exsolved sulfide morphologies that we observe in our samples are similar to those reported by Lauretta *et al.* (1997) for pentlandite synthetized via gas-solid reactions under nebular conditions suggesting that at least some of the Tagish Lake exsolved

sulfides formed at higher temperatures in a nebular environment. In comparison, some exsolved pentlandite, *e.g., the* "flame" texture, could possibly be a product of metal diffusion from Ni-bearing monosulfide solid solution (MSS) during cooling in the solar nebula at temperatures < 600 °C over extended periods of time (~ 3000 – 30,000 years) (Brearley and Martinez 2010).

It was reported that pentlandite can also form at lower temperatures (≤ 200 °C) or more rapid cooling forming non-exsolved granular pentlandite at interstices between grains and along grain boundaries (Vaughan and Craig 1997; Durazzo and Taylor 1982). Non-exsolved pentlandite has also been observed as a product of high oxygen fugacity conditions during aqueous alteration (Godlevskiy *et al.* 1971), which is thought to be consistent with conditions of non-exsolved pentlandite observed in hydrous IDPs (Zolensky and Thomas 1995). Comparison of morphologies in our samples with those previously reported suggests that pentlandite found along the pyrrhotite grain boundaries is a product of aqueous alteration on the parent body. Similarly, the 'bulls-eye' morphology consisting of a core and rim separated by a gap (Fig. 1.8e, f) and sulfide rims found around highly altered chondrules (Fig. 1.7c, d) possibly fall into the same generation of sulfides, which were formed by multiple precipitation episodes during low-temperature alteration (Zolensky *et al.* 2002).

1.6.4 Formation of magnetite

The majority of magnetite grains we observed occur in association with sulfides, as pseudomorphs of sulfides, or as clustered framboids and plaquettes with sulfides and surrounded by more magnetite. Based on the observed morphologies it appears that the majority of magnetite found in our samples is secondary and probably the product of aqueous alteration and multiple precipitation events. Although Zolensky et al. (2002) were unable to determine the order of precipitation, they observed that the majority of magnetite forms thin rims around sulfides or perfect pseudomorphs after sulfides similar to our samples. They concluded that magnetite is a product of late-stage oxidation/replacement event.

Our thermodynamic modeling indicates that low temperatures and neutral to basic pH is necessary for magnetite to form and be stable. These inferred conditions are consistent with previous estimates of pH during chondrite alteration (DuFresne and Anders 1962; Zolensky et al. 1989). The model of Schulte and Shock (2004) also show that magnetite can be stable up to 100°C at pressure of 1 bar. If we consider magnetite to

be a secondary mineral based on the morphologies observed, it appears that magnetite formed during parent-body alteration at low temperature and neutral to basic pH. Zolensky et al. (2002) also noted at least two stages of alteration, suggesting that oxidation of sulfides occurred in a later stage to transform them into magnetite. Our observations of magnetite morphologies and modeling also corroborate this conclusion. We hypothesize that the differences in magnetite abundances observed in EPMA and XRD calculations in the four studied samples are most likely due to the original variations in sulfides prior to the second stage of alteration.

1.6.5 Formation of 'flower'-like microstructure in the lithic fragment

To our knowledge, the coronal, 'flower'-like serpentine microstructure observed in the FIB section of lithic fragment TL11i (Fig. 1.13) has not been reported in other chondrites. The closest forms are polygonal serpentine reported by Zega *et al.* (2003, 2004, 2006) in CM chondrites. These structures contain polygonal sectors formed by concentric lizardite layers with periodic inversion of the tetrahedral sheet, resulting in kinked layers wrapped around a tube axis. The kinking is due to the structural mismatch between the tetrahedral silica sheet and the octahedral Mg-bearing sheet (*e.g.*, Dodony 1997). Such structures were inferred to have formed through intense alteration under oxidizing conditions (Zega *et al.* 2004, 2006). The 'flower'-like textures that we observe in Tagish Lake, while exhibiting a round morphology similar to polygonal forms, do not show polygonal geometry and appear to be of a different nature than those described by Zega *et al.* (2004, 2006).

Cressey (1979) reported radial structures in vein margins in serpentinized peridotite from the Lizard, Cornwall, England (Fig. 1.13e, f), and described these objects as consisting of radial bundles or blades of lizardite laths surrounded by fine-grained serpentine with no apparent core. These authors also noted that although these structures closely resemble spherulites in polymers, they are cylindrical, not spherical, in three dimensions. Cressey (1979) postulated that observed terrestrial lizardite structures probably formed under unique conditions in a hydrothermal vein. The formation was probably facilitated by high nucleation and growth rates producing skeletal-type structures followed by a rapid quenching similar to conditions in the chilled margins of a basic intrusion (Cressey 1979). In comparison, these terrestrial textures, although similar at first glance to those we observe in the Tagish Lake meteorite, differ in mineralogy and overall geometry, *i.e.*, the terrestrial forms appear to lack a distinct core (Cressey 1979).

We cannot infer from the data at hand whether the observed radial structures in TL11i have a spherical or cylindrical three-dimensional space. However, based on lattice-fringe measurements of localized areas within the structure, the cores contain serpentine and the radial bundles a combination of serpentine and saponite. We hypothesize that pore space played a role in producing the radial bundles observed in the coronal, 'flower'-like texture in TL11i.

It is widely accepted that hydrous processing of asteroidal bodies occurred after accretion (Brearley and Jones 1998; Brearley 2004). The hydration process varied in duration and chemistry. For example, there are local regions within the studied Tagish Lake samples where alteration appears to have been nearly complete, *e.g.* the embayment in the phosphate grain in TL11h (Fig. 1.10c) and partially altered silicate grain at the boundary of the top and bottom portions of TL11i-2 (Fig. 1.11c). These observations suggest a possible intermittent availability of fluids or the porosity of the grain to allow fluids to penetrate into some areas of the grain more readily than others. In other areas the mineralogy suggests variation in fluid composition, *e.g.* change in carbonate grain composition from Fe-rich to more Mg-rich (Fig. 1.14). In addition, the presence of both fine-grained and coarse-grained textures observed in the sheet silicates (Fig. 1.12) argues for changes in duration of crystallization (Jones and Brearley 2006; Brearley and Burger 2007). The coronal, 'flower'-like textures in TL11i-2 show both compositional (saponite and serpentine mixture in the radial arrays, and serpentine only in the core) and textural (fine-grained in the core, and coarse-grained in the arrays) changes (Fig. 1.13). We suspect that these textures formed as a result of different pulses of fluids with changing composition and varying duration in alteration.

We hypothesize that loosely packed clusters of anhydrous semi-rounded silicate grains (a few microns in diameter) were subjected to alteration from the outside (Fig. 1.16a). At first, these clusters were subjected to Fe-bearing fluids, which percolated through the cracks/pore space between and around these semi-rounded grains. Serpentine formed in this space in a radial fashion (Fig. 1.16b) similar to a terrestrial hydrothermal vein environment (*e.g.*, Cressey 1979). The radial arrays show evidence of intermixing during growth, indicating that the alteration was ubiquitous. The radial arrays had more time to crystallize to form coarse-grain morphology. The fluids then proceeded to alter the semi-rounded grains to produce fine-grained cores of the future 'flower'-like textures (Fig. 1.16c). Any excess Fe was precipitated as sulfides and/or magnetite found in and around the cores of these structures (Fig. 1.16c). The last stage of the alteration is late

introduction of Al-bearing fluid to alter the radial arrays only to produce a mixture of serpentine-saponite that we observe (Fig. 1.16d).

An alternative hypothesis is that the 'flower'-like textures were produced by altering the grains first to generate the cores followed by the growth of radial bundles into the pore spaces. Although hydrothermal experiments depicting the models' conditions are necessary to determine the formation stages of such texture, the fact that we observe similar 'flower'-like textures in the altered chondrule of TL11h (Fig. 1.7c) is consistent with our first preferred hypothesis. This chondrule was subjected to alteration fluids that appear to have percolated through the cracks between the olivine grains to produce radial bundles in the cracks, followed by alteration of the grains to produce fine-grained cores in a similar fashion to our proposed model. The altered chondrule in Figure 1.7a is also consistent with our proposed model. This chondrule preserves a snapshot of the alteration in progress showing serpentine radial arrays growing around partially altered olivine grains (Fig. 1.7b).

1.6.6 Mineral alteration index (MIA) – Browning et al. (1996) model

In this last section we discuss the alteration index of Browning et al. (1996) that is routinely used to determine the alteration sequence of CM chondrites. We attempted to apply the algorithm for calculating the mineral alteration index of Browning et al. (1996) to the Tagish Lake specimens. We, like others, encountered several difficulties in these calculations (see summary by Velbel and Palmer 2011). Preliminary filters are proposed by Browning et al. (1996) to ensure that the mineral assemblage used for calculation reflects phyllosilicates only. In these screens unwanted carbonates and oxides are excluded based on the following criteria: analytical totals > 83wt%; elements such as Ca, Cr, Na < 0.5 wt%; and S < 2 wt%. Initially we followed the same recommended screening procedure; however, out of 200 microprobe analyses with a defocused beam and 400 analyses with a focused beam this resulted in exclusion of 99% of the data. One of the main reasons is that the sulfur content in all studied Tagish Lake specimens typically varies between 3 to 6 wt% and could go as high as 10 wt%, and only rarely below 1wt%. We then modified these initial screens to include S content with up to 10 wt% and other elements (in particular Ca and Na) up to 2 wt%.

Once we selected satisfactory analyses we reduced our data further by subtracting an idealized pyrrhotite formula from each analysis following the Browning et al. (1996) algorithm. More than 50% of selected analyses produced negative values of Fe, Ni, and S

atoms after following this procedure. This had an effect on the sulfide-corrected cation totals that were recalculated to 5 based on the fundamental assumption that the atomic proportions reflect a stoichiometric serpentine composition. This could be due to the fact that our initial S content was set at much higher values than Browning et al. (1996). Another possibility is that we overgeneralized the sulfide composition by assuming pyrrhotite. Although we agree that the predominant sulfide phase in the Tagish Lake is pyrrhotite (Zolensky et al. 2002), similar to CM chondrites (Zolensky et al. 1993), we also have noted that there is a large variation in sulfide composition in the studied specimens with intermediate and high Ni compositions (Fig. 1.2) as well as exsolved compositions present (Fig. 1.7).

At the end of the calculations we were left with less than ten analyses that produced MIA values between 0 and 2 similar to Browning et al. (1996). Although these modified MIA values were reasonable for the index, they were not consistent with alteration degrees inferred from the petrology. We conclude that the MIA algorithm of Browning et al. (1996) is not suitable for the Tagish Lake meteorite specimens that are highly enriched in S, have various sheet silicate compositions (not only serpentine as assumed by Browning et al., 1996, for CM chondrites) as well as variable composition sulfides.

1.7 CONCLUSION

(1) Based on petrological and mineralogical observations we conclude that the Tagish Lake parent body was a heterogeneous mixture of anhydrous precursors of nebular origin, which were brecciated and aqueously altered. The degree to which the studied samples experienced aqueous alteration is in the order TL5b < TL11h < TL11i. Specimen TL11v, which consists of disaggregated material, is heterogeneous on the microscale and encompasses the petrologic characteristics of other three specimens as seen through EPMA observation. This conclusion is also supported by variations in organic matter and whole rock oxygen data (Herd *et al.* 2011, 2012).

(2) The presence of the abundant amorphous material in the TL5b argues that this sample experienced relatively milder parent-body alteration to preserve this indigenous nebular material and produce fine-grained sheet silicates. Other samples were subjected to a longer duration of hydrous alteration because they are dominated by coarse-grained sheets silicates

(3) We observed two generations of sulfides in the studied samples. The first generation consists of exsolved pentlandite morphologies, which formed at higher temperature in the changing nebular conditions or metal diffusion from Ni-bearing MSS during cooling of the solar nebula below temperatures < 600 °C. The second generation includes non-exsolved pentlandite along grain boundaries, the 'bulls-eye' sulfide morphology, and rims around highly altered chondrules, which all formed by multiple precipitation episodes during low temperature aqueous alteration (≤ 100 °C) on the parent body.

(4) The coronal, 'flower'-like microtexture consisting of core and radial arrays, observed in a lithic fragment from sample TL11i, shows both compositional changes from serpentine in the core to saponite-serpentine in the radial arrays and textural changes from fine-grained in the core to coarse-grained in the arrays. Our preferred model for production of this texture involves serpentine precipitation in the pore spaces around silicate grains to produce coarse-grained radial arrays, subsequent alteration of silicate grains to form fine-grained cores, and later introduction of Al-bearing fluid to precipitate the saponite in the already serpentinized cracks.

1.8 REFERENCES

Abreu, N.M., and Brearley, A.J. 2010. Early solar system processes recorded in the matrices of two highly pristine CR3 carbonaceous chondrites, MET 00426 and QUE 99177. Geochimica et Cosmochimica Acta 74:1146-1171.

Ashworth, J.R. 1985. Transmission electron-microscopy of L-group chondrites. 1. Natural shock effects. Earth and Planetary Science Letters 73:17-32.

Baker, L., Franchi, I.A., Wright, I.P., and Pillinger, C.T. 2002. The oxygen isotopic composition of water from Tagish Lake: its relationship to low-temperature phases and to other carbonaceous chondrites. Meteoritics and Planetary Science 37:977-985.

Benedix, G.K., Leshin, L.A., Farquhar, J., Jackson, T., and Thiemens, M.H. 2003. Carbonates in CM2 chondrites: Constraints on alteration conditions from oxygen isotopic compositions and petrographic observations. Geochimica et Cosmochimica Acta 67:1577-1588.

Blinova, A., Herd, C.D.K., Zega, T., De Gregorio, B., and Stroud, R. 2009. Preliminary SEM and TEM study of pristine samples of Tagish Lake Meteorite (abstract #2039). 40th Lunar and Planetary Science Conference. CD-ROM.

Blinova, A., Zega, T., Herd, C.D.K., and Stroud, R. 2011. A TEM stidy of the pristine matrix from the Tagish Lake meteorite (abstract #2517). 42nd Lunar and Planetary Science Conference. CD-ROM.

Blinova, A., Alexander, C.M.O'D., Wang, J., and Herd, C.D.K. 2012. Mineralogy and Mn-Cr extinct radionuclide dating of a dolomite from the pristine Tagish Lake Meteorite (abstract #1188). 43nd Lunar and Planetary Science Conference. CD-ROM.

Boctor, N.Z., Kurat, G., and Alexander, C.M.O'D. 2003. Sulfide-oxide assemblage in Tagish Lake carbonaceous chondrite (abstract #1705). 34th Lunar and PLanetary Science. CD-ROM.

Bradley, J.P., Keller, L.P., Snow, T.P., Hanner, M.S., Flynn, G.J., Gezo, J.C., Clemett, S.J., Brownlee, D.E., and Bowey, J.E. 1999. An infrared spectral match between GEMS and interstellar grains. Science 285:1716-1718.

Brandelik, A. 2009. CALCMIN – an EXCEL Visual Basic application for calculating mineral structural formulae from electron microprobe analyses. Computers and Geosciences 35:1540-1551.

Brearley, A.J. 1993. Matrix and fine-grained rims in the unequilibrated CO3 chondrite, ALHA77307: origins and evidence for diverse, primitive nebular dust components. Geochimica et Cosmochimica Acta 57:1521-1550.

Brearley, A.J. 2004. Nebular versus parent-body processing, in: Treatise on Geochemistry, edited by Davis, A.M. Elsevier Ltd. pp. 247-268.

Brearley, A.J., and Burger, P.V. 2009. Mechanisms of aqueous alteration of type IIA chondrule glass in the CR chondrite EET92105: Insights from FIB/TEM analysis. Meteoritics and Planetary Science 44:A39-A39.

Brearley, A.J., and Jones, A. 1998. Chondritic meteorites, in: Planetary materials, dited by Papike, J.J. Washington, DC,: Mineralogical Society of America. pp. 3-1 - 3-398.

Brearley, A.J., and Martinez, C. 2010. Ubiquitous exsolution of pentlandite and troilite in pyrrhotite from the TIL 91722 CM2 carbonaceous chondrite: a record of low temperature solid state processes (abstract #1689). 41st Lunar and Planetary Science Conference. CD-ROM.

Brown, P.G., Hildebrand, A.R., Zolensky, M.E., Grady, M., Clayton, R.N., Mayeda, T.K., Tagliaferri, E., Spalding, R., MacRae, N.D., Hoffman, E.L., Mittlefehldt, D.W., Wacker, J.F., Bird, J.A., Campbell, M.D., Carpenter, R., Gingerich, H., Glatiotis, M., Greiner, E., Mazur, M.J., and McCausland, P.J.A. 2000. The fall, recovery, orbit, and composition of the Tagish Lake Meteorite: a new type of carbonaceous chondrite. Science 290:320-325.

Brown, P.G., ReVelle, D.O., Tagliaferri, E., and Hildebrand, A.R. 2002. An entry model for the Tagish Lake fireball using seismic, satellite and infrasound records. Meteoritics and Planetary Science 37:661-675.

Browning, L.B., McSween, H.Y., and Zolensky, M.E. 1996. Correlated alteration effects in CM carbonaceous chondrites. Geochimica et Cosmochimica Acta 60:2621-2633.

Bullock, E.S., Gounelle, M., Lauretta, D.S., Grady, M.M., and Russell, S.S. 2005. Mineralogy and texture of Fe-Ni sulfides in CI1 chondrites: Clues to the extent of aqueous alteration on the CI1 parent body. Geochimica et Cosmochimica Acta 69:2687-2700.

Chizmadia, L., and Brearley, A.J. 2008. Mineralogy, aqueous alteration, and primitive textural characteristics of fine-grained rims in the Y-791198 CM2 carbonaceous chondrite: TEM observations and comparison to ALHA81002. Geochimica et Cosmochimica Acta 72:602-625.

Chizmadia, L., and Lebron-Rivera, S.A. 2010. Thermal and pH conditions during hydration of amorphous silicate smokes. Meteoritics and Planetary Science 45:A35-A35.
Cressey, B.A. 1979. Electron microscopy of serpentinite textures. Canadian Mineralogist 17:741-756.

Day, K.L. and Donn, B. 1978. Condensation of non-equilibrium phases of refractory silicates from vapor. Science 202:307-308.

David, W.I.F. 2004. Power diffraction: least-squares and beyond. Journal of Research of the National Institute of Standards and Technology 109(1):107-123.

Dódony, I. 1997. Structure of the 30-sector polygonal serpentine: A model based on TEM and SAED studies. Physics and Chemistry of Minerals 24:39-49.

Droop, G.T.R. 1987. A general equation for estimating Fe3+ concentrations in ferromagnesian silicates and oxides from microprobe analyses, using ctoichiometric criteria. Mineralogical Magazine 51:431-435.

Durazzo, A. and Taylor, L.A. 1982. Exsolution in the MSS-Pentlandite system - textural and genetic implications for Ni-sulfide ores. Mineralium Deposita 17:313-332.

Endress, M. and Bischoff, A. 1996. Carbonates in CI chondrites: Clues to parent body alteration. Geochimica et Cosmochimica Acta 60(3):489-507.

Fuchs, L.H., Olsen, E.J., and Gebert, E. 1973. New x-ray and compositional data for farringtonite, $Mg_3(PO_4)_2$. American Mineralogist 58:949-951.

Godlevskiy, M.N., Likhachev, A.P., Chuvkin, N.G. and Andronov, A.D. 1971. Geothermal synthesis of pentlandite. Dokldy Akademii Nauk USSR 196(5):1182.

Greshake, A. 1997. The primitive matrix components of the unique carbonaceous chondrite Acfer 094: A TEM study. Geochimica et Cosmochimica Acta 61:437-452.

Greshake, A., Krot, A.N., Flynn, G.J., and Keil, K. 2005. Fine-grained dust rims in the Tagish Lake carbonaceous chondrite: evidence for parent body alteration. Meteoritics and Planetary Science 40:1413-1431.

Hanowski, N.P., Brearley, A.J. 2000. Iron-rich aureoles in the CM carbonaceous chondrites Murray, Murchison, and Allan Hills 81002: Evidence for in situ aqueous alteration. Meteoritics and Planetary Science 35:1291-1308.

Hanowski, N.P., and Brearley, A.J. 2001. Aqueous alteration of chondrules in the CM carbonaceous chondrite, Allan Hills 81002: implications for parent body alteration. Geochimica et Cosmochimica Acta 65:495-518.

Herd, R.K., and Herd, C.D.K. 2007. Towards systematic study of the Tagish Lake meteorite (abstract #2347). 38th Lunar and Planetary Science Conference. CD-ROM.

Herd, C.D.K., Blinova, A., Simkus, D.N., Huang, Y., Tarozo, R., Alexander, C.M.O'D., Gyngard, F., Nittler, L.R., Cody, G.D., Fogel, M.L., Kebukawa, Y., Kilcoyne, A.L.D., Hilts, R.W., Slater, G.F., Glavin, D.P., Dworkin, J.P., Callahan, M.P., Elsila, J.E., De

Gregorio, B.T., and Stroud, R.M. 2011. Origin and evolution of prebiotic organic matter as inferred from the Tagish Lake Meteorite. Science 332:1304-1307.

Herd, C.D.K., Sharp, Z.D., Alexander, C.M.O'D., and Blinova, A. 2012. Oxygen isotopic composition of Tagish Lake lithologies: insights into parent body alteration (absract #1688). 43d Lunar and Planetary Science Conference. CD-ROM.

Hildebrand, A.R., McCausland, P.J.A., Brown, P.G., Longstaffe, F.J., Russell, S.S., Tagliaferri, E., Wacker, J.F., and Mazur, M.J.,2006. The fall and recovery of the Tagish Lake meteorite. Meteoritics and Planetary Science 41:407-431.

Howard, K.T., Benedix, G.K., Bland, P.A., and Cressey, G. 2009. Modal mineralogy of CM2 chondrites by X-ray diffraction (PSD-XRD). Part 1. Total phyllosilicate abundance and the degree of aqueous alteration. Geochimica et Cosmochimica Acta 73:4576-4589.

Howard, K.T., Benedix, G.K., Bland, P.A., and Cressey G. 2009. Modal mineralogy of CM2 chondrites by X-ray diffraction (PSD-XRD). Part 2. Degree, nature and settings of aqueous alteration. Geochimica et Cosmochimica Acta 75:2735-2751.

Izawa, M.R.M., Flemming, R.L., King, P.L., Peterson, R.C., and McCausland, P.J.A. 2010. Mineralogical and spectroscopic investigation of the Tagish Lake carbonaceous chondrite by X-ray diffraction and infrared reflectance spectroscopy. Meteoritics and Planetary Science 45:675-698.

Jarosewich, E. 2002. Smithsonian Microbeam Standards. Journal of Research National Institute of Standards and Technology 107:681-685.

Jones, C.L., and Brearley, A.J. 2006. Experimental aqueous alteration of the Allende meteorite under oxidizing conditions: Constraints on asteroidal alteration. Geochimica et Cosmochimica Acta 70:1040-1058.

Klimentidis, R.E. and Mackinnon, I.D.R. 1986. High-resolution imaging of ordered mixed-layer clays. Clays and Clay Minerals 34:155-164.

Kminek, G., Botta, O., Glavin, D.P. and Bada, J.L. 2002. Amino acids in the Tagish Lake meteorite. Meteoritics and Planetary Science 37:697-701.

Lauretta, D.S., and Lodders, K., Jr, B.F. 1997. Experimental simulations of sulfide formation in the Solar Nebula. Science 277:358-360.

Marhas, K.K., and Hoppe, P. 2005. Presolar grains in the Tagish Lake meteorite. Meteoritics and Planetary Science 40:A95.

McSween, H.Y. Jr. 1977. Carbonaceous chondrites of the Ornans type: a metamorphic sequence. Geochimica et Cosmochimica Acta 44:477-491.

Metzler, K., Bischoff, A., and Stōffler, D. 1992. Accretionary dust mantles in CM chondrites: Evidence for solar nebula processes. Geochimica et Cosmochimica Acta 56:2873-2897.

Nakamura, K., Zolensky, M.E., Tomita, S., Nakashima, S., and Tomeoka, K. 2002. Hollow organic globules in the Tagish Lake meteorite as possible products of primitive organic reactions. Inter. Journal of Astrobiology 1:179-189.

Nakamura, T., Noguchi, T., Zolensky, M.E., and Tanaka, M. 2003. Mineralogy and noble-gas signatures of the carbonate-rich lithology of the Tagish Lake carbonaceous chondrite: evidence for an accretionary breccia. Earth and Planetary Science Letters 207:83-101.

Nuth, J.A., and Donn, B. 1983. Laboratory studies of the condensation and properties of amorphous silicate smokes. Journal of Geophysical Research 88:A847-A852.

Petitat, M., Birck, J.-L., Luu, T.H. and Gounelle, M. 2011. The chromium isotopic composition of the ungrouped carbonaceous chondrite Tagish Lake. The Astrophysical Journal 736:23.

Ramdohr, P. 1973. The Opaque minerals in stony meteorites. New York: Elsevier Publ. Co., 245 p.

Russell, S.D.J., Longstaffe, F.J., King, P.L., and Larson, T.E. 2008. Whole-rock, clay mineral, and olivine oxygen and hydrogen isotope compositions of the Tagish Lake carbonaceous chondrite (abstract #1709). 39th Lunar and Planetary Science Conference. CD-ROM.

Schrader, D.L., Connoly Jr., H.C. and Lauretta, D.S. 2010. On the nebular and aqueous signatures in the CR chondrites (abstract# 1262). 41st Lunar and Planetary Science Conference. CD-ROM.

Simon, S.B., and Grossman, L. 2003. Petrography and mineral chemistry of the anhydrous component of the Tagish Lake carbonaceous chondrite. Meteoritics and Planetary Science 38:813-825.

Takayama, A., and Tomeoka, K. 2012. Fine-grained rims surrounding chondrules in the Tagish Lake carbonaceous chondrite: Verification of their formation through parent-body processes. Geochemica et Cosmochimica Acta 98:1-18.

Tomeoka, K., and Buseck, P.R. 1984. Transmission electron-microscopy of the low-Ca hydrated interplanetary dust particle. Earth and Planetary Science Letters 69:243-254.

Tomeoka, K., and Buseck, P.R. 1988. Matrix mineralogy of the Orgueil CI carbonaceous chondrite. Geochimica et Cosmochimica Acta 52:1627-1640.

Vaughan, D.J., and Craig, J.R. 1997. Sulfide ore mineral stabilities, morphologies, and intergrowth textures. In: Geochemistry of hydrothermal ore deposits, 3d ed., edited by Barnes, H.L. John Wiley and Sons, Inc. pp. 367-434.

Weisberg, M., and Huber, H. 2007. The GRO95577 CR1 chondrite and hydration of the CR parent body. Meteoritics and Planetary Science 42:1495-1503.

Weisberg, M., Prinz, M., Clayton, R.N., and Mayeda, T.K. 1993. The CR (Renazzo-type) carbonaceous chondrite group and its implications.

Zega, T.J., Garvie, L.A.J., and Buseck, P.R. 2003. Nanometer-scale measurements of iron oxidation states of cronstedtite from primitive meteorites. American Mineralogist 88:1169-1172.

Zega, T.J., Garvie, L.A.J., Dodony, I., and Buseck, P.R. 2004. Serpentine nanotubes in the mighei CM chondrite. Earth and Planetary Science Letters 223:141-146.

Zega, T.J., Garvie, L.A.J., Dodony, I., Friedrich, H., Stroud, R.M., and Buseck, P.R. 2006. Polyhedral serpentine grains in CM chondrites. Meteoritics and Planetary Science 41:681-688.

Zega, T.J., Nittler, L.R., Busemann, H., Hoppe, P., and Stroud, R.M. 2007. Coordinated isotopic and mineralogic analyses of planetary materials enabled by in situ lift-out with a focused ion beam scanning electron microscope. Meteoritics and Planetary Science 42:1373-1386.

Zega, T.J., Alexander, C.M.O'D., Busemann, H., Nittler, L.R., Hoppe, P., Stroud, R.M., and Young, A.F. 2010. Mineral associations and character of isotopically anomalous organic material in the Tagish Lake carbonaceous chondrite. Geochimica et Cosmochimica Acta 74:5966-5983.

Zolensky, M.E., and Thomas, K.L. 1995. Iron and iron-nickel sulfides in chondritic interplanetary dust particles Geochimica et Cosmochimica Acta 59:4707-4712.

Zolensky, M., Barrett, R., and Browning, L. 1993. Mineralogy and composition of matrix and chondrule rims in carbonaceous chondrites. Geochimica et Cosmochimica Acta 57:3123-3148.

Zolensky, M.E., Bourcier, W.L. and Gooding, J.L. 1989. Aqueous alteration on the hydrous asteroids: Results of EQ3/6 computer simulations. Icarus 78:411-425.

Zolensky, M.E., Nakamura, K., Gounelle, M., Mikouchi, T., Kasama, T., Tachikawa, O., and Tonui, E., 2002. Mineralogy of Tagish Lake: An ungrouped type 2 carbonaceous chondrite. Meteoritics and Planetary Science 37:737-761.

FIGURE CAPTIONS CHAPTER 1:

Figure 1.1:
Compositional diagrams showing (a) the Mg-Fe range of olivine and (b) Mg-Fe-Ca pyroxene compositions in all studied Tagish Lake samples.

Figure 1.2:
Fe-Ni-S ternary diagram (atom %) showing range of sulfide compositions in the studied Tagish Lake samples. The light blue is the approximate range of compositions of sulfides studied by Zolensky *et al.* (2002).

Figure 1.3:
Ternary diagram showing carbonate compositions (in mol%) with respect to $MgCO_3$-$CaCO_3$-$FeCO_3$+$MnCO_3$ from TL5b, TL11i and TL11h along with three analyses of carbonates from Zolensky *et al.* (2002) and approximate fields of CI and CM dolomites (Endress and Bichoff 1996; Petitat *et al.* 2011).

Figure 1.4:
Back-scattered electron images of (a) A large chondrule from TL5b, diameter approximately 2 cm in diameter (b, c, d) Enlargement of a partially crystallized mesostasis (see text for details). In (c): the light grey mineral is clinopyroxene and dark grey is orthopyroxene. (e) A broken chondrule with a thick rim from TL5b. The rim consists of two parts divided by the white line (see text for details). (f) Chondrule from TL11i with normally and oscillatory zoned olivines. The largest olivine has a euhedral shape and exhibits oscillatory zoning (Fo_{70-79}). Other olivine grains within it have normal zoning from Mg-rich cores (Fo_{79-99}) to Fe-rich rims (Fo_{61-74}).

Figure 1.5:
Si-Mg-Fe ternary diagrams (wt%) showing compositional variations of matrix from the Tagish Lake samples: (a) defocused (10 μm) beam; (b) focused (2 μm) beam. CM, CR and CI fields are from Zolensky *et al.* (1993) and Weisberg and Huber (2007).

Figure 1.6:

Back-scattered electron images of the studied Tagish Lake samples: (a) TL5b; (b) TL11h; (c) TL11i; (d) TL11v-1 and (e) TL11v-2. The last two images are of two chips from TL11v.

Figure 1.7:

Back-scattered electron images of (a) chondrule from TL11h with extensively altered silicate grains replaced by sheet silicates. (b) A close up of (a) to show the morphology of the sheet silicates that are growing as distinctive arrays into the voids (black areas); ol = olivine; s = sulfides; (c) an altered chondrule from TL11h with a sulfide/magnetite rim and 'flower-like' morphology produced by sheet silicates, and (d) an altered chondrule from TL11h with a fine-grained, dense texture. (e) pseudomorphed chondrule from TL11i containing remnant olivine grains (centre) altered by sheet silicates and surrounded by magnetite/sugfide grains. (d) Ca-P aggregate [BSE map (left image), Ca (lower right) and P (upper right) elemental maps of the same BSE map] found in TL11h only. It has a cracked lithic fragment in the lower right corner of the aggregate.

Figure 1.8:

Back-scattered electron images of individual sulfide grains showing the variety of morphologies found in the Tagish Lake samples: (a-d) exsolved pentlandite (light grey, 'pe') in pyrrhotite (dark grey, 'py'); (e-f) 'bulls-eye' morphology exhibiting distinctive core and shell separated by a gap. Image (a) is from a pseudomorphed chondrule in TL11i (b) is from TL5b; images (c) and (e) are from TL11i; images (d) and (f) are from TL11h;

Figure 1.9:

(a) Interpreted XRD difractograms for powdered TL5b, TL11h, TL11i, and TL11v samples. Peaks are: sap, saponite; serp, serpentine; pe, pentlandite; M, magnetite; ol, olivine; sid, siderite; cal, calcite; dol, dolomite; pyr, pyrrhotite; pr, prism reflection of saponite. (b-left) Graphical representation of modal differences in samples calculated by Rietveld refinement method. Colours: grey – amorphous material; light pink –clinochlore; light blue – calcite; dark blue – dolomite; orange – enstatite; yellow – pyrrhotite; red – forsterite; turquoise – siderite; green – magnetite; (b-right) Graphical representation of modal differences in samples manually observed using EPMA. Colours: purple – lithic fragments; light pink –isolated silicates; dark blue – carbonates; green – magnetite; yellow – sulfides; turquoise – matrix; red – chondrules.

Figure 1.10:

Bright-field and HAADF TEM images showing the FIB sections of TL5b (a, b) and TL11h (c, d). The middle part of the TL11H FIB section (c,d) contains a pseudo core-shell structure in which the core (white arrow) is composed of ribbon-like sheet silicates and a sulfide shell (arrowheads) that is discontinuous around the core. A phosphate-rich grain (black arrow) occurs near to the bottom-right of the structure and is partially embayed by sheet silicates on its lower edge. Pt = platinum; Au = gold; H = hole; Ep = epoxy; S = sulfides; C = carbonates; P = phyllosilicates; Am = amorphous material

Figure 1.11:

Bright-field and HAADF TEM images showing the FIB sections from TL11i. The FIB 11i-1 (a, b) was extracted from the part of the matrix that appears dark and porous on the macroscopic scale in BSE images, which is interpreted as a typical Tagish Lake matrix. FIB 11i-2 (c, d) was extracted from a lithic fragment, which is a more compact object with relatively higher contrast in BSE images. The lower part of this FIB section contains a fractured nanoglobule (black arrow). Pt = platinum; Au = gold; Ep = epoxy; S = sulfides; Ol = olivine; Ng = nanoglobule; P = phyllosilicates

Figure 1.12:

Sheet silicates on this image, which is a part of 11i-1 FIB section, exhibit sinuous textures with regions of coarse- and fine-grained sheets silicates that are intermixed with amorphous material in some areas. HRTEM measurements of both fine- and coarse-grained regions reveal an inter- mixture of saponite (lattice-fringe spacings of ~ 0.11 nm) and chlorite-type phase (lattice-fringe spacings of 0.14 nm).

Figure 1.13:

TEM images of (a) the top section of 11i-2 FIB section composed entirely of sheet silicates with a ‘flower’-like texture; (b, c) close-up of the core consisting of sulfide/oxide grain and fine-grained sheet silicates with 0.7-nm basal spacing, consistent with serpentine structure; (d) close-up of ‘flower’-like texture from the top of the section showing radial bundles radiating from the core having 0.9 nm basal spacing, consistent with smectite/saponite structure; (e-f) Radial bundles of lizardite laths surrounded by

fine-grained serpentine from terrestrial specimen 18515 (Cressey 1979; see text for detailed discussion). Reprinted with permission from the Canadian Mineralogist.

Figure 1.14:

(a) HAADF spectral imaging of a carbonate grain from TL11h FIB section. (b) Si enrichment outside the grain (matrix). (c) Ca enrichment in the shell. (d) Mg enrichment in the shell. (e) Mn enrichment in the shell. (f) Fe enrichment in the core. (g) Ni and (h) S enrichment spots in the core consistent with sulfides.

Figure 1.15:

Phase diagrams of modeling the magnetite formation (see text for details). (a) Magnetite stability field on pH vs. Eh phase diagram at 0 °C and 1 bar. (b) Minimum pressure at which magnetite is stable at 0 °C. (c) Stability of magnetite at 100 °C and 1 bar. (d) Maximum temperature at which magnetite is stable at pressure of 10^{-6} bar. (e) Stability of magnetite at fixed Eh = -0.25, T = 0 °C and P = 0.001 bar and various CO_2. (f) Stability of magnetite at maximum Eh = -0.155. (g, h) Stability of magnetite with changing Fe^{2+} (g) and Ca^{2+} activity (h) at fixed $CO_2 = 10^{-4}$.

Figure 1.16:

Schematic representation of the model for the formation of the 'flower'-like textures of 11i-2 FIB section, found within the lithic fragment (see text for details). (a) Precursor loosely packed clusters of anhydrous semi-rounded silicate grains (a few microns in diameter) were subjected to alteration from the outside. (b) Clusters were subjected to Fe-bearing fluids, which percolated through the cracks/pore space between and around these semi-rounded grains. Serpentine formed in this space in a radial fashion. The radial arrays had more time to crystallize to form coarse-grain morphology. (c) The fluids then proceeded to alter the semi-rounded grains to produce fine-grained cores of the future 'flower'-like textures. Excess of Fe was precipitated as sulfides and/or magnetite. (d) Introduction of Al-bearing fluid percolated through the bundles, which produced a mixture of serpentine-saponite.

Colours: orange – serpentine precipitation from Fe-bearing fluids; grey - excess of precipitated Fe as sulfides and/or magnetites: green – saponite precipitation from Al-bearing fluid.

Figure 1.1

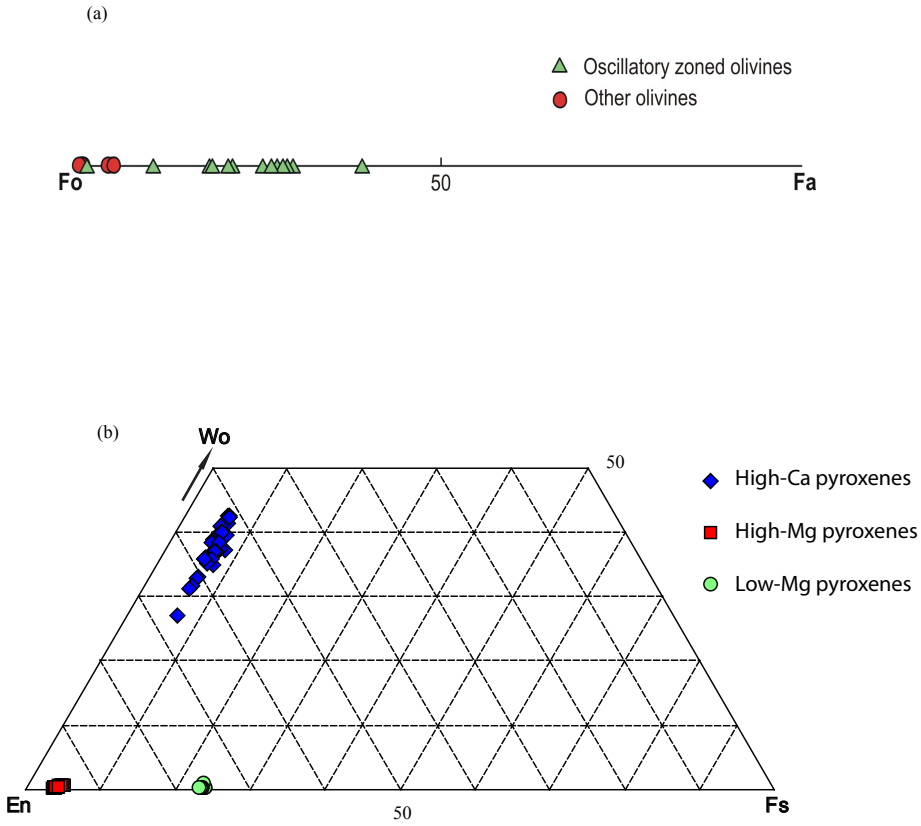
(a)
Oscillatory zoned olivines
Other olivines
Fo
50
Fa
(b)
Wo
50
High-Ca pyroxenes
High-Mg pyroxenes
Low-Mg pyroxenes
En
50
Fs

Figure 1.2

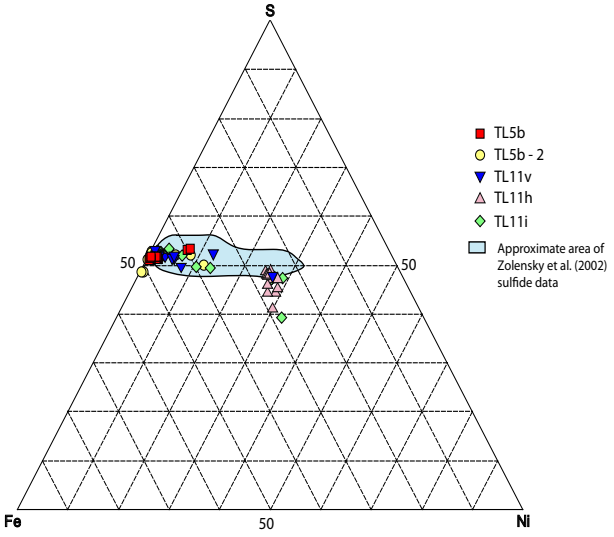
S
Fe
Ni
50
50
50
TL5b
TL5b - 2
TL11v
TL11h
TL11i
Approximate area of Zolensky et al. (2002) sulfide data

Figure 1.3

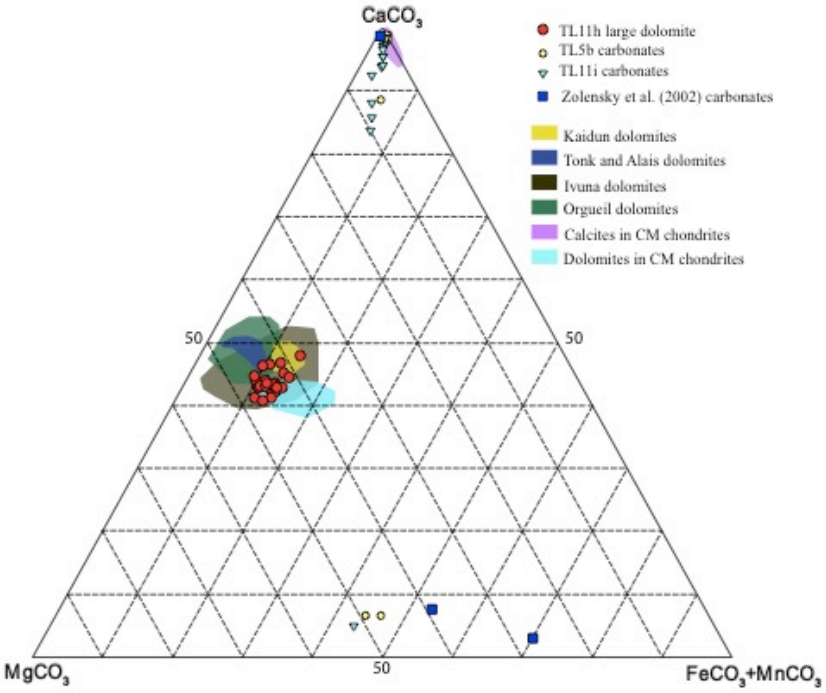
CaCO3
MgCO3
FeCO3+MnCO3
50
50
50
TL11h large dolomite
TL5b carbonates
TL11i carbonates
Zolensky et al. (2002) carbonates
Kaidun dolomites
Tonk and Alais dolomites
Ivuna dolomites
Orgueil dolomites
Calcites in CM chondrites
Dolomites in CM chondrites

Figure 1.4

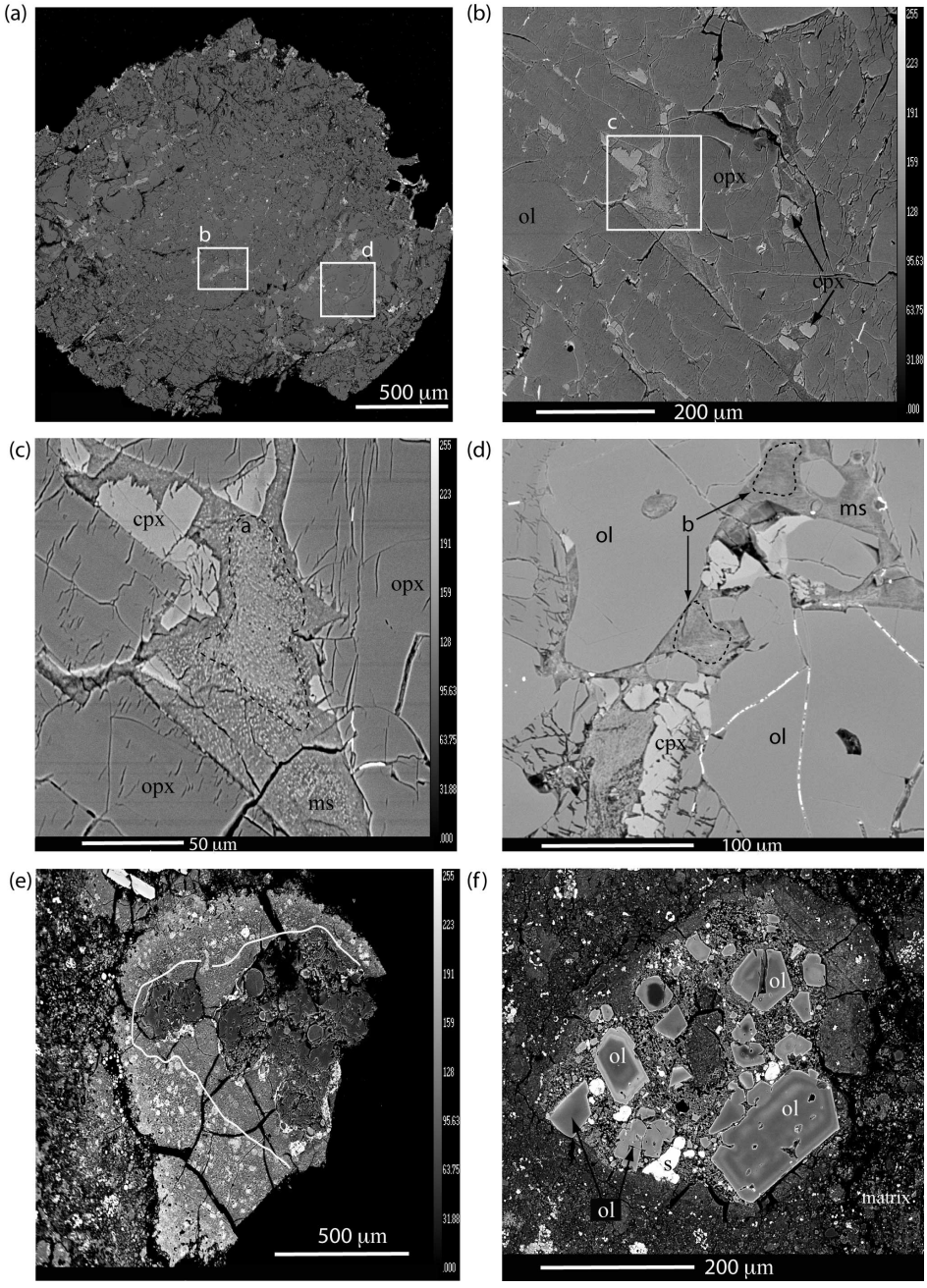
(a)
b
d
500 µm
(b)
c
opx
ol
cpx
200 µm
(c)
cpx
a
opx
opx
ms
50 µm
(d)
ol
b
ms
cpx
ol
100 µm
(e)
500 µm
(f)
ol
ol
ol
s
ol
matrix
200 µm

Figure 1.5

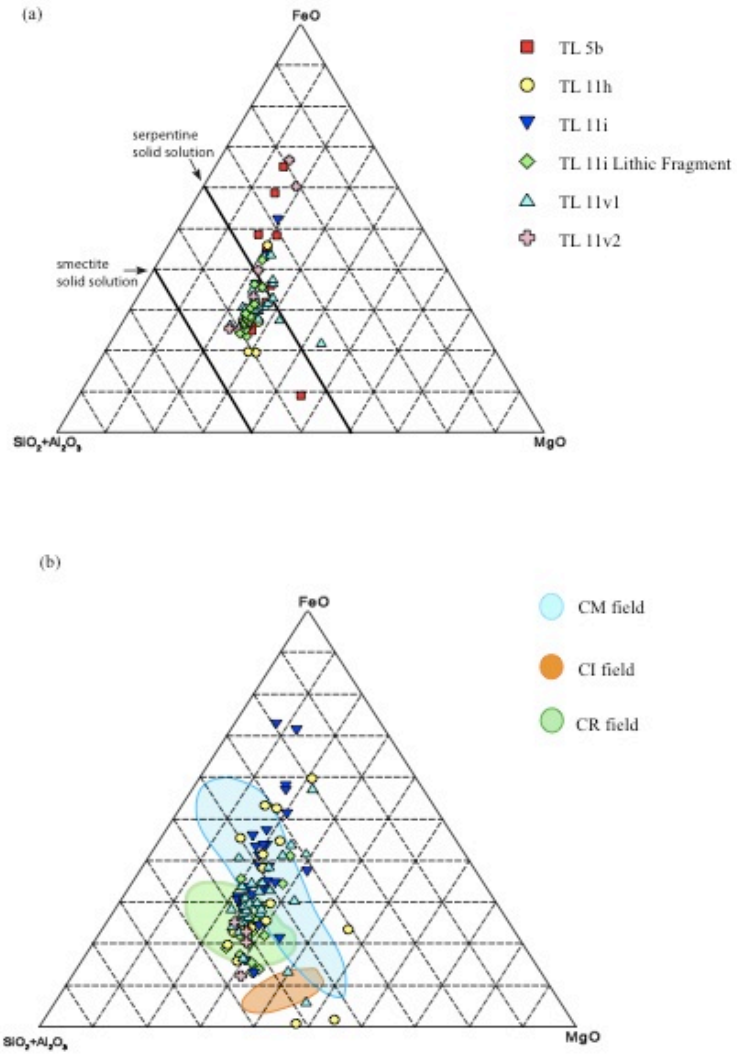
(a)
FeO
serpentine solid solution
smectite solid solution
SiO2+Al2O3
MgO
TL 5b
TL 11h
TL 11i
TL 11i Lithic Fragment
TL 11v1
TL 11v2
(b)
FeO
SiO2+Al2O3
MgO
CM field
CI field
CR field

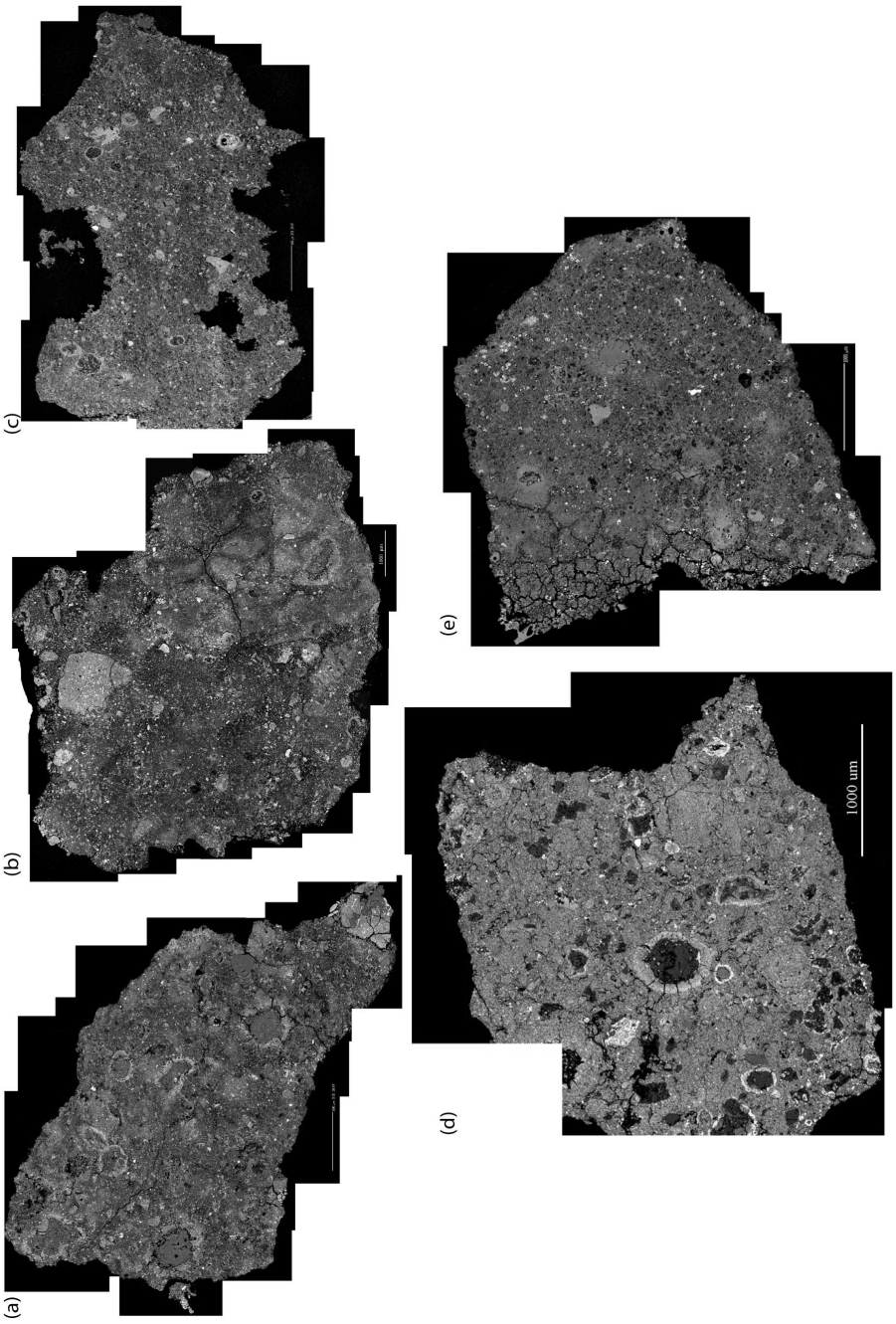

Figure 1.6

Figure 1.7

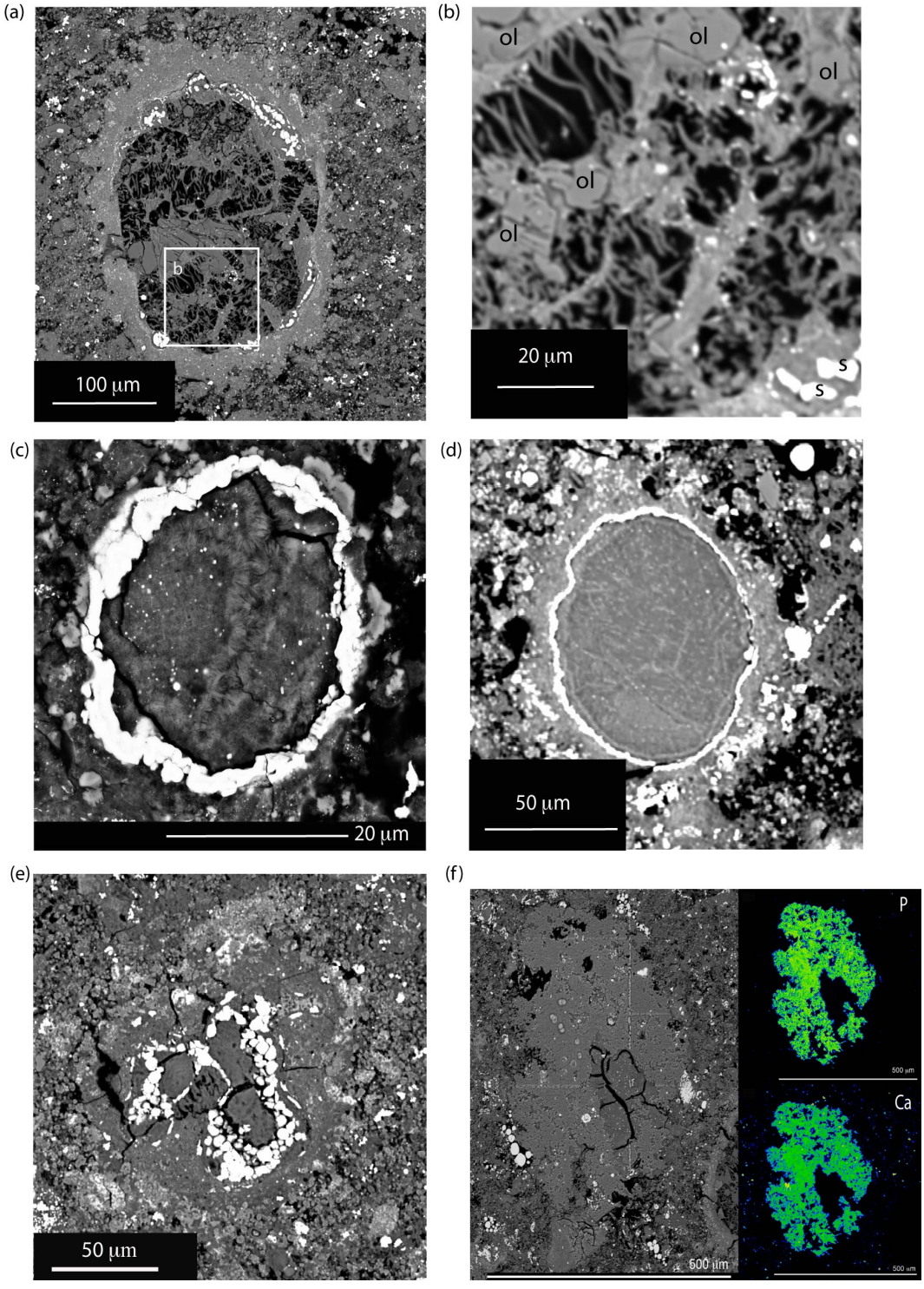

Figure 1.8

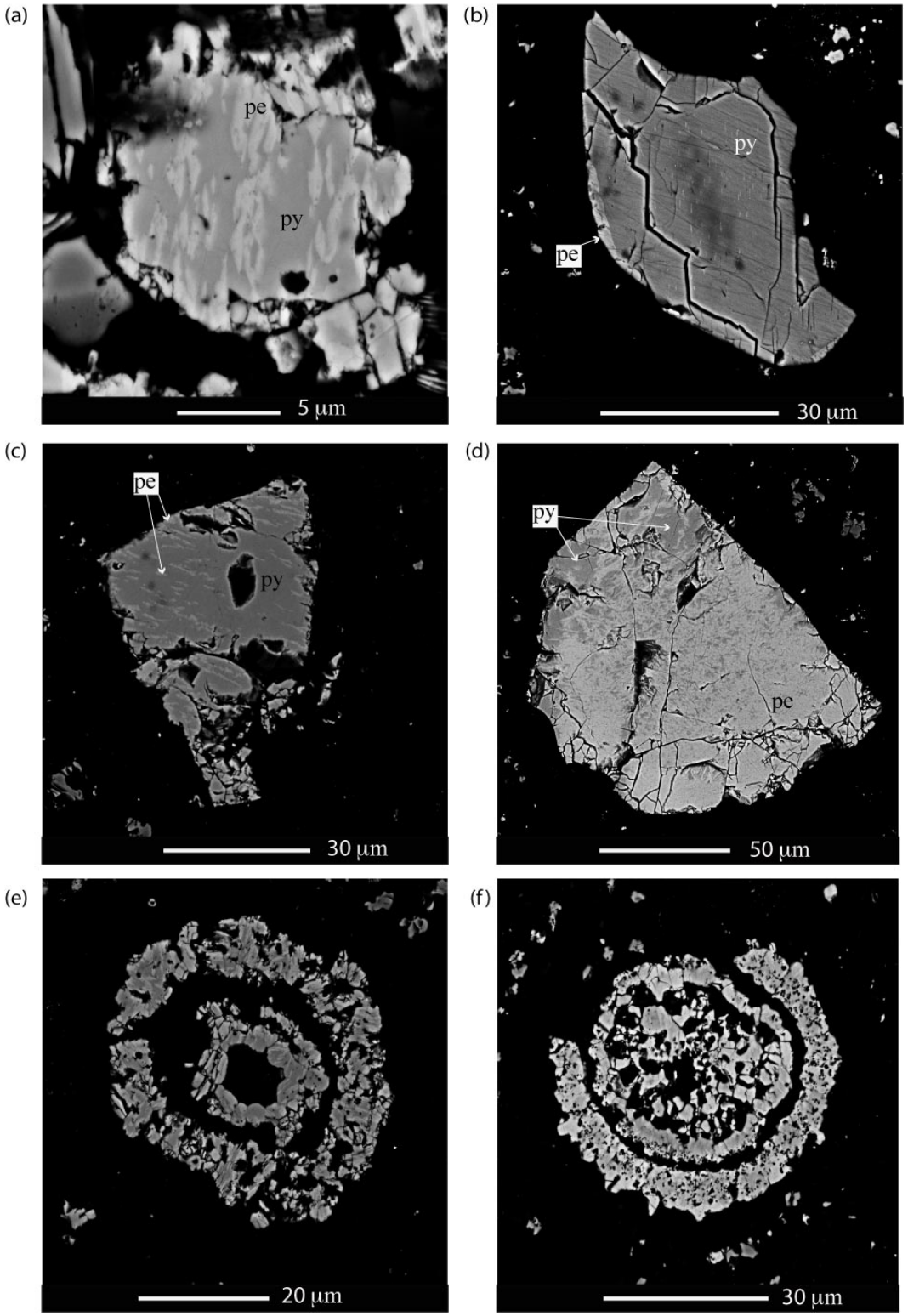

Figure 1.9

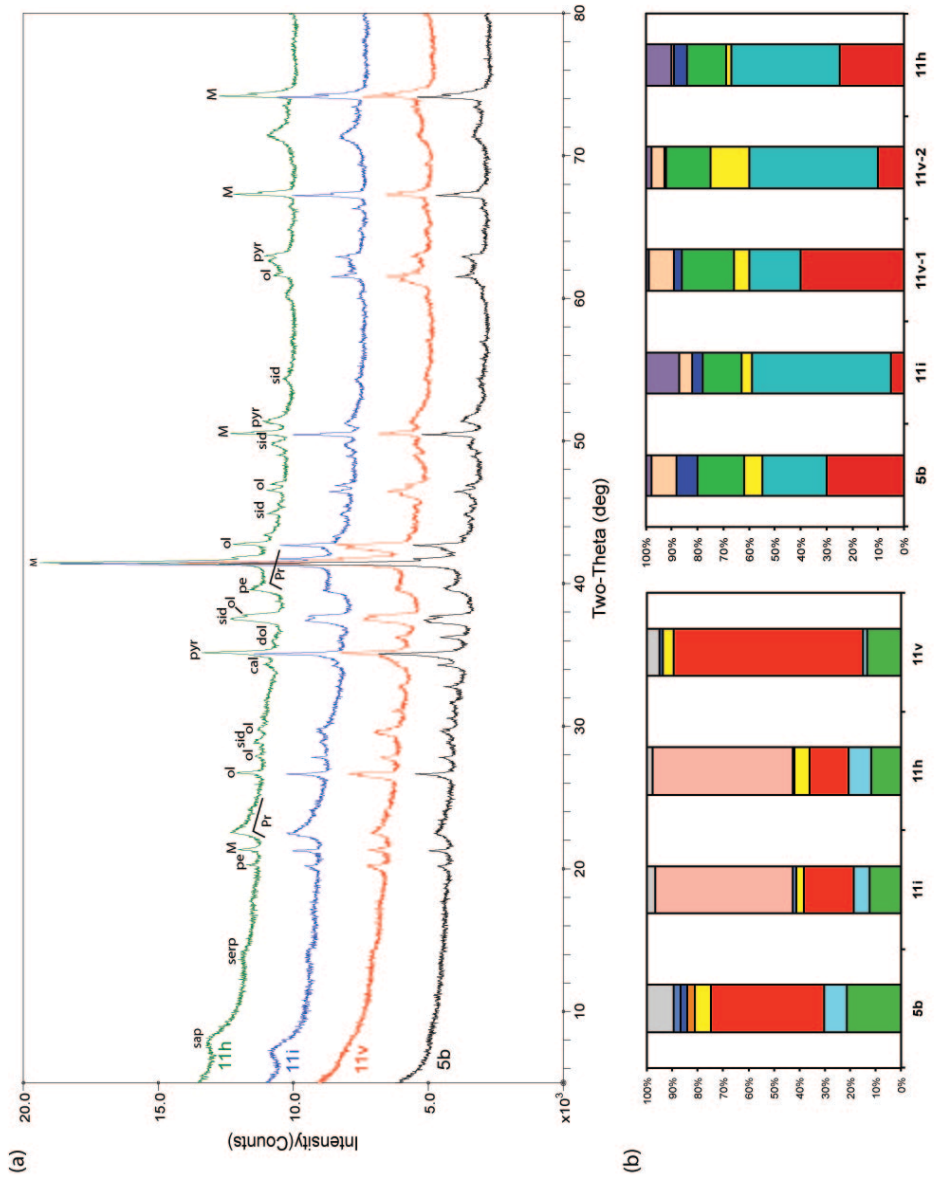
(a)
Intensity(Counts)
x10^3
Two-Theta (deg)
11h
11i
11v
5b
sap
serp
pe
M
Pr
ol
sid
cal
dol
pyr
(b)
5b
11i
11h
11v
11v-1
11v-2

Figure 1.10

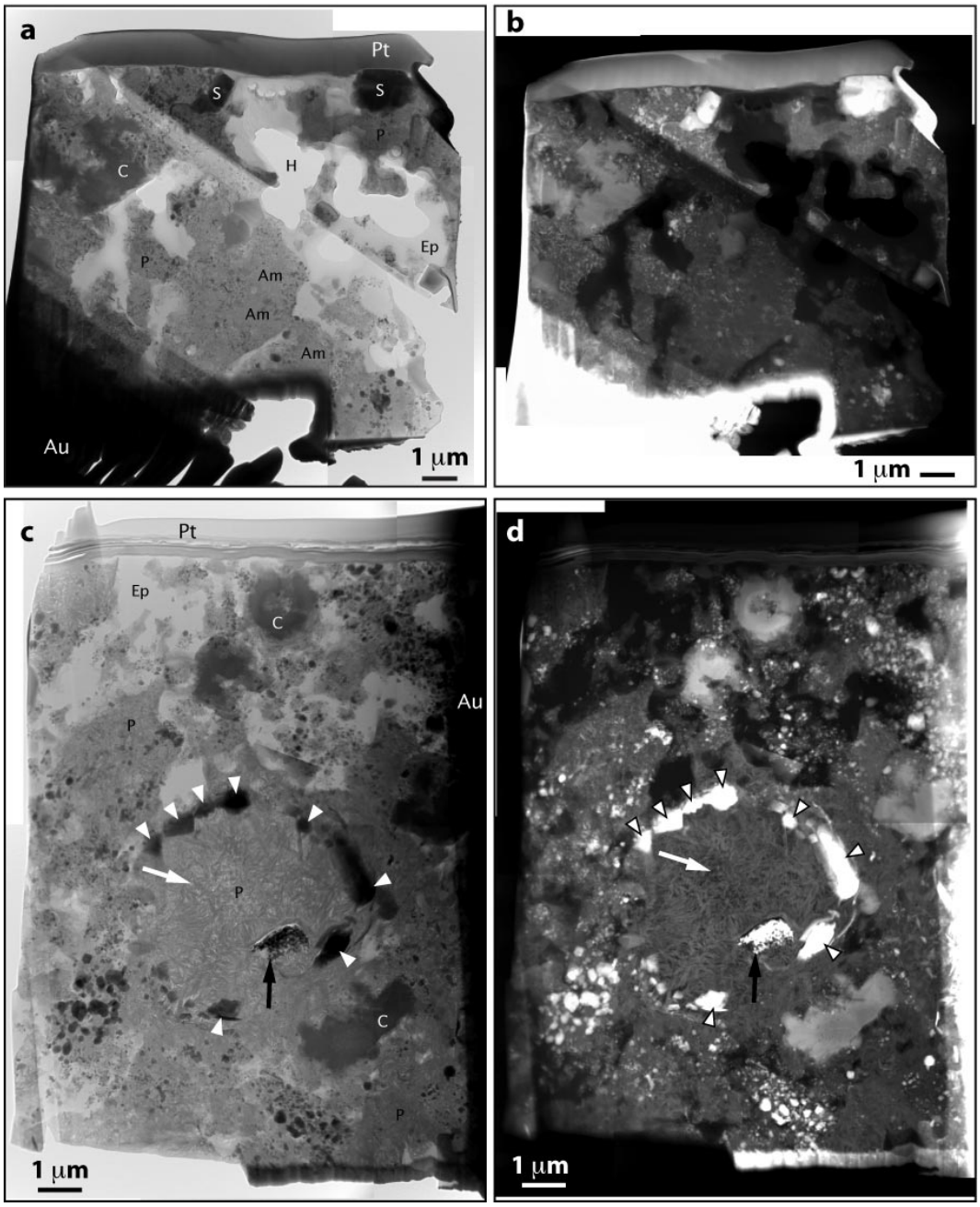

Figure 1.11

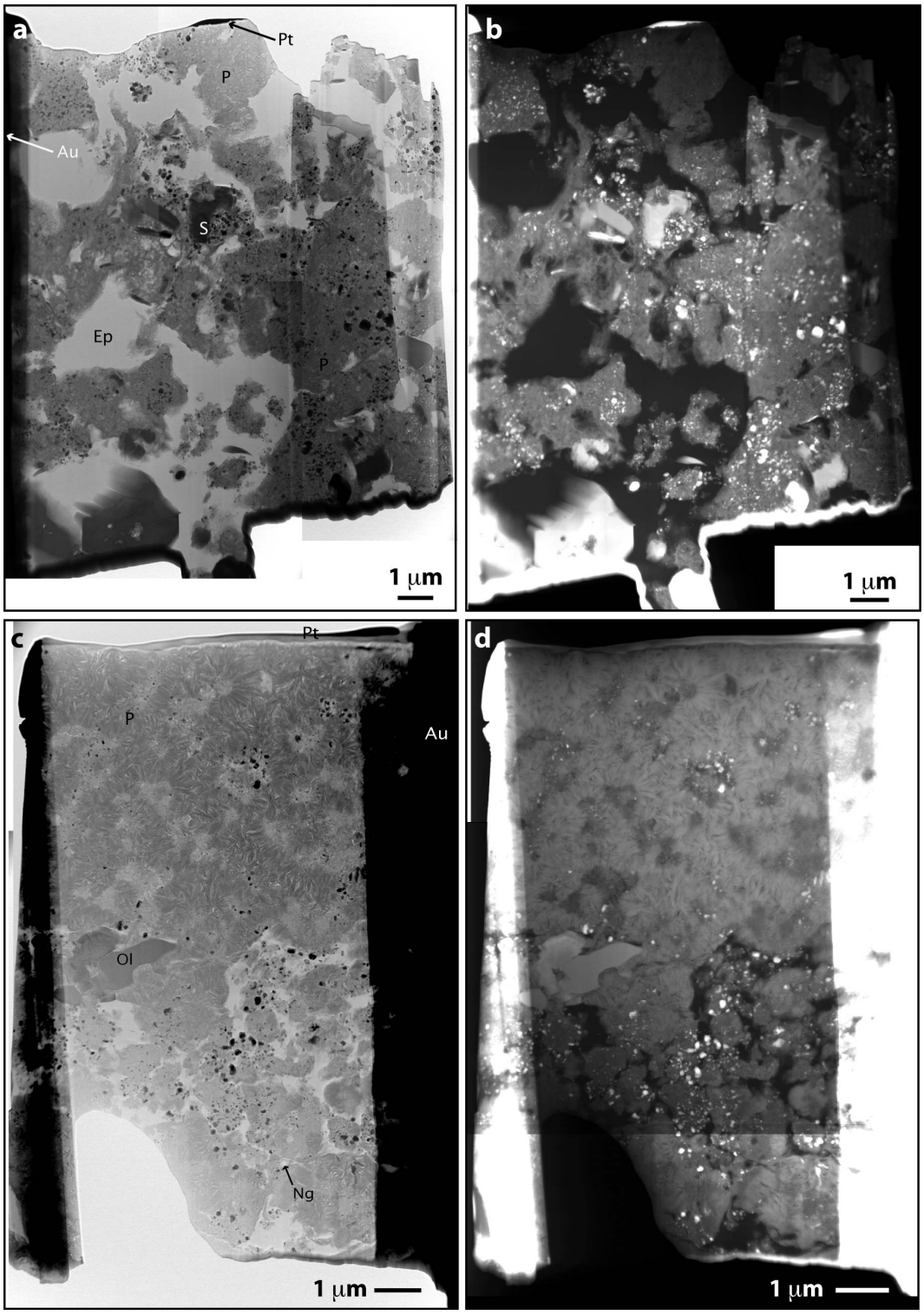

Figure 1.12

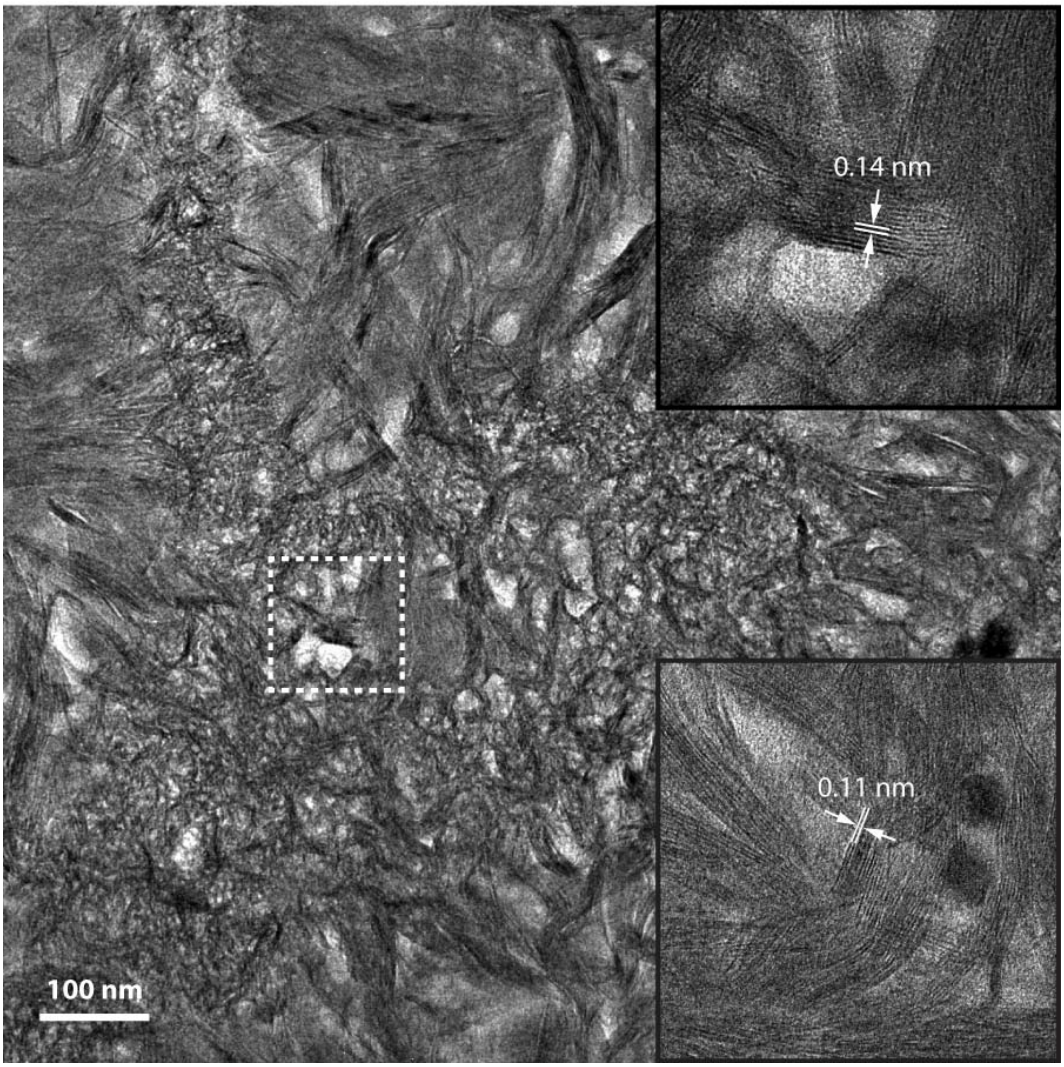

Figure 1.13

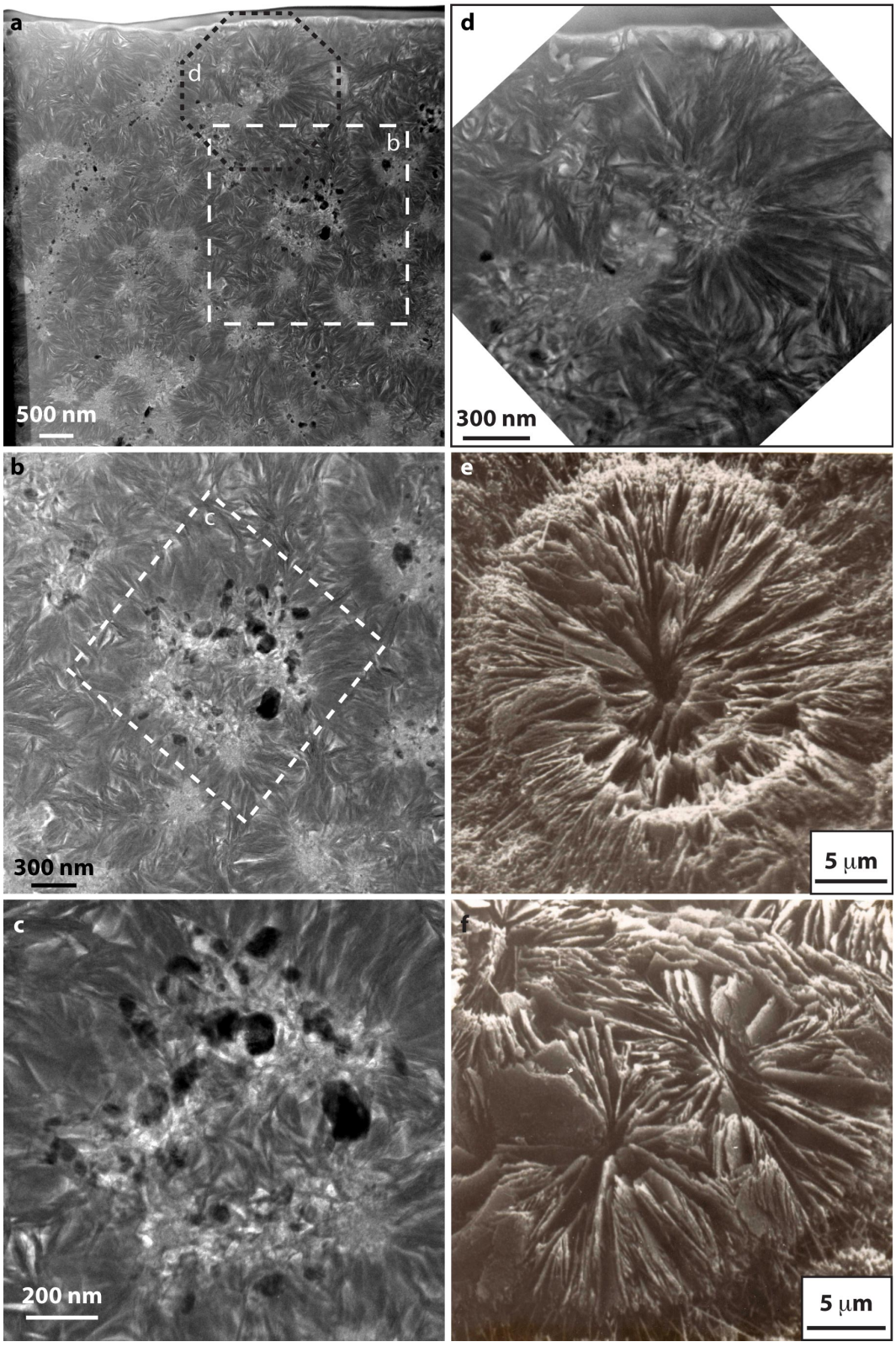

Figure 1.14

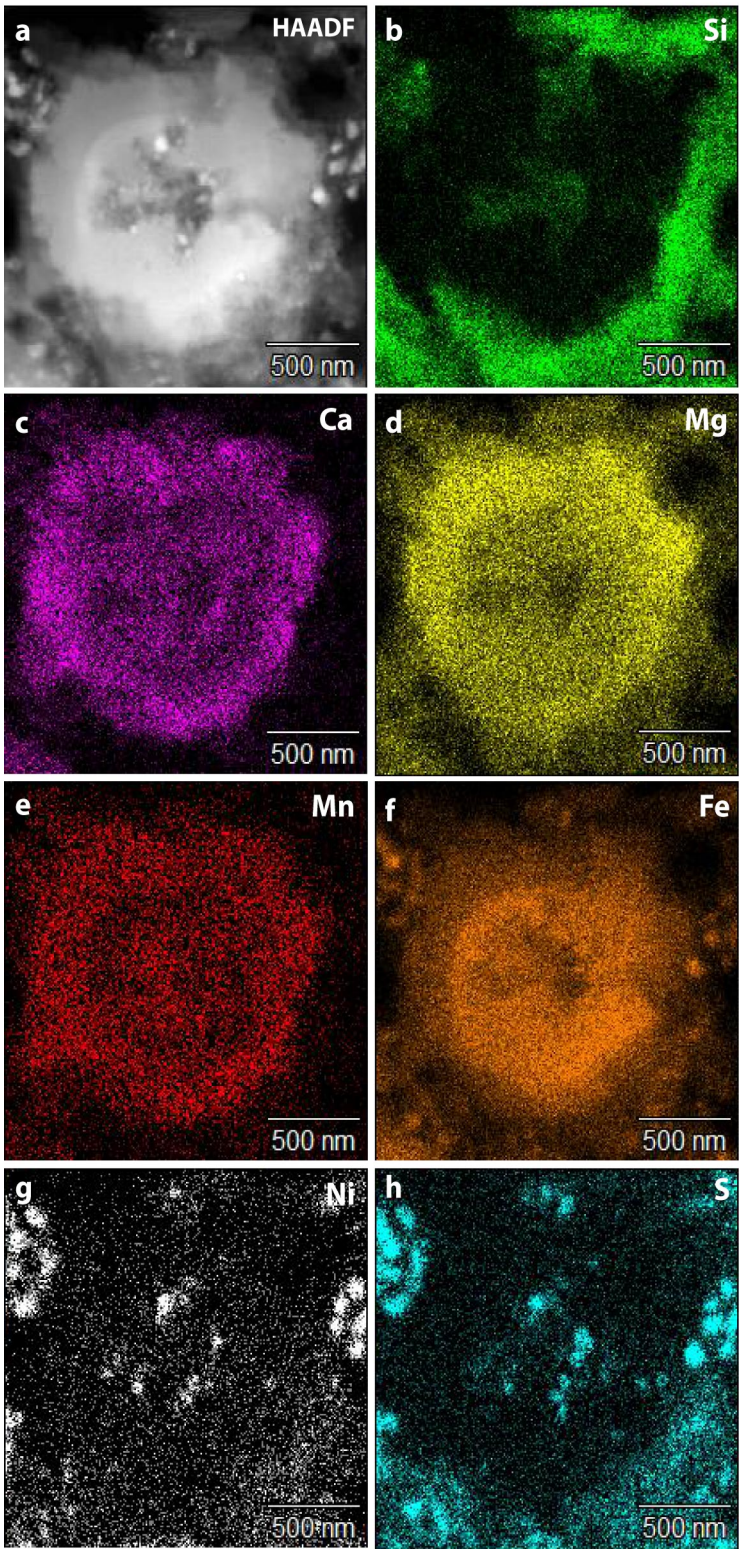
a
HAADF
500 nm
b
Si
500 nm
c
Ca
500 nm
d
Mg
500 nm
e
Mn
500 nm
f
Fe
500 nm
g
Ni
500 nm
h
S
500 nm

Figure 1.15

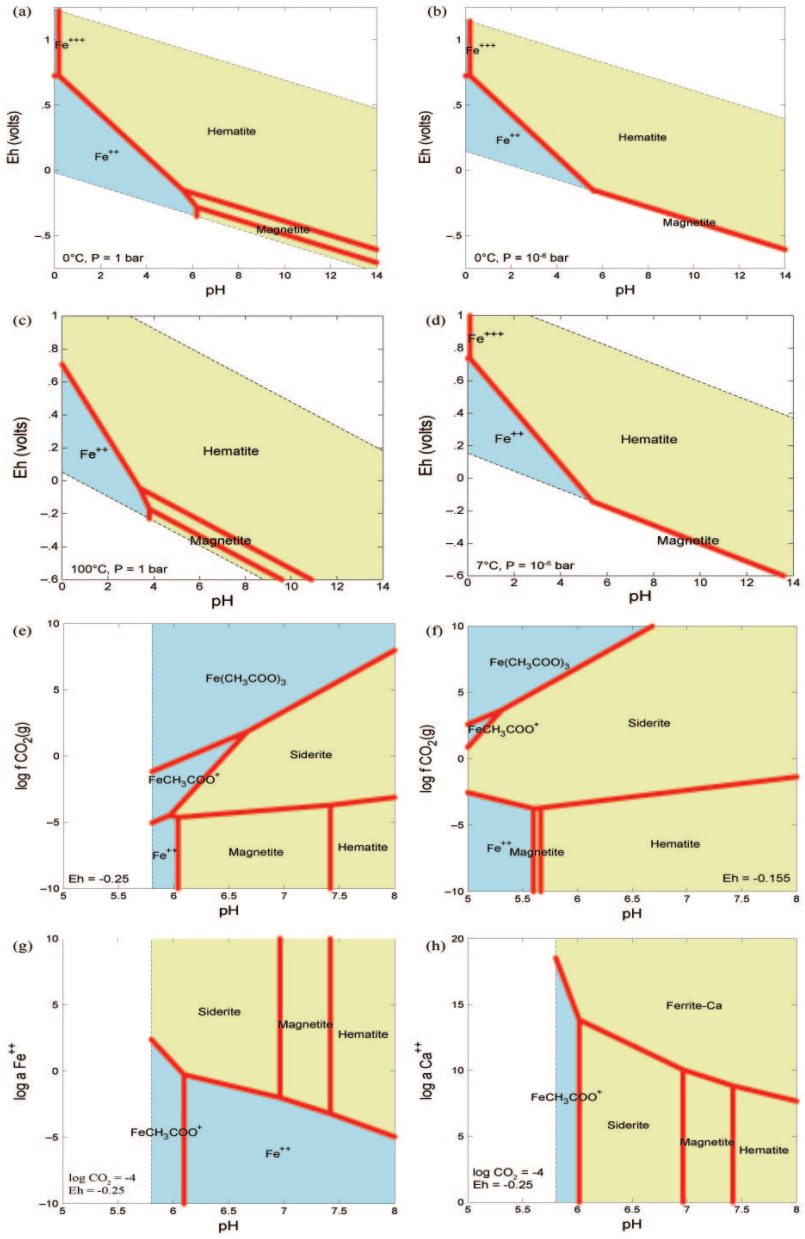
(a)
Fe+++
Hematite
Fe++
Magnetite
0°C, P = 1 bar
Eh (volts)
pH
(b)
Fe+++
Fe++
Hematite
Magnetite
0°C, P = 10-6 bar
Eh (volts)
pH
(c)
Fe++
Hematite
Magnetite
100°C, P = 1 bar
Eh (volts)
pH
(d)
Fe+++
Fe++
Hematite
Magnetite
7°C, P = 10-6 bar
Eh (volts)
pH
(e)
Fe(CH3COO)3
Siderite
FeCH3COO+
Fe++
Magnetite
Hematite
Eh = -0.25
log f CO2(g)
pH
(f)
Fe(CH3COO)3
FeCH3COO+
Siderite
Fe++
Magnetite
Hematite
Eh = -0.155
log f CO2(g)
pH
(g)
Siderite
Magnetite
Hematite
FeCH3COO+
Fe++
log CO2 = -4
Eh = -0.25
log a Fe++
pH
(h)
Ferrite-Ca
FeCH3COO+
Siderite
Magnetite
Hematite
log CO2 = -4
Eh = -0.25
log a Ca++
pH

Figure 1.16

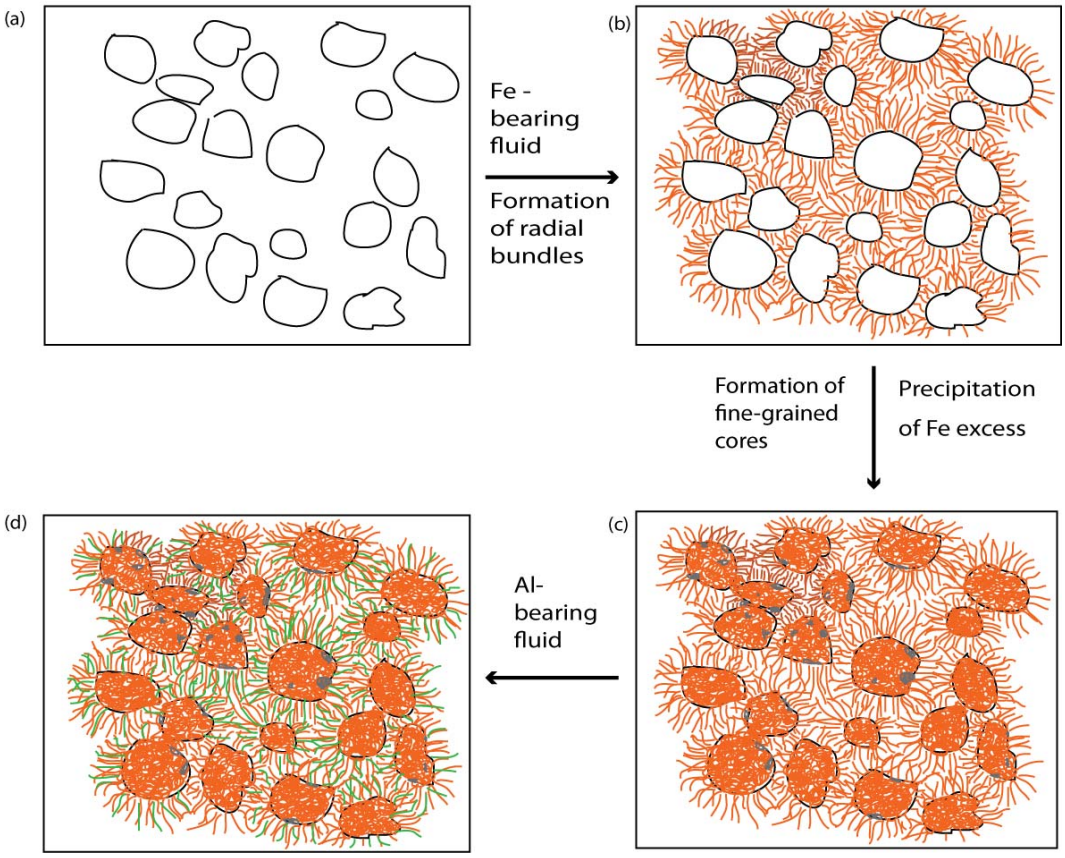
(a)
Fe - bearing fluid
Formation of radial bundles
(b)
Formation of fine-grained cores
Precipitation of Fe excess
(c)
Al- bearing fluid
(d)

Table 1.1: Average mineral composition in all studied Tagish Lake samples.

	OLIVINE		PYROXENE (CHOND)				PYROXENE (MATRIX)		CHROMITE		MAGNETITE		PHOSPHATE		CARBONATE				SULFIDES								MESOSTASIS AND OTHER PHASES							
	Average	stdev	Average	stdev	Average	stdev	Average	stdev	Average	stdev	Average	stdev	11h	11i	Average	stdev	11h ^	stdev		Average	stdev	Average	stdev	Average	stdev			1#	stdev	B&J	2#	stdev	3*	stdev
N	*20*		*34*		*40*		*11*		*10*		*45*		*23*	*20*	*30*		*23*			*23*		*18*		*10*				*14*			*15*		*4*	
Wt% oxides																				**troilite**		**pentlandlite**		**pyrrhotite**										
SiO_2	42.01	0.45	49.07	1.00	59.25	0.85	38.23	0.36	0.49	0.07	0.11	0.14	0.19	0.09	1.26	1.52	0.03	0.01	**S**	38.23	0.61	32.73	1.50	36.85	1.91		**SiO_2**	53.04	1.52	58.70	21.42	4.36	34.79	0.35
TiO_2	0.02	0.02	0.87	0.16	0.05	0.02	0.01	0.01	0.41	0.02	0.00	0.01	0.00	0.00	0.00	0.00	0.01	0.01	**Fe**	59.08	1.07	31.02	1.19	50.56	4.26		**TiO_2**	0.62	0.12	0.63	0.32	0.10	0.42	0.06
Al_2O_3	0.12	0.05	8.07	1.22	0.30	0.17	0.15	0.18	28.52	3.93	0.08	0.10	0.05	0.01	0.10	0.11	0.03	0.01	**Ni**	2.60	0.77	33.67	1.18	10.64	3.54		**Al_2O_3**	23.22	0.95	13.60	17.24	2.12	1.74	0.16
Fe_2O_3	0.00	0.00	0.00	0.47	0.00	0.09	21.94	0.29	0.69	0.75	68.09	0.76	0.00	0.00	0.00	0.00	0.00	0.00	**Co**	0.18	0.12	0.90	0.00	0.45	0.13		**FeO**	2.83	0.52	8.84	10.37	1.35	0.14	0.06
FeO	2.41	1.90	2.58	0.49	2.45	0.27	0.00	0.00	7.76	0.70	31.01	0.30	1.37	0.11	1.66	1.00	7.80	0.75	**Cu**	0.00	0.00	0.03	0.05	0.01	0.22		**MnO**	0.71	0.18	0.00	0.22	0.13	25.34	0.48
MnO	0.11	0.09	1.14	0.18	0.24	0.09	0.19	0.01	1.82	0.04	0.01	0.02	0.17	0.02	0.03	0.04	1.81	0.84	**Zn**	0.00	0.02	0.00	0.00	0.01	0.01		**MgO**	4.97	1.22	0.70	25.22	2.41	2.19	0.96
MgO	54.50	1.43	18.38	1.62	37.07	0.71	40.23	0.35	18.18	0.66	0.03	0.10	12.25	23.21	0.87	1.10	19.54	1.30	**As**	0.06	0.03	0.03	0.04	0.03	0.03		**CaO**	11.35	0.41	8.60	0.71	1.24	29.52	0.48
CaO	0.13	0.02	16.97	1.27	0.26	0.06	0.24	0.14	0.08	0.04	0.04	0.03	30.77	0.01	54.22	4.92	26.84	1.17	**Rh**	0.00	0.01	0.00	0.01	0.00	0.01		**Na_2O**	2.87	0.21	7.69	0.19	0.35	0.09	0.02
Na_2O	0.01	0.01	0.11	0.03	0.00	0.01	0.01	0.02	0.00	0.01	0.01	0.05	0.48	0.22	0.10	0.06	0.15	0.08	**Pd**	0.00	0.01	0.01	0.01	0.01	0.01		**K_2O**	0.10	0.02	0.37	0.10	0.06	0.00	0.00
K_2O	0.00	0.00	0.00	0.01	0.00	0.01	0.00	0.01	0.01	0.01	0.01	0.02	0.00	0.03	0.01	0.01	0.00	0.01	**Ag**	0.01	0.01	0.01	0.02	0.01	0.01		**P_2O_5**	0.04	0.02	-	0.57	0.15	0.14	0.07
P_2O_5	0.01	0.02	0.02	0.01	0.00	0.01	0.04	0.02	0.01	0.01	0.00	0.01	39.77	45.92	0.11	0.04	0.25	0.13	**Cd**	0.02	0.04	0.00	0.00	0.01	0.02		**Cr_2O_3**	0.23	0.05	-	0.40	0.16	0.42	0.06
Cr_2O_3	0.38	0.22	2.87	0.25	0.70	0.11	0.33	0.01	42.58	3.47	0.05	0.03	0.00	0.01	0.01	0.03	0.00	0.00	**Sn**	0.00	0.00	0.00	0.01	0.00	0.00		**NiO**	0.01	0.01	-	na	na	0.00	0.00
NiO	0.02	0.03	0.00	0.01	0.00	0.01	0.06	0.01	0.01	0.01	0.00	0.00	0.03	0.01	0.00	0.00	0.01	0.01	**Sb**	0.00	0.00	0.01	0.02	0.00	0.00									
BaO	-	-	-	-	-	-	-	-	-	-	-	-	0.00	0.00	0.03	0.03	0.00	0.00	**Pt**	0.00	0.02	0.01	0.02	0.01	0.01											
SO_3	0.01	0.03	-	-	-	-	-	-	-	-	-	-	-	-	-	-	-	-	**Au**	0.02	0.09	0.00	0.00	0.01	0.03											
Total	99.72		100.1		100.3		101.4		100.6		99.48		85.08	69.78	58.40		56.48		**Bi**	0.00	0.00	0.01	0.04	0.07	0.21											
																			Mg	0.00	0.00	0.00	0.00	0.00	0.02											
Anions	*Based on 4O*		*Based on 6O*						*Based on 4O*		*Based on 32O*		*Based on 26O*		*Based on 2 positive charges*[$]				**Al**	0.02	0.01	0.00	0.00	0.02	0.01											
SiO_2	2.00		3.55		4.00		2.94		0.03		0.09		0.07	0.04	**C**	1.00	0.00	1.00	0.00	**Si**	0.04	0.02	0.04	0.02	0.12	0.17											
SO_3	0.00		0.00		0.00		0.00		0.00		0.00		0.00	0.00	**P**	0.00	0.00	0.003	0.002	**Ti**	0.00	0.00	0.00	0.00	0.00	0.01											
Na_2O	0.00		0.00		0.00		0.00		0.00		0.00		0.17	0.10					**Cr**	0.05	0.02	0.02	0.02	0.05	0.04											
P_2O_5	0.00		0.00		0.00		0.00		0.00		0.00		6.25	9.27																			
FeO (t)	0.05		0.08		0.07		0.71		0.20		31.74		0.42	0.05	**Si**	0.02	0.02	0.00	0.00	**Total**	100.0		97.65		98.48			99.99		99.07	76.75		94.78	
Cr_2O_3	0.01		0.12		0.03		0.02		1.46		0.02		0.00	0.00	**Ti**	0.00	0.00	0.00	0.00																	
MgO	1.93		0.99		1.87		2.31		0.78		0.02		6.78	16.51	**Al**	0.00	0.00	0.00	0.00																	
K_2O	0.00		0.00		0.00		0.00		0.00		0.00		0.00	0.01	**Cr**	0.00	0.00	0.00	0.00																	
Al_2O_3	0.00		0.52		0.02		0.01		1.46		0.05		0.01	0.00	**Fe**	0.06	0.12	0.10	0.01																	
MnO	0.00		0.04		0.01		0.01		0.04		0.01		0.05	0.01	**Mn**	0.00	0.01	0.02	0.01																	
TiO_2	0.00		0.05		0.00		0.00		0.02		0.00		0.00	0.00	**Mg**	0.08	0.15	0.44	0.02																	
CaO	0.00		0.66		0.01		0.01		0.00		0.02		12.24	0.01	**Ni**	0.00	0.00	0.00	0.00																	
NiO	0.00		0.00		0.00		0.00		0.00		0.00		0.01	0.00	**Ca**	0.81	0.28	0.43	0.02																	
BaO	0.00		0.00		0.00		0.00		0.00		0.00		0.00	0.00	**Ba**	0.00	0.00	0.00	0.00																	
															Na	0.01	0.01	0.00	0.00																	
Cations															**K**	0.00	0.00	0.00	0.00																	
Si	1.00		1.77		2.01		1.47		0.01		0.03		0.03	0.02																			
S	0.00		0.00		0.00		0.00		0.00		0.00		0.34	0.21																			
Na	0.00		0.01		0.00		0.00		0.00		0.01		2.50	3.71																			
P	0.00		0.00		0.00		0.00		0.00		0.00		0.42	0.05																			
Fe^{3+}	0.00		0.00		0.01		0.71		0.02		15.85		0.00	0.00																			
Fe^{2+}	0.05		0.08		0.06		0.00		0.19		8.02		0.00	0.00																			
Cr	0.01		0.08		0.02		0.01		0.97		0.01		6.78	16.51																			
Mg	1.93		0.99		1.87		2.31		0.78		0.02		0.00	0.02																			
K	0.00		0.00		0.00		0.00		0.00		0.00		0.01	0.00																			
Al	0.00		0.34		0.01		0.01		0.97		0.03		0.05	0.01																			
Mn	0.00		0.04		0.01		0.01		0.04		0.00		0.00	0.00																			
Ti	0.00		0.02		0.00		0.00		0.01		0.00		12.24	0.01																			
Ca	0.00		0.66		0.01		0.01		0.00		0.01		0.01	0.00																			
Ni	0.00		0.00		0.00		0.00		0.00		0.00		0.00	0.00																			
Ba	0.00		0.00		0.00		0.00		0.00		0.00		0.00	0.00																			
Fo	97.46																																
Fa	2.54																																
En			56.3		95.6		76.2																										
Fs			6.4		3.89		23.5																										
Wo			37.3		0.48		0.32																										
Chr									0.49	0.05	0.00	0.00																					
Mg									0.01	0.01	1.00	0.00																					
Sp									0.49	0.05	0.00	0.00																					
Usp									0.02	0.00	0.00	0.00																					
Fe^{3+}/Fe^{2+}											1.98	0.03																					

^ large 11h carbonate enriched in Mn

1# average analyses of 5b chondule mesostasis in area "a" on Fig. 4c

2# average analyses of 5b chondrule mesostasis in area "b" on Fig. 4d

3* average analyses of Mn-Ca silicate in 11v

$ Following Brandelik (2009) CALCMIN calculations

B&J Brearley and Jones (1998) - comparative glass analyses for Y-790123 (CM2)

Table 1.2: Average matrix composition.

Sample	N	SiO_2	Al_2O_3	Cr_2O_3	FeO	MnO	MgO	CaO	Na_2O	K_2O	NiO	TiO_2	V_2O_3	Cl	S	Total
(1)		34.02	11.97	0.33	16.61	0.38	22.96	0.65	0.18	0.05	0.05	0.10	na	na	0.06	87.43
(2)		42.33	1.07	0.71	10.72	0.15	32.18	0.09	0.05	0.02	0.05	0.08	na	na	0.06	87.57
(3)		30.62	13.66	0.31	27.14	0.35	15.73	0.60	0.39	0.06	0.05	0.09	na	na	0.06	89.06
(4)		39.35	3.56	0.56	14.34	0.20	28.26	0.14	0.13	0.05	0.15	0.09	na	na	0.05	86.96
(5)		26.42	19.24	0.08	20.47	0.23	16.97	0.10	0.26	0.11	0.03	0.09	na	na	0.11	85.45
G*		22.40	1.90	0.32	16.30	0.20	15.20	0.97	0.22	0.06	1.50	na	na	na	3.90	63.00
10 µm (defocused) beam																
TL5b	13	24.77	3.01	0.37	28.50	0.23	17.78	0.91	0.34	0.16	1.82	0.11	0.01	0.29	5.74	84.01
stdev		6.36	0.81	0.15	12.79	0.11	6.91	0.94	0.13	0.06	1.50	0.04	0.01	0.08	2.23	3.98
TL11i LF[#]	18	32.18	2.44	0.60	22.11	0.19	18.73	0.51	0.50	0.18	2.15	0.22	0.01	0.06	6.76	86.62
stdev		2.09	0.18	0.17	4.16	0.06	1.26	0.16	0.05	0.03	0.73	0.04	0.01	0.01	2.09	1.89
TL11i	5	27.44	2.05	0.32	28.27	0.10	16.75	0.26	0.47	0.15	1.19	0.09	0.01	0.23	5.60	82.90
stdev		4.93	0.33	0.06	8.63	0.02	1.55	0.13	0.10	0.07	0.71	0.03	0.01	0.06	2.80	2.61
TL11v-1	32	29.28	2.30	0.38	23.23	0.26	19.02	1.37	0.73	0.05	1.66	0.12	0.01	0.06	6.22	84.69
stdev		2.55	0.42	0.07	3.62	0.07	3.73	1.59	0.15	0.01	0.39	0.05	0.01	0.04	1.63	3.08
TL11v-2	6	24.54	1.84	0.42	29.69	0.12	14.85	0.34	0.83	0.11	1.28	0.12	0.01	0.26	5.93	80.32
stdev		9.30	0.63	0.25	12.65	0.05	2.73	0.12	0.13	0.04	0.47	0.03	0.01	0.05	2.24	4.40
TL11h	4	31.15	2.48	0.38	20.78	0.11	20.48	0.44	0.52	0.10	0.91	0.14	0.01	0.35	3.85	81.67
stdev		6.11	0.51	0.07	8.79	0.07	3.88	0.17	0.14	0.03	0.42	0.06	0.00	0.10	2.45	1.86
2 µm (focused) beam																
TL11i LF[#]	28	34.92	2.65	0.49	18.13	0.15	21.16	0.44	0.40	0.18	1.26	0.20	0.01	0.05	5.07	85.07
stdev		3.96	0.41	0.24	5.13	0.07	3.21	0.22	0.13	0.04	0.71	0.05	0.01	0.01	2.69	2.52
TL11i	31	26.37	1.99	0.32	27.48	0.12	16.34	0.48	0.39	0.17	1.38	0.13	0.01	0.19	7.61	82.96
stdev		6.16	0.45	0.10	12.55	0.07	3.98	0.55	0.16	0.10	1.03	0.06	0.01	0.10	4.65	3.16
TL11h	19	30.16	2.15	0.44	23.03	0.17	21.44	0.33	0.44	0.08	0.94	0.10	0.01	0.25	4.31	83.81
stdev		7.55	0.80	0.40	12.94	0.19	9.57	0.22	0.21	0.05	0.84	0.07	0.01	0.08	3.44	3.08
TL11v-1	31	30.38	2.69	0.43	23.03	0.30	19.56	0.83	0.72	0.06	1.69	0.12	0.01	0.06	6.13	86.00
stdev		5.77	2.01	0.23	6.62	0.15	4.90	1.04	0.20	0.02	0.61	0.03	0.01	0.03	1.89	3.65
TL11v-2	4	35.55	2.65	0.65	14.47	0.06	20.38	0.28	0.64	0.11	1.05	0.10	0.02	0.22	3.77	79.93
stdev		5.26	0.38	0.25	3.04	0.03	4.21	0.07	0.22	0.00	0.61	0.02	0.01	0.11	2.48	3.91

(1)-(5) analyses from Zolensky et al. (2002), Table 3
G* - average matrix data from Greshake et al. (2005)
na - not available
LF - Lithic Fragment from sample TL 11i
TL11v-1 and TL11v-2 are two chips of the disagregated TL11v sample (See text for discussion)

Table 1.3: Bulk rock mineralogy of Tagish Lake samples: comparison by EPMA, XRD and literature data.

	Density (g/cm^3)*	XRD									EPMA						(a)		(b)					
		5b		5b		11i		11h		11v			5b	11i	11h	11v-1	11v-2			HG-42		HG-11		MM-38	
		wt% [1]	vol% [2]	wt% [1]	vol% [2]	wt% [1]	vol% [2]	wt% [1]	vol% [2]				vol% [3]	vol% [3]	vol% [3]	vol% [3]	vol% [3]		wt%	vol%	wt%	vol%	wt%	vol%	wt%	vol%
Forsterite	3.28	39	44	19	20	15	15	68	74	***Chondrules***	30	5	25	40	10	***Olivine (Fo_{100})***	8	7	4	3	9	7	8	7
Magnetite	5.18	30	21	19	12	18	12	19	13	***Magnetites***	18	15	15	20	17	***Magnetite***	8	5	13	7	9	5	12	6
Pyrrhotite	4.60	8	6	4	3	8	6	6	4	***Sulfides***	7	4	2	6	15	***Pyrrhotite***	9	5	10	6	16	11	10	6
Enstatite	3.20	3	3	n/d	n/d	n/d	n/d	n/d	n/d	***Isolated silicates***	10	5	1	10	5	***Pentlandite Fe-Mg***	1	0	≤ 3	≤ 3	≤ 3	≤ 3	≤ 3	≤ 3
Dolomite	2.84	2	3	n/d	n/d	n/d	n/d	1	1	***Carbonates***	8	4	5	3	1	***carbonate***	14	12	13	7	4	3	5	3
Siderite	3.96	10	9	7	6	10	9	2	2	***Lithic fragments***	2	13	10	1	2	***Calcite***			≤ 3	≤ 3	5	6	≤ 3	≤ 3
Calcite	2.71	2	2	1	1	0	1	n/d	n/d	***Matrix***	25	54	42	20	50	***Saponite-serpetine***	60	71	57	69	55	68	55	68
Clinochlore (the best fitted)	3.00	n/d	n/d	48	54	48	55	n/d	n/d							***Gypsum***			8	9	≤ 3	≤ 3	10	11
Amorphous ^	2.65	8	11	3	3	2	2	4	5							***Talc***			≤ 3	≤ 3	n/d	n/d	n/d	n/d
Total		100	100	100	100	100	100	100	100								100	100	105	101	98	100	100	101

* Source: www.mindat.org

^ Amorphous density = silica density

[1] Determined wt% of each phase by Rietveld refinment method (XRD)

[2] Calculated volume percent based on wt% from XRD

[3] Estimated volume percent by EPMA observations

Sources (a) Bland et al. (2004); (b) Izawa et al. (2010) selected samples

n/d not detected or determined by the method

CHAPTER 2:

TESTING VARIATIONS WITHIN THE TAGISH LAKE METEORITE – II: WHOLE-ROCK GEOCHEMISTRY OF PRISTINE SAMPLES[1]

Alexandra I. Blinova[1*], Christopher D. K. Herd[1], and M. John M. Duke[2].

[1]Dept. of Earth and Atmospheric Sciences, 1-23 Earth Sciences Building, University of Alberta, Edmonton, Alberta, T6G 2E3, Canada.
[2]SLOWPOKE Nuclear Reactor Facility, $^{c}/_{o}$ 1-20 University Hall, University of Alberta, Edmonton, Alberta, T6G 2J9, Canada

2.1 INTRODUCTION

The Tagish Lake meteorite is one of the most pristine meteorite samples available in the world's collection (Herd et al. 2011). Based on its mineralogy, Zolensky et al. (2002) classified Tagish Lake meteorite as an ungrouped type 2 carbonaceous chondrite. The pristine samples were collected by a local resident, Jim Brook, only a few days after the fall. He was aware of the importance of the meteoritic samples as he was working for the Geological Survey of Canada collecting snow samples for possible meteoritic dust, so he retrieved the samples with little contamination using plastic bags and stored them frozen, wrapped in aluminum foil, in Ziploc® bags (Hildebrand et al. 2006). A total of ~ 0.85 kg of pristine material was retrieved (Brown et al. 2000). The pristine nature of this material was confirmed by the stepped pyrolysis of 'waters' extracted from a bulk sample, which indicated little or minimal terrestrial signature (Baker et al. 2002). To date there are only two studies that have looked in detail at the bulk chemical composition of pristine Tagish Lake meteorite samples (Brown et al. 2000; Friedrich et al. 2002).

Brown et al. (2000) studied a few pieces of pristine material with the objective of classifying the newly fallen meteorite through mineralogical, bulk chemical and isotopic compositional data. They analyzed a total of 73 elements using various methods. They determined that the abundance of moderately volatile lithophile and siderophile elements fell between those of CM and CI chondrites. On the other hand the abundances of

[1] A version of this chapter has been submitted for publication to the Meteoritics and Planetary Science journal.

refractory lithophile elements were similar to those of CM chondrites while the refractory siderophile element abundances were similar to both CM and CI chondrites. Based solely on the bulk chemical composition these authors were unable to determine whether the Tagish Lake meteorite is CM or CI. However, using other evidence, from mineralogy and stable isotopes, they concluded Tagish Lake is a new type of meteorite, probably a CI2 chondrite.

Friedrich et al. (2002) developed an inductively coupled plasma mass spectrometry (ICP-MS) technique to quantify trace elements on extraterrestrial samples and applied it to three Tagish Lake samples (one pristine and two degraded) along with eight other carbonaceous chondrites. Their main goal was to establish the compositional relationship of Tagish Lake to other chemically well-characterized carbonaceous chondrites. The ICP-MS method was coupled with radiochemical neutron activation analysis (RNAA) to produce a data set of 47 elements, albeit without major element determination, in particular Si. These authors concluded that the pristine sample was compositionally distinct from other carbonaceous chondrites they characterized. This distinction was most pronounced by the 21% enrichment in refractory siderophile elements in the pristine Tagish Lake sample relative to Orgueil and from the highly volatile elements, which showed no evidence of loss due to thermal metamorphism. In addition, Friedrich et al. (2002) determined that Tagish Lake is not CI, and is not a mixture of two types of carbonaceous chondrites (CI and CM), but comes from a parent body with similar genetic processes as CI and CM chondrite parent bodies.

In an effort to further characterize the Tagish Lake meteorite and understand its alteration history, which was not the focus of previous authors' works, we initiated a mineralogical, petrological, textural, bulk-chemical and isotopic study of four pristine Tagish Lake specimens (TL5b, TL11h, TL11i, and TL11v). The mineralogical, petrological and textural results, using various methods such as electron microprobe, X-ray diffraction and Transmission Electron Microscopy (TEM), are published in the companion paper of this study (Chapter 1). In summary, these authors identified that the four studied specimens demonstrate varying degrees of aqueous alteration. Specimen TL5b contains the greatest number of least altered chondrule-like objects (~30 vol %) reaching 5 μm in diameter with accretionary fine-grained rims and the least amount of lithic fragments (~2 vol %). Specimen TL11i is dominated by the fine-grained matrix (up to 50 vol %), devoid of any well preserved chondrules, contains abundant framboidal and platelet magnetite clusters (15 vol %) and isolated olivine grains (up to 5 vol %).

Specimen TL11h represents an intermediate lithology between TL5b and TL11i. The abundance of chondrule-like objects in TL11h appears to be closer to that of TL5b (~20 vol%) but they are much smaller (50 to 200 μm) and more altered, and have more diverse morphologies than TL5b. Finally, specimen TL11v consists of disaggregated material (as collected), heterogeneous on the microscale, and encompassing the petrologic characteristics of the other three specimens as seen through EPMA observation. All the specimens have variable proportions of lithic fragments. Blinova et al. (submitted) concluded that the degree to which the specimens have undergone aqueous alteration, based on mineralogical and petrological observations, is in the order TL5b < TL11h < TL11i with specimen TL11v representing a physical mixture of the other three specimens.

In this study, we utilized a Parr bomb digestion method on small sample size (~50 mg) for ICP-MS and inductively coupled plasma atomic emission spectroscopy (ICP-AES) together with instrumental neutron activation analysis (INAA) producing a set of 65 elements, which we find analytically accurate and are able to compare to both Brown et al. (2000) for major and trace elements and Friedrich et al. (2002) for trace elements. Here we expand on the previous efforts by Blinova et al. (submitted) to add a geochemical parameter in establishing an overall mineralogical framework for determining the degree of alteration in the Tagish Lake meteorite. The main goal was to find out whether the alteration sequence described in Chapter 1 for four studied Tagish Lake samples was evident geochemically.

2.2 METHODOLOGY

2.2.1 Samples

In this work we determined the whole-rock composition of the same four pristine specimens of the Tagish Lake meteorite: TL5b, TL11h, TL11i, and TL 11v studied in Chapter 1. The specimens were obtained from the University of Alberta meteorite collection. Each sample was hand ground under acetone using an agate mortar and pestle. Once dried, each sample was sieved through a 200 mesh and re-ground to ensure homogeneity.

2.2.2 Instruments

Several analytical techniques and instruments were utilized to determine the whole-rock chemistry of the four specimens. We utilized the ICP-AES, housed at the Grant MacEwan University, the Perkin Elmer 's Elan 6000 NuPlasma multi-collector

inductively coupled mass spectrometer (MC-ICP-MS), housed in the Radiogenic Isotope Facility (RIF) at the University of Alberta, and the SLOWPOKE-II Nuclear Reactor and high-resolution gamma-ray spectrometers, housed in the SLOWPOKE Facility at the University of Alberta. The SLOWPOKE reactor was used as a source of neutrons for the instrumental neutron activation analysis (INAA).

2.2.3 ICP Digestion procedure

Approximately 50 mg of each ground specimen was used for sample digestion. The choice of the weight was governed by the availability of the specimens from the collection. TL11i had the smallest available weight in powder, 49.3 mg. Other samples were matched to avoid any bias. For quality accuracy and control purposes we also used two replicates of 50 mg aliquots of three USGS standards (GSP-2; SGR-1; BIR-1), four replicates of the Allende meteorite (MET7100/A-207 sample) from the University of Alberta collection, weighing between 63 and 65 mg, and a digestion blank to assess the digestion procedure and confirm the reproducibility of the method. The use of the Allende meteorite, although mineralogically different from the Tagish Lake meteorite, was governed by the availability of this abundant material in the collection and the fact that its chemical composition, which has been analyzed by other researchers, is well known.

The digestion protocol (details in Appendix) was developed based on a number of sources (Eggins et al. 1997; Yu et al. 2001; Takei et al. 2001; Jain et al. 2001; Navarro et al. 2008). We employed a Parr Bomb digestion method (heated under pressure Teflon bomb) using an HF/HNO_3 mixture to ensure complete digestion of samples, and in particular refractory minerals (e.g., chromites; Chapter 1). Prior to choosing the Parr Bomb method, we used a whole rock digestion method of HF/HNO_3 mix in an open Savillex® beaker on a hot plate that is routinely used at the RIF for silicate-mineral/whole rock analysis.

2.2.4 ICP-MS procedure

Routine running and instrument conditions were used for the measuring aliquots of the Tagish Lake samples. The flow rate is ~ 1 ml/minute with 35 sweeps per reading at 1 reading per replicate. Three replicates of all samples were done. Dwell times are 10 ms for Na, Al, K,, Cu, Zn and Sr, and 20 ms for other elements except Se, which is 150 ms. The integration time (dwell time x number sweeps) was 350 ms for Al, K, , Cu, Zn and Sr;

and for other samples are 700 ms, except for Se, which was 5250 ms. The final results were calculated as the average of 3 replicates.

Samples were measured in dual detector mode with auto lens one using 1300 W power. Blank was subtracted after internal standard correction. Scandium, Bi and In were used as internal standards for every sample. Four points calibration curves were used: 0, 0.25, 0.50, 1.00 ppm for Na, Ca, Mg, Fe, K and P; and 0, 0.005, 0.010, 0.020 ppm for other elements. Certified values of USGS GSP-2 standard were used to calculate the recovery % of measured elements.

2.2.5 INAA procedure

Aliquots of the ground Tagish Lake meteorite samples were prepared for INAA. The weight of the samples are: TL5b = 304 mg; TL11v = 346 mg; TL11h = 281.7 mg; TL11i = 217.2 mg. Powder from Cold Bokkeveld meteorite (weight = 80 mg) was analyzed at the same time as the Tagish Lake samples and used to compare our INAA method with the published values of Kallemeyn and Wasson (1981). All samples were ground in a similar manner as for ICP analyses. Samples were individually weighed into ~200 µL polyethylene microcentrifuge tubes and hermetically sealed in preparation for analysis.

The following elements were analyzed by INAA: Fe, Sc, Cr, Zn, Co, Se, As, Sb, La, Ce, Sm, Br, Na, Si, V, Mn, Ir, Al and Mg. Using a boron shield Si was determined *via* the fast neutron reaction $^{29}Si(n,p)^{29}Al$. Subsequently V, Mn, Al and Mg were determined by INAA utilizing a nominal thermal neutron flux of 1 x 10^{11} n cm^{-2} s^{-1} and a 300s – 600s – 300s irradiation-decay-count scheme. Following decay of the short-lived radionuclides samples were simultaneously irradiated as a batch for 2.50 hours at a nominal thermal neutron flux of 5 x 10^{11} n cm^{-2} s^{-1}. Following a decay period of 5-6 days samples and standards were individually counted for 12000 s using a 20% hyperpure Ge detector (FWHM resolution 1.86 keV), and following a total decay period of ~5 weeks they were individually counted using a 40% efficient Ortec GEM-FX Profile detector (FWHM resolution 1.76 keV) for 50000 to 60000 s. With the exception of the determination of Ir, all reported elements were quantified using the semi-absolute method of NAA (Bergerioux et al. 1979). Iridium was quantified *via* absolute NAA.

2.3 ANALYTICAL RESULTS

In Table 2.1 we present our data for the total 65 elements: 62 elements by ICP-MS with matching 16 elements by ICP-AES (both using Parr bomb digestion method) and 19 elements, out of which 3 elements are unique to this method only, by INAA along with 1σ errors where available. In addition, in the same table we list previously published data by Brown et al. (2000) and Friedrich et al. (2002), or B('00) and F('02) henceforth, for comparative purposes.

Duplicate analyses of split samples, using an open-vessel, mixed-acid digestion process on a hot plate gave inconsistent results. Consequently, we employed a high temperature, mixed-acid digestion process at pressure, the so-called Parr-bomb method, which is routinely applied for the total digestion of difficult to dissolve minerals such as zircon (e.g., Krogh 1973), for sample digestion and subsequent analysis by ICP techniques. Data from the hot plate method are used in several figures for comparison purposes only.

2.3.1 Reproducibility and Accuracy

As mentioned above we used three certified USGS standards (2 aliquots of each) and Allende meteorite (4 aliquots) powders as quality control for the Parr bomb digestion method followed by an ICP elemental analysis. In Table 2.2 we present average values from the two replicates of three USGS standards and average from four replicates of Allende meteorite along with published data for this meteorite. We also include data on two blanks from two different batches for the Parr bomb digestion method analyzed by ICP-MS.

The replicate analyses of the USGS standards were performed using the same procedure but in different batches and on different dates. At one standard deviation 12 elements (in BIR-1) out of 62 elements, such as Au, Be, Cd, Cs, Mo, Os, Pb, Rb, Re, Sb, Sn, Ta and W, reproduced within 20% to 80% of the published data. With the exception of Te (discussed below), the remaining 48 elements in BIR-1, 59 elements in SGR-1, and 50 elements in GSP-2 reproduced within 2% to 10%, which we consider an accomplishment in our digestion method using Parr bombs. Tellurium concentrations were below the detection of the ICP-MS methodology for all three USGS standards analyzed and no certified Te data are available for them.

In the case of Allende replicates, 41 out of 62 elements fall within 10% of the published values. Elements such as Ho, Li, Lu, Mo, Nb, Pb, Pt, Re, Tb, and Tm fall

within 20% of the published values. Other elements (Au, Hf, Os, Sn, Ta, Th, and Tl) reproduced within 20% to 70%. Tungsten did not reproduce among the Allende replicates. It is possible that our method is incapable of liberating this particular element, which could be held in a resistant mineral. Yet other chemically similar elements have a fair reproducibility in the replicates, such as Hf (reproduced within 1%), Ti (reproduced within 2%), Cr, Zr (both reproduced within 10%) and Sn (reproduced within 20%). We conclude tin our further discussions that W data should be considered qualitative at best.

In Table 2.2 we also compare Allende data with published data by Morgan et al. (1969); Wakita and Schmitt (1970); Malissa et al. (1972); Jarosewich et al. (1987); and Babechuk et al. (2010). For seven elements (Ge, Li, Nb, Pd, Ta, Te, Tl) we are unable to compare our results with the five published references as none report these data. Six elements (Au, Ba, Co, Hf, Ru, Sr) are identical within the uncertainty to Jarosewich et al. (1987) values. Eight elements (Ca, Cd, Cs, Fe, Mn, V, Yb, Zn) fall within 10% of the reported values by the above five references. Sixteen elements (Ce, Cr, Dy, Er, Eu, Ga, Gd, Ho, K, La, Nd, Ni, P, Pb, Pr, Tm) fall within 15-20% and seven other elements (Ir, Lu, Mg, Na, Rb, Tb, Ti) fall within 25% of the reported values. Ten elements (Al, As, Cu, Mo, Os, Pt, Sm, W, Y, Zr) differ by over 25% of the reported values by various authors mentioned above. Comparison of Re, Sb, and Sn to Malissa et al. (1972), and Th to Babechuk et al. (2010) show higher concentrations than reported by these authors. It is uncertain whether there is a deficiency in our method for these four elements or whether the Allende aliquot analyzed had different concentrations of these elements due to variations in mineralogy. A similar case is uranium, which is below the detection limit. Babechuk et al. (2010), however, reported measurable values of uranium in Allende. It is possible that our method is not capable of completely liberating this element. Our ICP-AES data for these elements are incomplete and are, therefore, not comparable. Overall, we believe that both the USGS and Allende replicates show that the accuracy and reproducibility of our digestion technique using pressurized Parr bombs is effective and overall is successful in attaining complete sample digestion.

Elemental data obtained by ICP-AES are less accurate compared to the previously published data. Out of 16 elements measured by this method only four elements (Co, Ti, V, Zn) fall within 10% of the reported values. Three elements (Na, Cu, Al) differ by more than 50% of the published values.

The INAA results for the Cold Bokkeveld meteorite are overall consistent with the published values of Kallemeyn and Wasson (1981). However, the results for three

elements (Br, La, Sb) are 50% greater relative to the published results (Table 2.3). Therefore, the INAA data for these elements for the studied Tagish Lake samples should be used with caution.

2.3.2 Analytical results by different methods

Fig. 2.1 compares element abundances, following cosmochemical classification of the elements based on condensation temperature (Palme and Jones 2004), for each sample by the Parr bomb and hot plate digestion methods, together with published data of B('00) and F('02).

On the chondrite normalized rare earth element (REE) diagram (Fig. 2.1a) the Parr bomb method results follow the lower abundance of these elements, similar to the selected duplicate samples by hot plate method. Data derived from the Parr bomb method are also comparable with the previous results on the Tagish Lake meteorite by B('00) and F('02). On a refractory lithophile element diagram (Fig. 2.1b) the majority of results of B('00) and F('02) straddle the middle ground of the hot plate and Parr bomb results, except for Nb, Hf, and U. The results for Nb of F('02), for Hf of B('00) and U from both papers are slightly lower than our results for these elements. The data on refractory siderophile and chalcophile elements (Fig. 2.1c) are mixed. Both previously published data have higher concentrations for Re and Ru than the data from Parr bomb method. In the case of Os, the hot plate method results are of similar magnitude to the published value. Although the reproducibility of Os is satisfactory for USGS standards and Allende sample (discussed above), the Parr bomb data show lower concentrations of Os than B('00). Main lithophile, siderophile and chalcophile data (Fig. 2.1d) from both methods show less scatter except for Li and Pd. Data for Li from B('00) are higher than our data using both methods and comparing to F('02). Results for Pd from the Parr bomb method is similar to those of F('02), while three duplicates (TL5b, Tl11i, TL11v) by the hot plate method have similar concentrations to B('00) data. The Parr bomb results of moderately and highly volatile elements (Fig. 2.1e,f) in general show similarity to the previously published data. Both Parr bomb and hot plate results for the K and Ge are twice as low as data from published sources. The Au content of TL11v is significantly greater than in the other samples analyzed and previously published data. This variation may be due to Au heterogeneity and the small sample size analyzed.

Three elements, which are not plotted on Fig. 2.1 (Ta, Th and W), produced inconsistent results among the samples in both Parr bomb and hot plate methods. There

appears to be a higher concentrations of these elements in our studied samples: Ta is 7 to 40 times greater than reported by B(’00); Th is 2 to 8 times that reported by B(’00) and F(’02); and W is 3 to 10 times greater than that reported by F (’02) (Table 2.1). We discussed above that although W is accurate, it is imprecise in our analyses of both Allende replicates and in the USGS standards. In the case of Ta, although both BIR-1 standard and Allende replicates reproduced this element fairly well (see above), its accuracy and precision cannot be evaluated due to the lack of published standard data for Ta. Thorium reproduced very well (within 4%) in the USGS standards; however, reproducibility in the Allende replicates for Th is 60% at best. Although Ta, Th, and W are accurate with variable reproducibility in standards, the concentrations of these elements in the studied Tagish Lake samples are two to three orders of magnitude higher than what was previously reported in B(’00) and F(’02). The concentrations of these elements are qualitative at best. Therefore, we have not plotted these results on Fig. 2.1 because the scale becomes too large and the reader is then unable to assess other elements.

Figure 2.2. compares data for 15 elements measured by INAA, ICP-MS/ICP-AES, and previously published results by B(’00) and F(’02) normalized to CI and Si. Silica as a major element is used here and in Fig. 2.3 for normalization, following convention, in order to allow comparisons with results of other workers. F(’02) data are missing results for Al, Cr, Fe, and Mg; so, no comparison can be made between our data and theirs. Overall our data by both methods and published results fall within the reported uncertainties. However, several elements by INAA do not match either previously published data or our ICP data. Sample TL5b shows a higher value for Sb by INAA; although for other samples this element is within the uncertainty. INAA data for Na for sample TL5b is much lower than by ICP-MS and B(’00) data. The same element measured by B(’00) has a much higher concentration than our data by both ICP-MS and INAA for TL11v, which are identical within the uncertainty. ICP-MS data for As for TL11h is much higher than INAA results, the latter is within the uncertainty of the previously published data. ICP-AES data for Al for sample TL11v is much lower than by INAA, ICP-MS and published data, which is consistent with the fact that Allende data for Al by this method is lower by a factor of 3 compared to published values. In general, there is good agreement between the ICP-MS Parr bomb and INAA methods, and published data for Cr, Fe, Mn, Sm, and partially for Co. Other elements are within the uncertainty, or just slightly above, or below, previously published data.

Finally, although we have not plotted Si data on any of our above diagrams, we use it for normalization. The NAA Si data are the only determinations of this element for the Tagish Lake meteorite since B(‘00). For three samples (TL5b, TL11h, TL11i) the Si values determined here agree within the analytical uncertainty, and with the Si value reported by B(‘00), whereas sample TL11v has a higher Si concentration by ~ 2 wt% than previous published data.

2.4 DISCUSSION

Carbonaceous chondrites have been affected by various secondary processes such as oxidation, metamorphism, and aqueous alteration. The location of the latter is under debate as either asteroidal or nebular (Brearley 2004). Brearley (2004) noted that evidence (or lack of) for isochemical bulk-compositional variation is most consistent with alteration after accretion on a parent body. The objectives of previous studies by B(‘00) and F(‘02), who studied bulk chemical variations in the Tagish Lake, did not focus on understanding the alteration history of this meteorite. Here we compare four studied samples to each other and with other carbonaceous chondrites to determine whether the alteration sequence observed through mineralogy is reflected in whole-rock geochemistry and whether the elemental variations, if any, tell us anything about the alteration history of this meteorite.

2.4.1 Whole-rock composition of pristine Tagish Lake samples

Following F(‘02), we plotted 51 elements from the studied samples in Fig. 2.3. The refractory and moderately lithophile elements are plotted based on condensation temperatures (e.g., McSween and Huss 2010; Palme and Jones 2004). Other elements are ordered by increasing vaporization and loss in artificially heated Allende and Murchison (Lipschutz and Woolum 1988). Both W and Ta are omitted from the diagram due to the reasons discussed in the results section.

We will first describe the variations seen on this diagram, as it will allow us to see whether any elements, or groups of elements, behave in accordance with our inferred alteration sequence (Chapter 1). When comparing the four studied samples, it is evident that refractory lithophile elements (Fig. 2.3a) do not show large variations and have three well-defined plateaus in Y-Er, Ho-Gd and Nd-Eu. Elements such as Hf, Lu, Zr, U, Nb, Sr and Ba show variations, in some cases beyond measurement uncertainty. Both Sr and Ba are elements that are considered to be mobile in aqueous fluids while Hf, Lu and Zr are

less so (Rollinson 1993; Wilson 2007). TL5b has the highest Hf, Zr and Nb contents. It has been shown that both Hf and Zr tend to partition more into pyroxene than olivine (e.g., Dunn 1987). As these two minerals are abundant in the studied samples (Chapter 1), it is possible that the higher concentrations of Hf and Zr in TL5b may be indicative of greater pyroxene abundance relative to other samples. As shown by the internal standards there could be a deficiency in our digestion method in liberating U; therefore, any U variations in the studied samples are most likely not real. Among siderophile elements (Fig. 2.3b) the fluctuations are stronger and there are no apparent plateaus. Elements such as Mo, Pt, Pd, Au and As have variations among the samples beyond measured uncertainty as well as above the detection limit of the ICP-MS. Therefore, we conclude that these fluctuations are real and could be attributed to mineralogical variations, such as volume % of sulfides, in the studied samples (Chapter 1)

The most volatile elements Sb to Cd overall show less variation, with TL11v having the lowest concentrations, and define a plateau characteristic of carbonaceous chondrites (Xiao and Lipschutz 1992). It was shown that in thermally metamorphosed meteorites the most labile elements (Cs to Cd) have strong depletions by an order of magnitude below the constant mean value of unaltered specimens (Wang and Lipschutz 1998). Although TL11v in general has lower concentrations of these elements than other samples (Fig. 2.3b), we rule out loss of these elements in this sample by an open-system thermal metamorphism because the mean value for Cs to Cd in TL11v is within the mean defined by the primary nebular condensates (Wang and Lipschutz 1998).

The alteration sequence (TL5b < TL11h < TL11i) is based on the mineralogical differences observed in primary nebular components such as chondrules, and modal abundance of other components, such as matrix, lithic fragments, carbonates, sulfides, etc. (Chapter 1). On Fig. 2.4 we tested the variation of selected major and trace elements for any correlation with inferred alteration. Major elements (e.g. Mg, Fe, Al, Ca) do not show any variation; however, trace elements, such as K and Br, show a positive correlation between the least (TL5b) and most altered (TL11i) samples. Homogeneity of major elements suggests that any elemental mass transfer occurred on a localized scale and aqueous alteration was isochemical in nature, consistent with observations in other primitive chondrites (Brearley 2004). The mineralogical differences in the studied samples are due to replacement of primary silicates (olivines and pyroxenes) mainly by phylloslicates (Chapter 1). Therefore, the behavior of the mobile trace elements is likely controlled by the abundance phylloslicates. Sample TL11v plots in the same region as

TL5b (Fig. 2.4) reflecting its mineralogy as a physical mixture of other studied samples (Chapter 1).

2.4.2 Comparison of TL whole-rock composition with other carbonaceous chondrites

Figures 2.5 – 2.8 show various diagrams comparing bulk chemical composition of the studied samples with other carbonaceous chondrites and published data on the Tagish Lake meteorite.

In lithophile and siderophile diagrams (Fig. 2.5) we plot fields for each sample from both ICP-MS and INAA derived data. The studied Tagish Lake samples have lower CI-normalized lithophile element abundances (Si-normalized) than mean CV and CO chondrites but follow the pattern of previously published data by B('00) and are similar to CM mean. Some exceptions can be noted. Samples TL11v and TL11h have lower Ca concentrations than the mean of other chondrites and other studied samples. Sample TL11v has twice the Lu concentration compared to the other TL samples analyzed but is similar within uncertainty to the mean Lu in CV and CO chondrites (Table 2.1). Another noticeable difference is the Na depletion (~ 0.3 x CI) in TL11v. Similar, although not to the same extent, Na depletion is found in Murray (CM2.4/2.5) chondrite (Fig. 2.6; e.g., Rubin et al. 2007). It is possible that the Na deficit in TL11v could be attributed to the mineralogy of the sample. Brearley and Jones (1998) reported analyses of rare chondrule glass from CM chondrites that show variations in concentrations of Ca, K, and especially in Na, with Na varying from less than 2 wt% up to 8 wt%. Our only analyses of slightly altered mesostasis of TL5b chondrule show Na_2O concentrations up to 3 wt% (Chapter 1). Because TL11v represents a physical mixture of other studied samples (Chapter 1), it is quite conceivable that the 50 mg piece that we have analyzed for bulk chemistry was devoid of chondrules. This is supported by the fact that the two pieces of TL11v that we have studied using EPMA have opposite component abundances: one contains up to 40% of chondrules, the other has less than 10% (Chapter 1).

In general mean siderophile concentrations of CV, CM and CO chondrites have a decreasing pattern from Ir to Cd with CO mean concentration much lower for Cd than other chondrites (Fig. 2.5b). In the studied samples, on the other hand, such a decrease in siderophile elements is not very pronounced. The Tagish Lake pattern has a few anomalies and is flatter overall because elements Ir, Ru, and Ni are lower in concentration than other chondrites. There are slight increases from Ni to Fe, Ga to Sb, and Se to Zn.

Overall bulk-composition variations in the studied Tagish Lake samples are comparable with the mean composition of other carbonaceous chondrites, regardless of their type (CV vs. CM).

Recently Rubin et al. (2007) developed a system for determining the degree of alteration of CM chondrites based on petrological observations and bulk elemental composition. Previously Browning et al. (1996) used an algorithm to establish a 'mineralogical alteration index' (MAI) based on EPMA analyses to identify the alteration sequence in CM chondrites. Regardless of their methodology, both agree that the alteration sequence for CM chondrites is as following: Murchison (least altered) < Murray < Nogoya < Cold Bokkeveld (most altered). On Fig. 2.6 we plot available data (Kallemeyn and Wasson 1981) for these four CM chondrites (least to most altered) and compare the patterns with our samples. The CI-normalized elements are plotted in order of decreasing volatility from left to right (McSween and Huss 2010). The objective of this diagram is to determine whether there is an obvious bulk-chemical composition variation from most to least altered CM chondrites and to ascertain whether Tagish Lake samples follow any of these variations. The CM meteorites follow an isochemical alteration pattern as other carbonaceous meteorites, except for a couple of elements, such as Na and K in Murray, and Sm in Nogoya (e.g., Rubin et al. 2007; McSween and Huss 2010). Altogether our Tagish Lake samples follow the same pattern as found in CM chondrites: a relatively flat plateaus at ~ 0.6 x CI and ~1.1 x CI, and a general increase from most volatile to least volatile elements. It has been proposed that the first plateau, which is formed by volatile elements, reflects matrix component composition, while the second plateau, which is formed by more refractory elements, reflects chondrule-CAI component, and both indicate a mixture of high-T and low-T condensates (e.g., Larimer and Anders 1970; McSween and Huss 2010). Our studied samples follow the pattern established for other carbonaceous chondrites.

Several elements in Fig. 2.6, however, show some variations. Relative to these four CM chondrites the most notable variations are a decrease in Cd, K and Na, an increase in Au in TL11v; and an increase in Sb in TL5b. Murray chondrite, although not the most altered in CM sequence, shows an extensive depletion in Na and K. Decrease in Cd in TL11v relative to other samples and CM chondrites could possibly be explained by the mineralogy of TL11v, as reproducibility for this element is satisfactory. Low Os concentrations in the studied samples versus CM are probably due to loss of this element during repeated evaporation (see Appendix). Overall, Fig. 2.6 shows that when

comparing our studied samples, which exhibit alteration sequence on the mineralogical scale, to the CM chondrites with established alteration sequence there is no major difference in a bulk-chemical composition among our samples and CM chondrites confirming the isochemical alteration.

Comparison of REE of the four studied samples with other carbonaceous chondrites is made in Fig. 2.7. Our data are much lower than the CV mean concentration and fall between the Murchison and Orgueil chondrites possibly reflecting a mineralogical difference between the studied samples and these chondrites. Sample TL11v has a higher concentration of La, although within the uncertainty with Murchison, and a Lu concentration much higher than other Tagish Lake samples making a 'bowl'-shaped REE pattern. Other samples have lower HREE concentrations than TL11v but higher than Orgueil. In general, the studied samples show comparable chondrite normalized REE patterns.

To conclude our compositional comparison with other carbonaceous chondrites, we plot Zn/Mn vs. Sc/Mn atomic ratios similar to Friedrich et al. (2002) in Fig. 2.8. Such plots have been shown to be successful at distinguishing carbonaceous chondrite clans based on the on the abundance of volatile and refractory elements, such as Zn, Mn and Al (Kallemeyn and Wasson 1981). Here I use Sc as proxy for tripositive Al, similar to F('02), to enable comparison with their results. In Fig. 2.8 we can see that samples TL5b and TL11h, which we consider to be the least altered among the four studied samples, plot in the general region as the pristine Tagish Lake samples from F('02). Sample TL11i plots just below TL5b and TL11h, but in the same region. This could be a result of TL11i's greater degree of alteration, i.e., longer exposure to alteration water. It was noted previously that none of the known carbonaceous chondrite groups fall in this region of the diagram (vertical lines in Fig. 2.8; Kallemeyn and Wasson 1981). Our data add three additional points to the area defined by the Tagish Lake data of F('02) and confirm their conclusion that this meteorite is not a simple mixture of CI and CM material as the line joining these two groups will by-pass the Tagish Lake region. Interestingly, TL11v plots well below the other three samples in the CM region but on the same line connecting TL11h and TL11i. We do not believe that TL11v is a 'true' representative of the CM group due to the nature of this sample. As described in Chapter 1, TL11v is a physical mixture of the other samples, heterogeneous on the microscale, and encompassing the petrologic characteristics of the other three specimens as seen through EPMA observation. The whole-rock chemistry also indicates that TL11v could contain an additional, more

altered than TL11i, component. This could also explain several minor differences in the chemical analyses of some elements in TL11v as discussed above.

2.5 CONCLUSION

We obtained whole-rock data for a total of 65 elements for four pristine Tagish Lake samples (TL5b, TL11h, TL11i, TL11v) utilizing ICP-MS, ICP-AES and INAA. Mineralogical, petrological and organic chemistry observations demonstrate that the alteration sequence (from least to most altered) in the studied samples is TL5b < TL11h < TL11i (Chapter 1). In general, when comparing the samples with each other, homogeneity of major and minor elements shows us that elemental mass transfer occurred on a localized scale and alteration was isochemical. This conclusion is supported when comparing our whole-rock data with other carbonaceous chondrites. Mobile trace elements, such as K and Br, on the other hand, have a positive correlation with an alteration sequence observed through mineralogy, which we believe is controlled by an increase in phyllosilicates from least to most altered sample. We have added additional data points on the Tagish Lake region defined by Friedrich et al. (2002) in Zn/Mn vs. Sc/Mn space, a plot which is traditionally used (here with Sc as a proxy for Al) for distinguishing between established carbonaceous groups. Three of the studied samples (TL5b, TL11h, TL11i) plot in the same region as Friedrich et al. (2002) data in a previously unoccupied area of this diagram, confirming that the Tagish Lake meteorite is not a simple mixture of CI and CM material. The location of TL11v sample on the Zn/Mn vs. Sc/Mn diagram is lower than other samples but on the line connecting TL11h and TL11i, consistent with its nature as a physical mixture of other Tagish Lake samples.

2.6 REFERENCES

Baker, L., Franchi, I.A., Wright, I.P., and Pillinger, C.T. 2002. The oxygen isotopic composition of water from Tagish Lake: its relationship to low-temperature phases and to other carbonaceous chondrites. Meteoritics and Planetary Science 37:977-985.

Bergerioux, C., Kennedy, G., and Zikovsky, L. 1979. Use of the semi-absolute method in neutron activation analysis. Journal of Radioanalytical Chemistry 50:229-234.

Brearley, A.J. 2004. Nebular versus parent-body processing, In Treatise on Geochemistry, edited by Davis, A.M. Elsevier Ltd., pp. 247-268.

Brearley, A.J., and Chizmadia, L.J. 2005. On the behavior of phosphorus during the aqueous alteration of CM2 carbonaceous chondrites (abstract #2176). 36th Lunar and Planetary Science Conference. CD-ROM.

Brearley, A.J., and Jones, A. 1998. Chondritic meteorites, In Planetary materials, edited by Papike, J.J. Washington D.C., USA: Mineralogical Society of America. pp. 3-1 - 3-398.

Brown, P.G., Hildebrand, A.R., Zolensky, M.E., Grady, M., Clayton, R.N., Mayeda, T.K., Tagliaferri, E., Spalding, R., MacRae, N.D., Hoffman, E.L., Mittlefehldt, D.W., Wacker, J.F., Bird, J.A., Campbell, M.D., Carpenter, R., Gingerich, H., Glatiotis, M., Greiner, E., Mazur, M.J., and McCausland, P.J.A. 2000. The fall, recovery, orbit, and composition of the Tagish Lake Meteorite: a new type of carbonaceous chondrite. Science 290: 320-325.

Browning, L.B., McSween, H.Y., and Zolensky, M.E. 1996. Correlated alteration effects in CM carbonaceous chondrites. Geochimica et Cosmochimica Acta 60:2621-2633.

Dunn, T. 1987. Partitioning of Hf, Lu, Ti, and Mn between olivine, clinopyroxene and basaltic liquid. Contributions to Mineralogy and Petrology 96:476-484.

Eggins, S.M., Woodhead, J.D., Kinsley, L.P.J., Mortimer, G.E., Sylvester, P., McCulloch, M.T., Hergt, J.M., and Handler, M.R. 1997. A simple method for the precise

determination of ≥ 40 trace elements in geological samples by ICPMS using enriched isotope internal standardisation. Chemical Geology 134:311-326.

Friedrich, J.M., Wang, M.-S., and Lipschutz, M.E. 2002. Comparison of the trace element composition of Tagish Lake with other primitive carbonaceous chondrites. Meteoritics and Planetary Science 37:677-686.

Hanowski, N.P., and Brearley, A.J. 2001. Aqueous alteration of chondrules in the CM carbonaceous chondrite, Allan Hills 81002: implications for parent body alteration. Geochimica et Cosmochimica Acta 65:495-518.

Herd, C.D.K., Blinova, A., Simkus, D.N., Huang, Y., Tarozo, R., Alexander, C.M.O'D., Gyngard, F., Nittler, L.R., Cody, G.D., Fogel, M.L., Kebukawa, Y., Kilcoyne, A.L.D., Hilts, R.W., Slater, G.F., Glavin, D.P., Dworkin, J.P., Callahan, M.P., Elsila, J.E., De Gregorio, B.T., and Stroud, R.M. 2011. Origin and evolution of prebiotic organic matter as inferred from the Tagish Lake Meteorite. Science 332:1304-1307.

Hildebrand, A.R., McCausland, P.J.A., Brown, P.G., Longstaffe, F.J., Russell, S.S., Tagliaferri, E., Wacker, J.F., and Mazur, M.J. 2006. The fall and recovery of the Tagish Lake meteorite. Meteoritics and Planetary Science 41:407-431.

Jain, J.C., Neal, C.R., and Hanchar, J.M. 2001. Problems associated with the determination of rare earth elements of a "Gem" quality zircon by inductively coupled plasma-mass spectrometry. Geostandards Newsletter-the Journal of Geostandards and Geoanalysis 25:229-237.

Jarosewich, E. 1987. Bulk chemical analysis of the Allende Meteorite reference sample. Smithsonian Contributions to the Earth Sciences 27.

Kallemeyn, G.W. and Wasson, J.T. 1981. The compositional classification of chondrites; I, The carbonaceous chondrite groups. Geochimica et Cosmochimica Acta 45:1217-1230.

Krogh, T.E. 1973. A low-contamination method for hydrothermal decomposition of zircon and extraction of U and Pb for isotopic age determinations. Geochimica et Cosmochimica Acta 37:485-494.

Larimer, J.W., and Anders, E. 1970. Chemical fractionations in meteorites; III, Major element fractionations in chondrites. Geochimica et Cosmochimica Acta 34:367-387.

Lipschutz, M.E., and Woolum, D.S. 1988. Labile elements, In Meteorites and the early Solar System, edited by Kerridge, J.F. and Matthews, M.S. Tucson, Arizona, USA: University Arizona Press. pp. 462-487.

Malissa, H., Kluger, F., Kiesl, W., and Hermann, F. 1972. Chemical and microprobe investigations of Allende-meteorite. Mikrochimica Acta:434-450.

McSween Jr, H.Y., and Huss, G.R. 2010. Cosmochemistry, 1st ed. Cambridge: Cambridge University Press. 549 p.

Morgan, J.W., Rebagay, T.V., Showalte, D., Nadkarni, R.A., Gillum, D.E., McKown, D.M., and Ehmann, W.D. 1969. Allende meteorite - some major and trace element abundances by neutron activation analysis. Nature 224:789-791.

Navarro, M.S., Andrade, S., Ulbrich, H., Gomes, C.B., and Girardi, V.A.V. 2008. The direct determination of rare earth elements in basaltic and related rocks using ICP-MS: Testing the efficiency of microwave oven sample decomposition procedures. Geostandards and Geoanalytical Research 32:167-180.

Palme, H., and Jones, A. 2004. Solar System abundances of the elements, In Treatise on Geochemistry, edited by Davis, A.M. Elsevier Ltd. pp. 41-61.

Rollinson, H. 1993. Using geochemical data: evaluation, presentation, interpretation, 1st ed. Harlow, Essex, England: Pearson Education Ltd. 352 p.

Rubin, A.E., Trigo-Rodriguez, J.M., Huber, H., and Wasson, J.T. 2007. Progressive aqueous alteration of CM carbonaceous chondrites. Geochimica et Cosmochimica Acta 71:2361-2382.

Takei, H., Yokoyama, T., Makishima, A., and Nakamura, E. 2001. Formation and suppression of AIF(3) during HF digestion of rock samples in Teflon bomb for precise trace element analyses by ICP-MS and ID-TIMS. Proceedings of the Japan Academy Series B-Physical and Biological Sciences 77:13-17.

Wakita, H., and Schmitt, R.A. 1970. Rare earth and other elemental abundances in Allende meteorite. Nature 227:478-479.

Wang, M.-S., and Lipschutz, M.E. 1998. Thermally metamorphosed carbonaceous chondrites from data for thermally mobile trace elements. Meteoritics and Planetary Science 33:1297-1302.

Wilson, M. 2007. Igneous Petrogenesis: a global tectonic approach, 9th ed. Dordrecht, The Netherlands: Springer. 466 p.

Xiao, X.Y., and Lipschutz, M.E. 1992. Labile trace-elements in carbonaceous chondrites - a survey. Journal of Geophysical Research-Planets 97:10199-10211.

Yu, Z.S., Robinson, P., and McGoldrick, P. 2001. An evaluation of methods for the chemical decomposition of geological materials for trace element determination using ICP-MS. Geostandards Newsletter-the Journal of Geostandards and Geoanalysis 25:199-217.

Zolensky, M.E., Nakamura, K., Gounelle, M., Mikouchi, T., Kasama, T., Tachikawa, O., and Tonui, E. 2002. Mineralogy of Tagish Lake: An ungrouped type 2 carbonaceous chondrite. Meteoritics and Planetary Science 37:737-761.

FIGURE CAPTRIONS CHAPTER 2:

Figure 2.1:
Comparison of Parr bomb ICP-MS and hot plate ICP-MS results with literature data. Normalized to CI, units on y-axis are parts per million (ppm).

Figure 2.2:
Comparison of results from INAA and Parr bomb ICP-MS methods with literature data from Brown et al. (2000) and Friedrich et al. (2002). (a) TL5b; (b) TL11h; (c) TL11i; (d) TL11v. Units on y-axis are parts per million (ppm).

Figure 2.3:
CI- and Si-normalized atomic abundances of 51 elements following Friedrich et al. (2002) for four Tagish Lake samples. See text for details.

Figure 2.4:
CI- and Si-normalized concentration of (a) K vs. Br, showing a positive correlation with the alteration sequence (see text for details); (b) K vs. Mg; (c) K vs. Ca; (d) K vs. Al

Figure 2.5:
Bulk composition of pristine Tagish Lake samples including the uncertainty, literature data on Tagish Lake meteorite (Brown et al. 2000; Friedrich et al. 2002) and the mean compositions of CM, CV and CO chondrites (Kallemeyn and Wasson 1981). (a) Lithophile elements. (b-c) Siderophile elements.

Figure 2.6:
Comparison of bulk compositions of pristine Tagish Lake and four CM chondrites: Murchison (least altered), Murray, Nogoya, Cold Bokkeveld (most altered) (Rubin et al. 2007).

Figure 2.7:
CI-normalized REE data comparison for pristine Tagish Lake samples and other carbonaceous chondrites (Orguiel and Murchison data are from Friedrich et al. 2002; CV mean is from Kallemeyn and Wasson 1981).

Figure 2.8:

Zn/Mn vs. Sc/Mn (atomic ratios following Friedrich et al., 2002) of studied pristine Tagish Lake samples, previously published data and other carbonaceous chondrites (all are from Friedrich et al. (2002) unless noted). Shown on the left are Zn/Mn ratio ranges established for CI, CM, CV, and CO by Kallemeyn and Wasson (1981). See text for details.

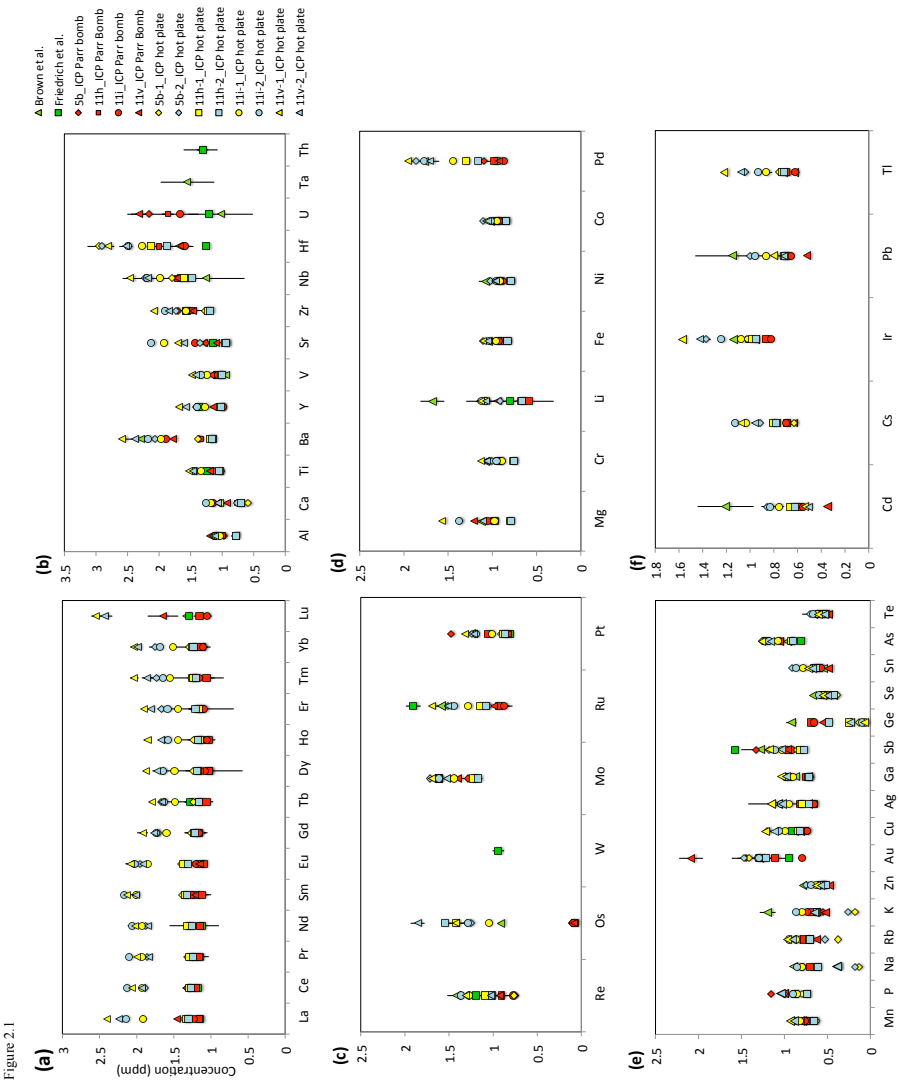
Brown et al.
Friedrich et al.
5b_ICP Parr bomb
11h_ICP Parr Bomb
11i_ICP Parr bomb
11v_ICP Parr Bomb
5b-1_ICP hot plate
5b-2_ICP hot plate
11h-1_ICP hot plate
11h-2_ICP hot plate
11i-1_ICP hot plate
11i-2_ICP hot plate
11v-1_ICP hot plate
11v-2_ICP hot plate
(a)
(b)
(c)
(d)
(e)
(f)
Concentration (ppm)
La Ce Pr Nd Sm Eu Gd Tb Dy Ho Er Tm Yb Lu
Al Ca Ti Ba Y V Sr Zr Nb Hf U Ta Th
Re Os W Mo Ru Pt
Mg Cr Li Fe Ni Co Pd
Mn P Na Rb K Zn Au Cu Ag Ga Sb Ge Se Sn As Te
Cd Cs Ir Pb Tl

Figure 2.1

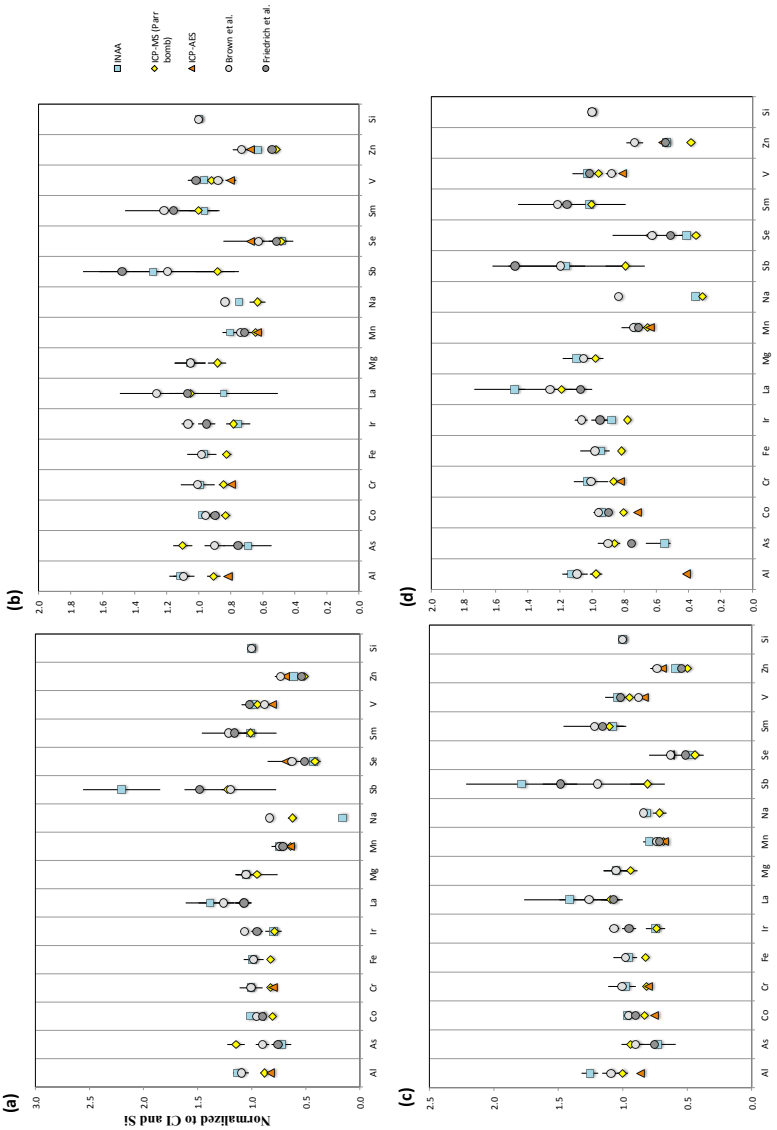
INAA
ICP-MS (Parr bomb)
ICP-AES
Brown et al.
Friedrich et al.
(a)
(b)
(c)
(d)
Normalized to CI and Si
Al As Co Cr Fe Ir La Mg Mn Na Sb Se Sm V Zn Si

Figure 2.2

Figure 2.3

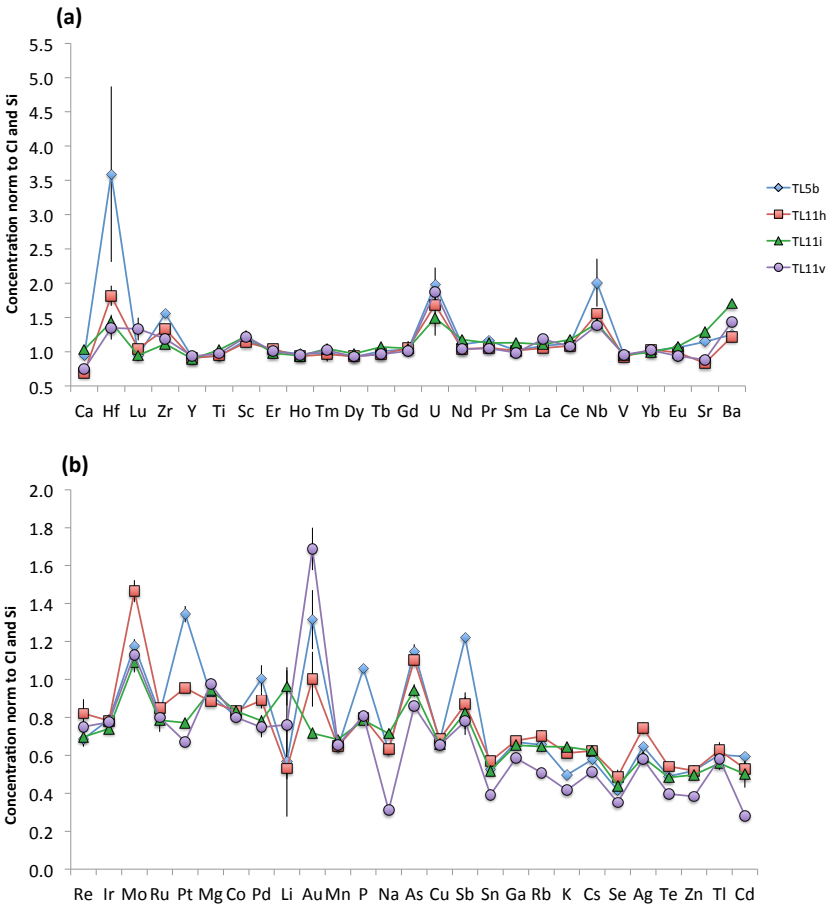
(a)
Concentration norm to CI and Si
5.5
5.0
4.5
4.0
3.5
3.0
2.5
2.0
1.5
1.0
0.5
Ca Hf Lu Zr Y Ti Sc Er Ho Tm Dy Tb Gd U Nd Pr Sm La Ce Nb V Yb Eu Sr Ba
TL5b
TL11h
TL11i
TL11v
(b)
Concentration norm to CI and Si
2.0
1.8
1.6
1.4
1.2
1.0
0.8
0.6
0.4
0.2
0.0
Re Ir Mo Ru Pt Mg Co Pd Li Au Mn P Na As Cu Sb Sn Ga Rb K Cs Se Ag Te Zn Tl Cd

Figure 2.4

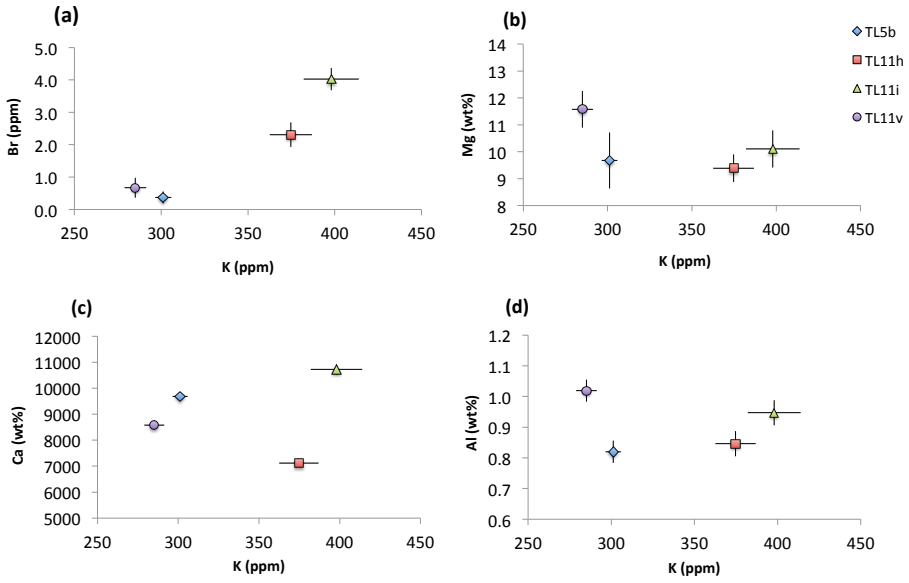
(a)
Br (ppm)
K (ppm)
(b)
Mg (wt%)
K (ppm)
TL5b
TL11h
TL11i
TL11v
(c)
Ca (wt%)
K (ppm)
(d)
Al (wt%)
K (ppm)

Figure 2.5

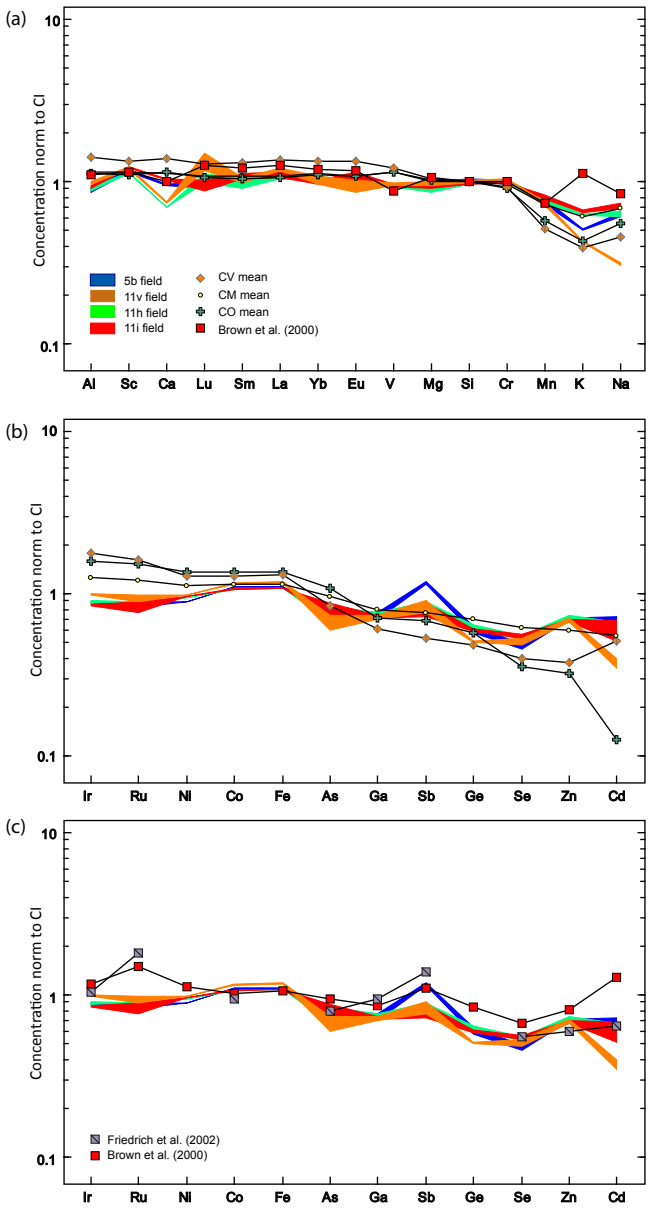
(a)
10
1
0.1
Concentration norm to CI
5b field
11v field
11h field
11i field
CV mean
CM mean
CO mean
Brown et al. (2000)
Al Sc Ca Lu Sm La Yb Eu V Mg Si Cr Mn K Na
(b)
10
1
0.1
Concentration norm to CI
Ir Ru Ni Co Fe As Ga Sb Ge Se Zn Cd
(c)
10
1
0.1
Concentration norm to CI
Friedrich et al. (2002)
Brown et al. (2000)
Ir Ru Ni Co Fe As Ga Sb Ge Se Zn Cd

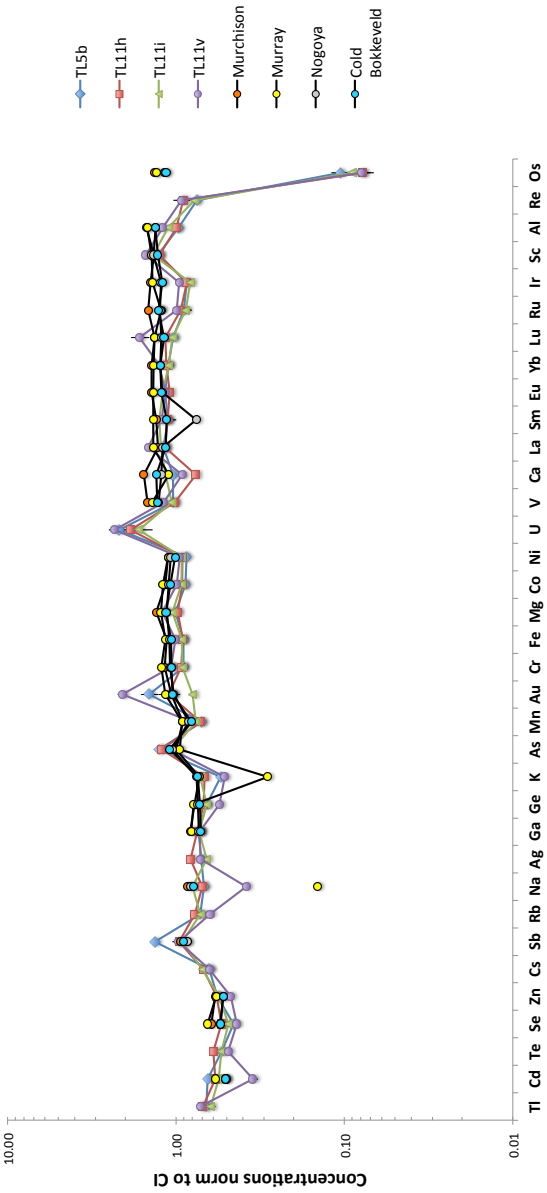
TL5b
TL11h
TL11i
TL11v
Murchison
Murray
Nogoya
Cold Bokkeveld
Concentrations norm to CI
10.00
1.00
0.10
0.01
Tl Cd Te Se Zn Cs Sb Rb Na Ag Ga Ge K As Mn Au Cr Fe Mg Co Ni U V Ca La Sm Eu Yb Lu Ru Ir Sc Al Re Os

Figure 2.6

Figure 2.7

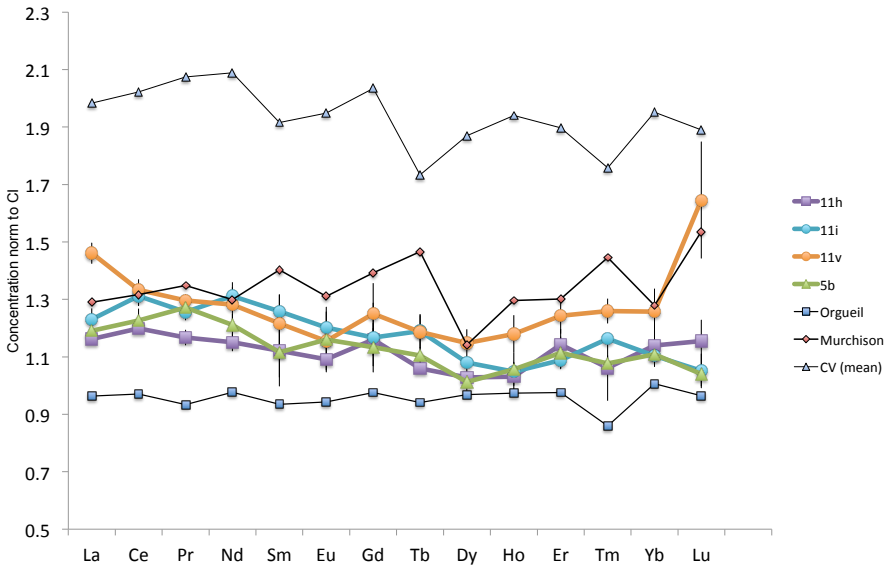
Concentration norm to CI
2.3
2.1
1.9
1.7
1.5
1.3
1.1
0.9
0.7
0.5
La
Ce
Pr
Nd
Sm
Eu
Gd
Tb
Dy
Ho
Er
Tm
Yb
Lu
11h
11i
11v
5b
Orgueil
Murchison
CV (mean)

Figure 2.8

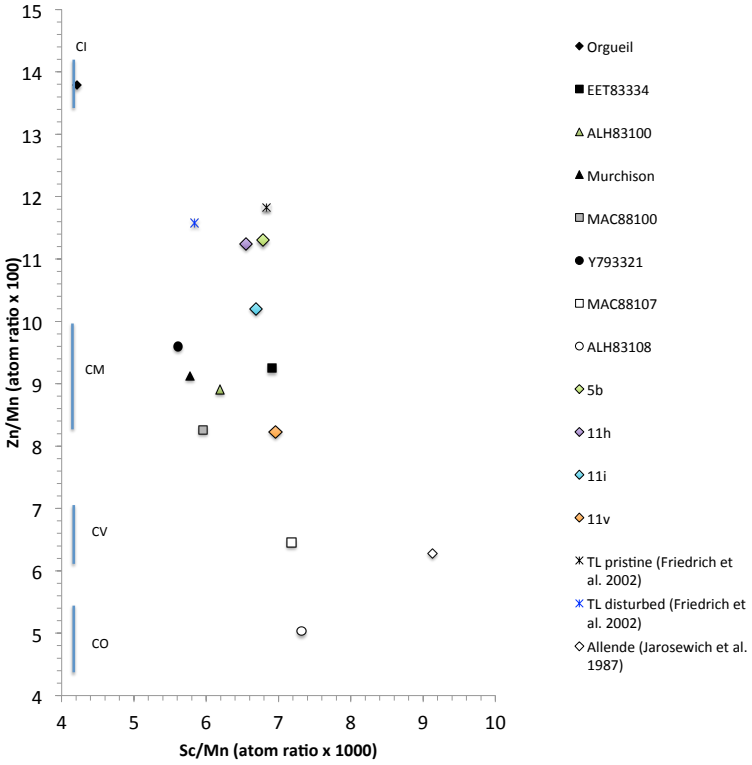
15
14
13
12
11
10
9
8
7
6
5
4
CI
CM
CV
CO
Zn/Mn (atom ratio x 100)
4
5
6
7
8
9
10
Sc/Mn (atom ratio x 1000)
Orgueil
EET83334
ALH83100
Murchison
MAC88100
Y793321
MAC88107
ALH83108
5b
11h
11i
11v
TL pristine (Friedrich et al. 2002)
TL disturbed (Friedrich et al. 2002)
Allende (Jarosewich et al. 1987)

Table 2.1: Anhydrous bulk rock composition of the Tagish Lake samples and comparison with literature data.

		ICP-MS												ICP-AES								INAA							
Element		**1**	**σ**	**2**	**σ**	**TL5b**	**σ**	**TL11h**	**σ**	**TL11i**	**σ**	**TL11v**	**σ**	**TL5b**	**σ**	**TL11h**	**σ**	**TL11i**	**σ**	**TL11v**	**σ**	**TL5b**	**σ**	**TL11h**	**σ**	**TL11i**	**σ**	**TL11v**	**σ**
Ag	ppm	0.21	*0.07*	0.128		0.139	*0.004*	0.16	*0.01*	0.130	*0.001*	0.141	*0.004*																
Al	wt%	0.99	*0.03*			0.82	*0.02*	0.85	*0.02*	0.95	*0.02*	1.02	*0.02*	0.767	*0.008*	0.814	*0.009*	0.816	*0.003*	0.432	*0.001*	1.05	*0.02*	1.05	*0.03*	1.19	*0.03*	1.18	*0.03*
As	ppm	1.74	*0.06*	1.46	*0.02*	2.27	*0.08*	2.20	*0.06*	1.90	*0.07*	1.92	*0.04*									1.44	*0.09*	1.4	*0.2*	1.5	*0.1*	1.2	*0.1*
Au	ppm	0.19	*0.03*	0.14		0.21	*0.03*	0.16	*0.02*	0.118	*0.004*	0.31	*0.02*																
Ba	ppm	7.4	*0.8*	2.77	*0.1*	3.30	*0.07*	3.24	*0.07*	4.57	*0.03*	4.28	*0.02*	3.12	*0.01*	3.15	*0.02*	4.52	*0.04*	4.18	*0.06*								
Be	ppm	0.052	*0.003*			0.01	*0.06*	0.03	*0.06*	0.03	*0.06*	0.030	*0.001*	0.073	*0.007*	0.069	*0.002*	0.074	*0.004*	0.065	*0.006*								
Br	ppm	2.8	*0.2*																			0.37	*0.09*	2.3	*0.2*	4.0	*0.2*	0.7	*0.2*
Ca	wt%	0.99	*0.09*			0.968	*0.005*	0.7117	*0.0005*	1.07	*0.01*	0.86	*0.01*	0.798	*0.009*	0.589	*0.005*	0.888	*0.006*	0.703	*0.003*								
Cd	ppm	0.82	*0.16*	0.408		0.44	*0.01*	0.40	*0.03*	0.38	*0.05*	0.24	*0.02*																
Ce	ppm	0.81	*0.06*	0.75	*0.03*	0.78	*0.03*	0.77	*0.01*	0.84	*0.02*	0.85	*0.02*									≤ 1.3	-	≤ 1.4	-	≤ 1.3	-	≤ 2.0	-
Co	ppm	517	*9*	485	*5.6*	446	*8*	465	*8*	470	*7*	500	*2*	510	*3*	439	*2*	425.4	*0.6*	448	*2*	561	*4*	548	*5*	547	*4*	588	*4*
Cr	ppm	2840	*150*			2395	*13*	2470	*44*	2418	*38*	2827	*23*	2331	*18*	2408	*27*	2356	*17*	2687	*10*	2920	*10*	2890	*10*	2890	*10*	3360	*10*
Cs	ppm	0.146	*0.006*	0.153		0.119	*0.003*	0.129	*0.003*	0.131	*0.005*	0.119	*0.004*																
Cu	ppm	116	*5*	120	*2.2*	97	*4*	99	*1*	96	*1*	106	*2*	89	*1*	100.3	*0.4*	92.9	*0.9*	101	*3*								
Dy	ppm	0.30	*0.04*	0.260	*0.002*	0.26	*0.01*	0.26	*0.01*	0.274	*0.005*	0.29	*0.01*																
Er	ppm	0.20	*0.02*	0.188	*0.001*	0.18	*0.01*	0.19	*0.01*	0.181	*0.005*	0.21	*0.01*																
Eu	ppm	0.072	*0.004*	0.0666	*0.0002*	0.067	*0.001*	0.063	*0.003*	0.070	*0.004*	0.07	*0.01*																
Fe	wt%	19.3	*0.9*			16.6	*0.3*	16.8	*0.3*	17.0	*0.3*	18.5	*0.2*									20	*0.1*	19.7	*0.1*	19.7	*0.1*	21.5	*0.1*
Ga	ppm	8.4	*0.3*	9.29		7.1	*0.3*	7.3	*0.2*	7.1	*0.08*	7.0	*0.2*																
Gd	ppm	0.24	*0.02*	0.25	*0.01*	0.23	*0.01*	0.24	*0.01*	0.24	*0.02*	0.26	*0.02*																
Ge	ppm	30	*2*			21	*1*	22.37	*0.45*	21.47	*0.41*	18.0	*0.1*																
Hf	ppm	0.18	*0.02*	0.134	*0.002*	0.4	*0.2*	0.21	*0.02*	0.17	*0.01*	0.18	*0.02*																
Ho	ppm	0.064	*0.006*	0.0662	*0.0005*	0.060	*0.003*	0.058	*0.003*	0.059	*0.002*	0.067	*0.004*																
Ir	ppm	0.547	*0.01*	0.487	*0.03*	0.414	*0.005*	0.415	*0.006*	0.396	*0.005*	0.460	*0.004*									0.42	*0.02*	0.4	*0.02*	0.4	*0.02*	0.52	*0.02*
K	ppm	650	*50*			301	*2*	375	*6*	398	*8*	285	*3*	291	*8*	365	*3*	392	*5*	263	*5*								
La	ppm	0.33	*0.03*	0.28	*0.02*	0.29	*0.01*	0.285	*0.004*	0.30	*0.01*	0.36	*0.01*									0.372	*0.03*	0.23	*0.05*	0.39	*0.05*	0.45	*0.04*
Li	ppm	2.5	*0.2*	1.2	*0.02*	0.93	*0.06*	0.9	*0.4*	1.6	*0.2*	1.4	*0.5*																
Lu	ppm	0.034	*0.006*	0.033	*0.001*	0.026	*0.001*	0.029	*0.002*	0.027	*0.002*	0.042	*0.005*																
Mg	wt%	10.8	*0.5*			10	*1*	9.4	*0.3*	10.1	*0.3*	11.6	*0.3*									11.1	*0.5*	11.2	*0.5*	11.3	*0.5*	13.0	*0.5*
Mn	ppm	1530	*77*	1470	*15.3*	1360	*22*	1382	*11*	1474	*30*	1561	*12*	1353	*10*	1404	*5*	1463	*15*	1522	*7*	1580	*50*	1620	*50*	1720	*50*	1730	*50*
Mo	ppm	1.13	*0.09*	1.5	*0.01*	1.20	*0.04*	1.50	*0.06*	1.13	*0.05*	1.30	*0.07*	0.58	*0.34*	0.52	*0.11*	0.08	*0.20*	0.11	*0.30*								
Na	ppm	4450	*60*			3404	*113*	3484	*137*	3967	*146*	1909	*33*									871	*6*	4130	*30*	4530	*30*	2190	*20*
Nb	ppm	0.3	*0.2*	0.41	*0.01*	0.54	*0.09*	0.42	*0.02*	0.39	*0.02*	0.42	*0.01*																
Nd	ppm	0.58	*0.03*	0.53	*0.01*	0.57	*0.02*	0.55	*0.01*	0.62	*0.02*	0.61	*0.03*																
Ni	wt%	1.16	*0.08*			0.93	*0.03*	0.99	*0.02*	1.00	*0.01*	1.02	*0.01*	0.861	*0.003*	0.903	*0.004*	0.882	*0.002*	0.887	*0.004*								
Os	ppm	0.46	*0.02*			0.05	*0.01*	0.039	*0.004*	0.046	*0.005*	0.040	*0.006*																
P	ppm	927	*50*			1073	*22*	818	*10*	810	*1*	926	*4*																
Pb	ppm	2.9	*0.8*			1.975	*0.004*	1.76	*0.01*	1.67	*0.01*	1.32	*0.01*	10.7	*0.4*	12.1	*0.1*	10.1	*0.9*	12.5	*0.6*								
Pd	ppm	0.98	*0.09*	0.528	*0.03*	0.61	*0.04*	0.55	*0.03*	0.48	*0.02*	0.51	*0.04*																
Pr	ppm	0.111	*0.007*	0.114	*0.004*	0.123	*0.004*	0.113	*0.003*	0.121	*0.002*	0.125	*0.002*																
Pt	ppm	1.22	*0.05*	0.8	*0.04*	1.45	*0.05*	1.04	*0.01*	0.84	*0.02*	0.81	*0.01*																
Rb	ppm	2	*0.2*	1.63	*0.02*	1.66	*0.09*	1.79	*0.08*	1.67	*0.06*	1.46	*0.02*																
Re	ppm	0.056	*0.004*	0.047	*0.003*	0.030	*0.002*	0.036	*0.003*	0.031	*0.002*	0.037	*0.004*																
Ru	ppm	1.08	*0.09*	1.3	*0.1*	0.61	*0.03*	0.641	*0.004*	0.60	*0.05*	0.68	*0.03*																
Sb	ppm	0.17	*0.03*	0.21		0.178	*0.004*	0.13	*0.01*	0.12	*0.01*	0.13	*0.01*									0.32	*0.03*	0.19	*0.03*	0.27	*0.03*	0.19	*0.03*
Sc	ppm	7.2	*0.3*	8.22	*0.5*																	7.55	*0.15*	7.41	*0.09*	8.1	*0.1*	8.9	*0.2*
Se	ppm	14.3	*0.4*	11.7		9.7	*0.6*	11.5	*0.9*	10.5	*0.8*	9.3	*0.2*	16	*2*	15	*2*	15	*2*	17	*3*	10.1	*0.4*	11.4	*0.4*	11.6	*0.3*	10.8	*0.6*
Si	wt%	11.4	*0.4*																			11.7	*0.3*	11.8	*0.3*	11.9	*0.4*	13.2	*0.3*

Sm	ppm	0.20	*0.02*	0.185	*0.003*	0.17	*0.02*	0.17	*0.01*	0.19	*0.01*	0.19	*0.02*									0.171	*0.005*	0.164	*0.008*	0.186	*0.007*	0.193	*0.007*
Sn	ppm	0.92	*0.09*	1.00	*0.04*	0.97	*0.03*	1.05	*0.03*	0.97	*0.03*	0.81	*0.02*																
Sr	ppm	9.4	*0.5*	8.3	*1.0*	9.1	*0.2*	6.7	*0.1*	10.4	*0.2*	7.9	*0.1*																
Ta	ppm	0.022	*0.006*			1.0	*0.4*	0.38	*0.07*	0.23	*0.03*	0.169	*0.001*																
Tb	ppm	0.049	*0.005*	0.048	*0.4*	0.041	*0.001*	0.040	*0.001*	0.045	*0.002*	0.045	*0.002*																
Te	ppm	1.5	*0.3*	1.35		1.22	*0.03*	1.36	*0.03*	1.22	*0.03*	1.11	*0.06*																
Th	ppm	0.040	*0.008*	0.039	*0.002*	0.4	*0.2*	0.10	*0.02*	0.07	*0.01*	0.060	*0.004*																
Ti	ppm	520	*56*	565	*20.0*	469	*3*	478	*1*	525	*4*	550	*5*	437	*2*	458	*2*	497	*3*	517.8	*0.8*								
Tl	ppm	0.090	*0.004*	0.101		0.094	*0.005*	0.10	*0.01*	0.09	*0.01*	0.103	*0.004*																
Tm	ppm	0.032	*0.002*	0.032		0.028	*0.001*	0.027	*0.003*	0.0298	*0.0004*	0.032	*0.001*																
U	ppm	0.008	*0.004*	0.0094	*0.0005*	0.017	*0.002*	0.015	*0.001*	0.013	*0.002*	0.018	*0.001*																
V	ppm	51	*1*	59	*1.6*	56.4	*0.2*	55.3	*0.2*	57.6	*0.9*	64.3	*0.9*	48	*1*	48.7	*0.2*	50.7	*0.5*	54.3	*0.5*	59	*3*	58	*3*	63	*3*	69	*3*
W	ppm			0.09	*0.01*	0.28	*0.02*	0.36	*0.01*	0.92	*0.02*	0.33	*0.02*																
Y	ppm	1.7	*0.1*	2.13	*0.04*	1.6	*0.1*	1.56	*0.02*	1.55	*0.02*	1.80	*0.02*																
Yb	ppm	0.21	*0.02*	0.185	*0.001*	0.183	*0.004*	0.19	*0.01*	0.18	*0.01*	0.21	*0.01*																
Zn	ppm	253	*9*	187		183	*6*	185	*2*	179	*5*	153	*3*	242.6	*0.5*	256	*1*	249.8	*0.4*	224.3	*0.2*	218	*4*	224	*4*	213	*4*	213	*6*
Zr	ppm	6	*1.3*	6.1	*0.2*	6.6	*0.2*	5.7	*0.1*	4.80	*0.04*	5.7	*0.2*																

1 - Brown et al. (2000)
2 - Friedrich et al. (2002)

Table 2.2: Internal standard replicates.

		ICP-MS Parr bomb						ICP-MS		ICP-AES		Published values for Allende meteorite							ICP-MS Parr bomb			
		GSP-2		SGR-1		BIR-1		Allende														
Element		Aver #	2σ	Aver #	2σ	Aver #	2σ	Aver *	2σ	Aver *	2σ	1	σ	2	σ	3	σ	4	5	blank #1	σ	blank #2	σ
Ag	ppm	0.55	*0.06*	0.25	*0.02*	0.045	*0.002*	0.07	*0.002*											0.055	*0.008*	0.022	*0.001*
Al	wt%	6.0	*0.7*	2.77	*0.04*	6	*1*	1.22	*0.07*	0.56	*0.03*			1.71	*0.05*	1.74	*0.04*	1.7		0.0005	*0.0001*	0.00047	*0.00001*
As	ppm	1.9	*2.0*	56	*1*	0.0	*0.0*	1.5	*0.3*									2.2		0.8	*0.3*	<DL	*<DL*
Au	ppm	0.1	*0.1*	0.08	*0.06*	0.1	*0.1*	0.2	*0.2*			0.26	*0.01*			0.15	*0.01*	0.2		0.22	*0.02*	0.12	*0.04*
Ba	ppm	1141	*136*	279	*99*	5.5	*0.4*	4.4	*0.6*	3.4	*0.3*					4	*1*		8.2	0.053	*0.003*	0.052	*0.008*
Be	ppm	1.29	*0.02*	0.9	*0.2*	0.2	*0.1*	<DL	*<DL*											0.1	*0.1*	0.02	*0.06*
Ca	wt%	1.24	*0.04*	4.8	*0.1*	6.9	*0.6*	1.65	*0.06*	1.24	*0.06*			2.0	*0.2*	1.84	*0.05*	1.8		<DL	*<DL*	<DL	*<DL*
Cd	ppm	0.1	*0.1*	0.9	*0.1*	0.09	*0.04*	0.18	*0.02*					0.19	*0.01*					0.002	*0.01*	0.003	*0.009*
Ce	ppm	385	*32*	30	*0.4*	1.6	*0.1*	1.1	*0.2*					1.25	*0.06*	1.33	*0.08*			0.014	*0.003*	0.0114	*0.0005*
Co	ppm	6.4	*0.4*	11.5	*0.2*	46	*3*	592	*32*	588	*14*	612	*54*	640	*20*	600	*100*	600		0.14	*0.01*	<DL	*<DL*
Cr	ppm	20	*8*	28.34	*0.07*	317	*28*	3229	*122*	2844	100	3900	*100*	3680	*100*	3626	*137*	3626		1.30	*0.06*	0.37	*0.02*
Cs	ppm	1.02	*0.08*	4.6	*0.3*	0.003	*0.002*	0.09	*0.02*					0.11	*0.01*			0.1		<DL	*<DL*	<DL	*<DL*
Cu	ppm	38.8	*0.3*	55.3	*0.2*	103	*5*	77	*11*	45	*4*					119	*19*			0.22	*0.02*	0.62	*0.02*
Dy	ppm	5.0	*0.2*	1.49	*0.01*	2.1	*0.1*	0.36	*0.05*					0.42	*0.02*	0.42	*0.03*			<DL	*<DL*	<DL	*<DL*
Er	ppm	2.3	*0.1*	0.91	*0.02*	1.47	*0.04*	0.24	*0.03*					0.31	*0.02*	0.29	*0.01*			0.0007	*0.001*	0.0003	*0.002*
Eu	ppm	2.3	*0.1*	0.50	*0.04*	0.44	*0.03*	0.09	*0.02*					0.107	*0.005*	0.11	*0.01*			<DL	*<DL*	<DL	*<DL*
Fe	wt%	2.8	*0.2*	1.71	*0.05*	6.0	*0.4*	21.9	*1.5*			24.4	*0.04*	21.9	*0.4*	23.57	*0.08*	23		0.0023	*0.0001*	0.0007	*0.0004*
Ga	ppm	22.08	*0.08*	7.68	*0.07*	13.2	*0.4*	4.9	*0.4*							6	*1*			<DL	*<DL*	<DL	*<DL*
Gd	ppm	13.0	*0.6*	1.93	*0.05*	1.6	*0.1*	0.35	*0.03*					0.43	*0.02*	0.42	*0.02*			0.002	*0.002*	<DL	*<DL*
Ge	ppm	1.7	*0.01*	1.68	*0.06*	1.4	*0.1*	13	*2*											0.04	*0.01*	0.038	*0.002*
Hf	ppm	13.63	*0.03*	1.22	*0.01*	0.580	*0.002*	0.21	*0.10*			0.16	*0.02*			0.21	*0.01*		0.18	0.024	*0.006*	0.012	*0.002*
Ho	ppm	0.83	*0.01*	0.302	*0.003*	0.49	*0.03*	0.08	*0.02*					0.12	*0.01*	0.10	*0.01*			0.001	*0.001*	0.0002	*0.0001*
Ir	ppm	0.0	*0.0*	0.0	*0.0*	0.0	*0.0*	0.57	*0.05*			0.71	*0.03*			0.74	*0.09*	0.5		<DL	*<DL*	<DL	*<DL*
K	wt%	3.9	*0.3*	1.18	*0.02*	0.015	*0.001*	0.029	*0.002*	0.029	*0.002*					0.033	*0.008*	0.06		0.001	*0.0001*	0.002	*0.0001*
La	ppm	153	*8*	15.5	*0.2*	0.49	*0.03*	0.42	*0.08*					0.44	*0.02*	0.52	*0.04*		0.48	0.007	*0.002*	<DL	*<DL*
Li	ppm	33	*5*	113	*10*	2.50	*0.01*	1.0	*0.3*											0.10	*0.02*	0.10	*0.08*
Lu	ppm	0.197	*0.003*	0.1322	*0.0005*	0.21	*0.02*	0.04	*0.01*					0.058	*0.002*	0.052	*0.006*			<DL	*<DL*	<DL	*<DL*
Mg	wt%	0.4	*0.2*	2.27	*0.06*	4.6	*0.7*	11.2	*1.0*							14.8	*0.1*	15		0.000143	0.000006	0.000127	0.000003
Mn	ppm	270	*13*	208	*5*	1031	*60*	1298	*68*	1190	*54*			1450	*40*	1472	*77*	2600		0.22	*0.01*	0.02	*0.01*
Mo	ppm	3	*1*	31	*1*	0.4	*0.3*	1.3	*0.3*									2.3		0.26	*0.06*	<DL	*<DL*
Na	wt%	1.81	*0.09*	1.97	*0.05*	1.06	*0.08*	0.26	*0.02*	0.157	*0.003*	0.33	*0.01*	0.3	*0.1*	0.341	*0.007*	0.5		0.0004	0.000025	0.0004	*0.00001*
Nb	ppm	22.4	*0.3*	5.5	*0.1*	0.57	*0.03*	0.50	*0.16*											0.047	*0.003*	0.028	*0.004*
Nd	ppm	179	*9*	12.2	*0.2*	1.95	*0.07*	0.81	*0.13*					0.91	*0.05*	0.99	*0.03*			0.0004	*0.005*	0.0006	*0.002*
Ni	ppm	16	*5*	26.5	*0.5*	139	*6*	1.21	*0.05*	0.99	*0.04*	1.43	*0.09*			1.42	*0.02*	1.4		0.75	*0.05*	<DL	*<DL*
Os	ppm	0.06	*0.01*	0.041	*0.002*	0.04	*0.01*	0.14	*0.19*									0.6		0.10	*0.02*	0.06	*0.01*
P	wt%	0.11	*0.01*	0.105	*0.002*	0.0074	*0.0006*	0.089	*0.004*							0.105	*0.004*	0.1		0.0027	*0.0005*	0.0028	*0.0002*
Pb	ppm	32	*13*	37.7	*0.9*	3	*2*	1.2	*0.4*	1.2	*0.4*					1.4	*0.3*			0.012	*0.003*	0.008	*0.002*
Pd	ppm	15.11	*0.05*	1.26	*0.01*	0.44	*0.02*	0.73	*0.12*											0.04	*0.01*	0.012	*0.002*
Pr	ppm	49	*3*	3.4	*0.1*	0.31	*0.03*	0.17	*0.03*					0.2	*0.01*	0.21	*0.01*			0.0009	*0.001*	0.0003	*0.0003*
Pt	ppm	0.12	*0.01*	0.02	*0.01*	0.0123	*0.0001*	1.2	*0.2*			1.8	*0.2*							0.005	*0.01*	<DL	*<DL*
Rb	ppm	180	*74*	71	*2*	0.27	*0.25*	0.9	*0.3*					1.3	*0.1*	1.2	*0.1*	1.4		<DL	*<DL*	<DL	*<DL*
Re	ppm	0.003	*0.002*	0.035	*0.001*	0.004	*0.001*	0.05	*0.02*									0.03		0.005	*0.001*	0.003	*0.002*
Ru	ppm	<DL	*<DL*	0.14	*0.01*	0.11	*0.02*	0.78	*0.06*									0.8		<DL	*<DL*	<DL	*<DL*
Sb	ppm	0.31	*0.05*	2.9	*0.2*	0.5	*0.3*	0.057	*0.008*	0.67	*0.12*							0.05		<DL	*<DL*	<DL	*<DL*
Se	ppm	<DL	*<DL*	2.7	*0.4*	<DL	*<DL*			7.52	*3.61*							11		<DL	*<DL*	<DL	*<DL*
Sm	ppm	23	*1*	2.17	*0.06*	0.88	*0.08*	0.24	*0.04*					0.29	*0.01*	0.34	*0.02*		0.3	<DL	*<DL*	<DL	*<DL*

Sn	ppm	5.82	*0.08*	1.38	*0.05*	0.7	*0.3*	0.6	*0.3*							0.29		0.06	*0.03*	0.044	*0.009*
Sr	ppm	200	*4*	337	*3*	94	*4*	13	*2*					12	*3*			0.041	*0.003*	0.0482	*0.0005*
Ta	ppm	0.9	*0.1*	0.40	*0.03*	0.4	*0.1*	0.18	*0.14*									0.040	*0.002*	0.025	*0.003*
Tb	ppm	0.81	*0.02*	0.23	*0.01*	0.297	*0.005*	0.06	*0.02*			0.074	*0.005*	0.08	*0.01*			<DL	*<DL*	<DL	*<DL*
Te	ppm	<DL	*<DL*	<DL	*<DL*	0.02	*0.04*	0.70	*0.11*									0.06	*0.04*	<DL	*<DL*
Th	ppm	97	*8*	4.11	*0.07*	0.083	*0.002*	0.16	*0.2*								0.06	0.019	*0.002*	0.0106	*0.003*
Ti	wt%	0.347	*0.004*	0.127	*0.001*	0.45	*0.02*	0.069	*0.003*	0.059	*0.002*			0.090	*0.006*	0.06		0.00085	0.000032	<DL	*<DL*
Tl	ppm	1.2	*0.1*	0.52	*0.03*	0.0133	*0.0005*	0.09	*0.06*									0.024	*0.001*	0.017	*0.003*
Tm	ppm	0.256	*0.002*	0.125	*0.004*	0.215	*0.003*	0.04	*0.02*			0.049	*0.001*					<DL	*<DL*	<DL	*<DL*
U	ppm	2.27	*0.06*	4.6	*0.02*	0.00944	*0.00001*	<DL	*<DL*								0.015	0.0019	*0.0004*	<DL	*<DL*
V	ppm	45	*3*	111	*2*	266	*11*	86	*2*	85.5	*1.8*	130	*10*	92	*6*			<DL	*<DL*	<DL	*<DL*
W	ppm	0.7	*0.2*	2.7	*0.2*	8	*14*	0.8	*1.8*			0.15	*0.02*	3.1	*0.1*		0.15	0.29	*0.03*	0.18	*0.01*
Y	ppm	21.8	*0.7*	8.2	*0.1*	12.0	*0.7*	2.08	*0.33*			3	*0.1*					<DL	*<DL*	<DL	*<DL*
Yb	ppm	1.6	*0.1*	0.87	*0.05*	1.4	*0.1*	0.27	*0.03*			0.32	*0.02*	0.30	*0.02*			0.002	*0.003*	0.000022	*0.0004*
Zn	ppm	100.4	*0.8*	65	*1*	62	*2*	102	*16*	102	*16*			110	*5*	120		<DL	*<DL*	<DL	*<DL*
Zr	ppm	504	*15*	39	*1*	12.4	*0.4*	5.7	*0.8*			12	*0.7*	9	*3*			0.57	*0.04*	0.15	*0.03*

1 - Allende values from Morgan et al. (1969)
2 - Allende values from Wakita and Schmitt (1970)
3 -Allende values from Jarosewich et al. (1987)
4 -Allende values from Malissa et al. (1972)
5 - Allende values from Babechuk et al. (2010)
- averge is based on 2 replicate analyses of the same powder
* - average is based on 4 replicate analyses of the same powder
< the values is less than detection limit given for a specific element
Note: Allende Ni content is in wt%

Table 2.3: Comparison of Cold Bokkeveld standard replicates by INAA.

Element		KW	INAA	σ
Al	wt%	1.13	1.07	0.03
As	ppm	1.97	1.83	0.14
Br	ppm	4.5	13.9	0.3
Ce	ppm	n/a	$\leq$ 1.8	-
Co	ppm	546	567	4
Cr	ppm	2820	2990	10
Fe	wt%	19.8	20.2	0.1
Ir	ppm	0.54	0.45	0.02
La	ppm	0.28	0.61	0.082
Mg	wt%	11.0	11.2	0.7
Mn	ppm	1565	1580	50
Na	ppm	3910	5120	40
Sb	ppm	0.12	0.548	0.055
Sc	ppm	7.54	7.96	0.07
Se	ppm	11.6	9.2	0.5
Si	wt%	n/a	11.7	0.5
Sm	ppm	0.176	0.182	0.011
V	ppm	69.5	66	4
Zn	ppm	170	176	6

KW - mean of two replicates from Kallemeyn and Wasson (1981)
n/a - not available

CHAPTER 3:

IN-SITU SIMS OXYGEN ISOTOPE MEASUREMENTS OF PYROXENE AND OLIVINE GRAINS IN CHONDRULES FROM THE PRISTINE TAGISH LAKE METEORITE

Alexandra Blinova[1], Christopher D.K. Herd[1], and Richard A. Stern[1,2]

[1]Dept. Earth and Atmospheric Sciences, 1-23 Earth Sciences Building, University of Alberta, Edmonton, Alberta, T6G 2E3, Canada

[2]Canadian Centre for Isotopic Microanalysis (CCIM), University of Alberta, Edmonton, Alberta, T6G 2E3, Canada

3.1 INTRODUCTION

Chondrules are the most common component present in all but one type (CI) of chondritic meteorites. These sub-millimeter-sized, spherical ferromagnesian silicate objects show evidence of an igneous origin and are composed of a mixture of silicates (olivine and pyroxene) with minor oxides, metals and sulfides set in a glassy or altered mesostasis (Brearley and Jones 1996). In this study we look at oxygen composition of chondrules from the pristine samples of the Tagish Lake meteorite. The Tagish Lake meteorite, pristine samples of which were collected just a few days after the fall from a frozen lake surface (Brown et al. 2000), is a brecciated carbonaceous Type 2 chondrite. (Van Schmus and Wood 1967). It consists of several lithological variations containing different chondrule abundances (Zolensky et al. 2002; Izawa et al. 2010; Blinova et al. 2010; Chapter 1). A recent mineralogical, petrological and whole-rock geochemistry study of four pristine Tagish Lake meteorite samples was undertaken, the results of which can be found in (Chapter 1).

Russell et al. (2010) measured the oxygen isotopic composition of individual hand picked olivines and forsterites, and forsterite-rich chondrules from Tagish Lake meteorite specimens, which were collected 3 months after the fall (so-called 'degraded' specimens; Brown et al. 2000), using a laser-fluorination method. Oxygen isotopic

compositions of the picked anhydrous mineral fractions (isolated matrix forsterite and olivine grains, and chondrules) define a line similar to the trend of other carbonaceous chondrites. Within these data the isolated matrix forsterite grains ($Fo_{99.6-99.8}$) are ^{16}O-rich compared to bulk chondrules, which overlap with both isolated matrix olivine ($Fo_{39.6-86.8}$) and forsterite grains. These authors speculated that the isolated matrix forsterite grains resemble refractory grains and formed from a condensed melt under conditions similar to the ones found in CM, while the isotopic composition of isolated matrix olivine grains is suggestive of formation from an evolving melt with ^{16}O-depleted gases.

Leshin et al. (2001) presented oxygen data for olivine and carbonate separates also from the 'degraded' Tagish Lake samples. They obtained a similar correlation as in other carbonaceous chondrites between the O-composition and mineral chemistry in that the more Mg-rich olivines tend to be more ^{16}O-rich. These authors also found that forsterites in the Tagish Lake meteorite are more ^{16}O-enriched than typical chondrules and isolated olivines from other carbonaceous chondrites.

A parallel study was conducted by Engrand et al. (2001) on the olivines, pyroxenes, calcium carbonates and matrix *in-situ* in the thick section of the Tagish Lake meteorite. In this study two of the most ^{16}O enriched olivine aggregates ($\delta^{17}O$ = -43.8‰ and -43.9‰, and $\delta^{18}O$ = - 43.3‰ and -41.4‰) thus far found in this meteorite, including the present study, were analyzed. The majority of the olivine data, which they called "normal", are compatible with values previously measured in other carbonaceous chondrites. However, these authors did not observe a correlation between Fo content and oxygen isotopic composition. Their pyroxene data show a bimodal distribution, and plot close to the Young and Russell line (Young et al. 1998) and oxygen composition of the Tagish Lake matrix. Although these authors were unable to discriminate between a CI1 and CM2 classification, their discovery of the extremely ^{16}O enriched olivines suggests a common chemical process for calcium aluminum inclusions (CAIs) and these olivines.

In this study we examine olivines and pyroxenes *in-situ* in two chondrules from two mineralogically different Tagish Lake meteorite specimens. Our aim is to compare chondrule oxygen isotopic compositions of these two different specimens to each other in order to understand the formation conditions of these chondrules. In addition, our results will assist in comparing and understanding the data from previous Tagish Lake oxygen studies. We also propose that the oscillatory zoned olivine found in TL11i chondrule is a product of changes in redox conditions in the Solar nebula.

3.2 SAMPLES AND METHODS

Two pristine Tagish Lake samples, TL5b and TL11i, were studied in detail for mineralogy and whole-rock bulk geochemistry and reported elsewhere (Chapter 1). In summary, specimen TL5b contains the most abundant number of chondrules up to 500 μm diameter set in a phyllosilicate-rich matrix. The more altered specimen TL11i contains fewer chondrules and is dominated by an altered matrix.

In this study we used a JEOL 8900 Superprobe and a Cameca SX100 located in the Department of Earth and Atmospheric Sciences at the University of Alberta for major and trace element analysis of olivines and pyroxenes in the studied chondrules. Both instruments were operated using a 1 to 2 μm diameter focused electron beam with a current of 20 nA and an accelerating voltage of 20 kV. As external standards for both instruments we used natural and synthetic minerals: chromite, albite, diopside, forsterite (Mg#93), Ni mental (synthetic), rutile, sanidine, tugtupite, hematite and willemite from the University of Alberta collection; and apatite, fayalite, ilmenite and pyrope from the Smithsonian Institute collection (Jarosewich 2002). The Phi-rho-Z correction algorithm was used to correct the electron microprobe data. The instrument calibration was deemed successful when the composition of standards was reproduced within the error margins defined by the counting statistics. A Zeiss EVO MA 15 scanning electron microscope (SEM) housed at the Canadian Centre for Isotopic Microanalysis (CCIM), was used for mapping the compositional heterogeneity of olivine and pyroxene with backscattered electrons and cathodoluminescence (ETP Semra, Pty. Ltd).

Oxygen isotope composition (^{18}O, ^{17}O, and ^{16}O) were determined in olivine and enstatite by secondary ion mass spectrometry (SIMS) using a Cameca IMS1280 ion microprobe CCIM. Three 25 mm diameter epoxy mounts were prepared containing the Tagish Lake samples and olivine or enstatite reference materials (RM). First mount contained the TL5b chondrule mounted along with the CCIM olivine (Fo_{93}) RM S0013D ($\delta^{18}O_{VSMOW}$=+5.26; R. Stern, unpublished data), and S0103 olivine (Fo_{74}) RM ($\delta^{18}O$ =+5.2, sample CI114 from Bindeman et al. 2008). The $\delta^{17}O$ values for these RMs were not independently known, but assumed to have a composition determined by a terrestrial fractionation curve $\delta^{17}O = 0.52 \times \delta^{18}O$ (Clayton 1993). The VSMOW ratios utilized for normalization were $^{18}O/^{16}O = 0.0020052$ and $^{17}O/^{16}O = 0.0003759$. The second mount contained the TL11i zoned olivine chondrule and RM S0013D olivine. The third mount

containing TL5b chondrule enstatite. was co-mounted with grains of enstatite RM S0170 ($\delta^{18}OV_{SMOW}$ =+5.64; R. Stern, unpublished data). All mounts were coated with 25 nm Au for SIMS analysis.

The primary beam consisted of 3 – 4 nA of $^{133}Cs^+$ having 20 keV impact energy, and focussed to a 15 micron diameter spot. The entrance slit used was 80 µm wide, and the field aperture 4x4 mm. A 50 eV energy window was utilized, rejecting a small fraction of high energy ions. The three oxygen isotopes were measured simultaneously in Faraday cups, namely at detector positions L'2, FC2, and H1, for $^{16}O^-$, $^{17}O^-$, and $^{18}O^-$, respectively. An exit slit width of 180 or 190 µm was selected for $^{17}O^-$, giving a mass resolution (m/Δm @10% peak height) of >4800, sufficient to resolve $^{16}O^1H$. For $^{16}O^-$ and $^{18}O^-$, the mass resolution using 500 µm exit slits was 1900 and 2350, respectively. Experiments were initiated with a 30 s raster of a rectangular area slightly larger than the primary spot, to clean the region of interest and to implant Cs^+. Subsequently, the $^{16}O^-$ transmission in the transfer section was optimized by an automated tuning routine, and then the three isotopes determined simultaneously by counting for 5 s x 30 or 40 cycles. Count rates (counts/s) were typically 3 x 10^9, 1 x 10^6, and 7 x 10^6 for $^{16}O^-$, $^{17}O^-$ and $^{18}O^-$, respectively, and typical within-spot counting uncertainties (±1 standard error) were ~ ±0.05–0.1‰ for $^{18}O^-/^{16}O^-$ and ±0.15–0.3 ‰ for $^{17}O^-/^{16}O^-$.

The instrumental mass fractionation (IMF) of $^{18}O^-/^{16}O^-$ and $^{17}O^-/^{16}O^-$ measured in S00113D olivine ranged from +2‰ to +6‰ and +9‰ to +10‰, respectively, and for enstatite was +5 ‰ and +11 ‰. It should be noted that the relative IMF values of $^{18}O^-/^{16}O^-$ and $^{17}O^-/^{16}O^-$ are of no significance, as they were not accurately calibrated because the IMF for the two ratios is independently measured and individually applied to the unknowns. A matrix effect due to varying Fo content was determined from analysis of S0013D and S0103 olivine during the analysis of the mount if both materials were available, or separately in another mount. The matrix effect for the IMF for $^{18}O^-/^{16}O^-$ $\delta^{18}O$ ranged from +0.02 – 0.05 ‰/Fo unit (0.03 is considered the typical value), and we assumed that the affect on $^{17}O^-/^{16}O^-$ was 0.52x that value. These values are higher than previously reported using similar instrumentation although slightly different transmission conditions (e.g., Bindeman et al. 2008), but the reason for this difference is currently unknown. Data for unknowns were corrected accordingly using the measured matrix effect and Fo contents determined from the same spots by Cameca SX100 EDS after SIMS analysis. Further evaluation of the Fo-related matrix effect is required using a wider compositional range of olivines, and with varying instrument conditions.

Uncertainties propagated to the final value of the unknowns include the within-spot counting uncertainties and the repeatability (~ standard deviation) of the ratios measured for the RMs, but do not include uncertainties in the matrix correction, estimated to potentially add up to ±0.2 ‰ for some spots. The 95% confidence uncertainties for $\delta^{18}O_{VSMOW}$ and $\delta^{17}O_{VSMOW}$ reported are ±0.2–0.3‰ and ±0.5 –1.3‰, respectively. The uncertainties in the values for $\Delta^{17}O$ (= $\delta^{17}O$ – 0.52 x $\delta^{18}O$; Clayton 1993) propagate uncertainties in both ratios.

3.3 RESULTS

3.3.1 Mineralogy of chondrules

3.3.1.1 TL5b chondrule

This is the largest (2000 μm in diameter) intact chondrule so far observed in the Tagish Lake meteorite. It was found in the least altered, chondrule-rich Tagish Lake specimen, TL5b (Chapter 1). The chondrule is a porphyritic, type IAB (Fe-poor; McSween 1977) dominated by olivine and two types of pyroxene and olivine set in an altered mesostasis (Fig. 3.1). The majority of pyroxene (~85%) are $En_{95.2\text{-}96.0}Fs_{3.6\text{-}4.2}Wo_{0.4\text{-}0.6}$ composition (Table 3.1; Fig. 3.2), and the remainder are Ca-rich pyroxenes with the composition of $En_{52.6\text{-}59.7}Fs_{5.8\text{-}7.0}Wo_{33.8\text{-}40.9}$ (Table 3.1; Fig. 3.2). Olivine composition is $Fo_{95.4\text{-}99.6}Fa_{0.5\text{-}4.5}$ (Table 3.1; Fig. 3.2). On Mg and Si maps (Fig. 3.1b, c) the majority of olivines are located around the perimeter of the chondrule (grains in red colour in Fig. 3.1b and green in colour in Fig. 3.1c). Enstatite dominates the chondrule (grains in green colour in Fig. 3.1b and yellow in colour in Fig. 3.1c), while Ca-rich pyroxenes are interspersed among the enstatite grains (grains in yellow colour in Fig. 3.1d). Three chromite grains were also observed in the chondrule.

3.3.1.2 TL11i chondrule

The more altered specimen TL11i contains fewer chondrule-like objects and is dominated by altered matrix (Chapter 1). This specimen contains a porphyritic chondrule with zoned olivines, type IIA (Fig. 3.3). The largest olivine (marked as "5" in Fig. 3.3b) has a euhedral shape and exhibits oscillatory zoning ($Fo_{70\text{-}79}$) (Fig. 3.4 and Table 3.2). The zoning is parallel to the crystal sides and ranges in thickness from a few microns (edges) to hundreds of microns (the core). The gradation between more Fe-rich and more Mg-rich zones is more diffuse than sharp, especially the core of the grain, which appears to be patchy. Other olivine grains are subhedral and exhibit normal zoning from Mg-rich cores

(Fo_{79-99}) to Fe-rich rims (Fo_{61-74}). One grain (marked as "4" in Fig. 3.3) has a Mg-rich core ($Fo_{98.63}$) (Table 3.2) and is readily visible in backscattered electrons (Fig. 3.3b) and cathodoluminesce. All olivines have a similar fayalitic outer edge (Fa < 40), which can be seen as a high brightness rim only a few microns in thickness around all grains in BSE image. The rest of the chondrule is extensively altered and dominated by phyllosilicates and sulfides. The chondrule is broken on one side (Fig. 3.3a). The chondrule rim, which is comprised of fine-grained phyllosilicates and sulfides, varies in thickness, however, surrounds the whole chondrule even at the broken area.

3.3.2 Oxygen isotopes

Within the TL5b chondrule, we analyzed 14 distinct olivines with one to four analyses per grain and 12 distinct enstatite grains with one analysis per grain. On a three-O isotopic plot, olivine data form a cluster just to the left of carbonaceous chondrite anhydrous mineral (CCAM) line and spread out by half a unit more in $\delta^{17}O$ than in $\delta^{18}O$ (Fig. 3.5 and 3.6). Average olivine $\Delta^{17}O$ is -2.6‰ (± 0.3) and mean $\delta^{17}O$ and $\delta^{18}O$ are -1.7‰ (± 0.3) and 1.7‰ (± 0.2), respectively (Table 3.3). Enstatite data overlap with olivine data but are more spread out in the $\delta^{18}O$ direction. Average enstatite $\Delta^{17}O$ is -2.07‰ (± 0.19), mean $\delta^{17}O$ is -1.57‰ (±0.09) and $\delta^{18}O$ is 0.97‰ (±0.31) (Table 3.3).

We analyzed seven zoned olivine grains in the TL11i chondrule (Fig. 3.3). Fourteen data points out of 22 are reliable and are presented in Table 3.3. Eleven analyses of olivines with Fo_{60-79} (Table 3.3) are more $^{17,18}O$-enriched than TL5b and make a scattered cluster (mean $\delta^{17}O$ = 1.0 ± 0.3 ‰ and $\delta^{18}O$ = 5.25 ± 0.54 ‰) that fall on the CCAM line (Fig. 3.5 and 3.6). These analyses have an average $\Delta^{17}O$ of -1.73 (± 0.22). Three other grains have ^{16}O-enriched cores (Fig. 3.5). One of these olivine grains (marked as "4" in Fig. 3.3 and 3.5) contains a core with diffuse boundaries and shows the most extreme core to rim variations in Fo content and $\Delta^{17}O$ differences amongst all zoned olivine grains. In this grain the core (Fo_{98}) has $\Delta^{17}O$ = -8.6 (± 0.68) and mean $\delta^{17}O$ and $\delta^{18}O$ of -11.3‰ (± 0.34) and -14.4‰ (± 0.6), respectively. The rim (Fo_{71}) has $\Delta^{17}O$ = -1.9 (± 0.62) and mean $\delta^{17}O$ and $\delta^{18}O$ of 5.5‰ (± 0.18) and 1.0‰ (± 0.6), respectively. Another ^{16}O-enriched grain (marked as "6" in Fig. 3.3 and 3.5) has Fo_{90} core and a similar $\Delta^{17}O$ of -8.3 (± 1.73) to the Fo_{98} core, although different mean $\delta^{17}O$ and $\delta^{18}O$ of -10.5‰ (± 1.19) and -13.8‰ (± 1.3), respectively. These two grains fall at the ^{16}O-enriched end of the CCAM line relative to the grain marked as "7" (Fig. 3.5). This latter grain falls exactly between the $^{17,18}O$-enriched eleven grains and ^{16}O-enriched grains (Fig. 3.5). It

has a similar core of Fo_{90} to the grain "7" but a different $\Delta^{17}O$ of -4.9 (± 0.73) and mean $\delta^{17}O$ and $\delta^{18}O$ of -5.9‰ (± 0.7) and -2.0‰ (± 0.15).

3.4 DISCUSSION

3.4.1 Oxygen variations in the Tagish Lake chondrules

It has been shown elsewhere that minerals from the most ferromagnesian chondrules from primitive chondrites are usually isotopically uniform within 2-3 ‰ in $\Delta^{17}O$ (Krot et al. 2006). Within chondrules there are some types that are more enriched in ^{16}O relative to others (e.g., Al-rich chondrules vs. type II or Fe-rich) (Connolly et al. 2003). Such ^{16}O-rich chondrules usually contain relict calcium-aluminum inclusions (CAIs); however, most of the carbonaceous chondrite chondrules are depleted in ^{16}O compared to amoeboid olivine aggregates (AOAs) and CAIs, which have $\Delta^{17}O < -20$ ‰ (Krot et al. 2006).

The majority of olivine grains in these two chondrules in Tagish Lake are similar to each other in $\Delta^{17}O$ despite the difference in Mg# (Fo_{97} in TL5b and $Fo_{60\text{-}79}$ in TL11i) (Fig. 3.7). There is, however, a noticeable variation in $\Delta^{17}O$ (~ 8 ‰) within a single TL11i chondrule. The major variation is seen between Mg-zoned olivine grains and forsteritic ^{16}O-enriched cores. One of these grains (#4) also cathodoluminesces (CL), which was suggested to be characteristic of primitive condensates (Steele 1986, 1989; Jones and Scott 1989; Alexander 1994). Based on the enrichment in ^{16}O and presence of CL we consider this grain as "relict". The relict grains are thought to represent the fragments of early generation of chondrules that were enriched in ^{16}O (Krot et al. 2006; Steele 1986).

The rest of the zoned olivines from TL11i and normal olivines from TL5b show similar variation in oxygen (~2 ‰) as other minerals in ferromagnesian chondrules from primitive chondrites (Krot et al. 2006). Engrand et al. (2001), however, analyzed extremely ^{16}O enriched olivine aggregate in the Tagish Lake meteorite with enrichment up to – 22 ‰ in $\Delta^{17}O$ (Fig. 1.8), which is equivalent to variations seen in CV3 and CM2 chondrites (Hiyagon and Hashimoto 1999). With a few exceptions (Kobayashi et al. 2003), such large variations in oxygen composition in chondrules from a single primitive carbonaceous chondrite are rarely observed (Clayton 1993).

The previously published oxygen data on this meteorite showed that the range of variations observed (Fig. 1.8) in this meteorite covers the oxygen isotopic composition seen in all other carbonaceous chondrites (Engrand et al. 2001). Our data corroborates

this conclusion. Such variation found in one meteorite suggests that the parent asteroid sampled the material from different oxygen isotope reservoirs, perhaps ^{16}O-rich and ^{17}O-rich gaseous reservoirs (e.g. Scott and Krot 2001; Yurimoto and Kuramoto 2004). The existence of relict forsteritic cores, which have a different oxygen composition than the rims that surround them, also suggests that the relict cores first condensed in a more reduced nebular environment prior to their accretion into a chondrule. In contrast, the rims around these cores formed later in a ^{16}O-depleted environment, perhaps concurrently with other zoned olivine grains during melting and formation of this chondrule. In addition, the similar variations in Δ^{17}O composition in the majority of olivines and pyroxene from such mineralogically different Tagish Lake specimens (Chapter 1) indicate that overall these two chondrules were formed in similar nebular environments prior to their incorporation into the Tagish Lake parent body.

3.4.2 Formation of TL11i chondrule with zoned olivines

In terrestrial settings zonation in major, minor and trace elements, especially oscillatory zoning, is common (e.g. Shore and Fowler 1996; Holten et al. 2000). In magmatic systems oscillatory zonation usually implies an open system with either an intermittent recharge of a more evolved magma chamber with more primitive melts or fluctuations in P-T conditions of the magmatic chamber (Holten et al. 2000). In some cases the crystal growth and thermal and chemical diffusion of the boundary layer, which surrounds the growing crystal, will lead to oscillatory zonation (Shore and Fowler 1996). Shore and Fowler (1996) also noted that oscillatory zoning in aqueous systems is formed in response to fluctuations in redox conditions.

It is believed that chondrules formed by melting of chondrule precursors such as aggregates of fine-grained matrix-like material and coarse-grained components including fragments of CAIs, AOAs and chondrules of earlier generations (Krot et al. 2009). This is thought to have happened during multiple transient flash-heating events, possibly by shock waves, in a dusty, inner solar nebula; however, the conditions of this process still remain unclear (e.g., Shu et al. 1996, 2001; Desch and Connolly 2002; Scott and Krot 2003; Krot et al. 2009). Nonetheless, it is evident that they formed in an isotopically distinct region, at lower ambient temperatures, and higher total pressure and/or dust/gas ratio than CAIs and AOAs (Krot et al. 2009).

Despite the fact that chondrules formed from a melt, the compositional variations such as oscillatory zoning caused by fractional crystallization are difficult to produce within

grains due to chondrule's small size, rapid melting and crystallization rates (e.g., Yurimoto and Wasson 2002; Hua et al. 2003). Therefore, oscillatory zoning in chondrule minerals is uncommon (Jones 1990; Steele 1995; Hua et al. 2003). In fact, only Hua et al. (2003) reported comparable oscillatory zoning in major (Fe and Mg) elements in an olivine from CM2 Lewis Cliff 90500. This olivine, however, is a solitary grain in the matrix with a fine-grained rim around it, whereas TL11i oscillatory zoned olivine is a part of a complex chondrule that contains other olivines with normal zoning and relict grains.

Let us suppose that TL11i oscillatory zoned olivine formed via solid-state diffusion between the grain and the surrounding medium as suggested by Hua et al. (2003). It has been shown that the interdiffusion of major elements (e.g. Mg and Fe) is a function of composition, temperature, and oxygen fugacity (e.g. Buening and Buseck 1973; Nakamura and Schmalzried 1984; Chakraborty 1997). Hua et al. (2003) proposed that fluctuations in temperature and oxygen fugacity would lead to oscillation in composition similar to the ones seen in the olivine grain from CM2 Lewis Cliff 90500. It is possible that TL11i oscillatory zoned olivine formed in a similar nebular environment at high temperatures and fluctuating oxygen fugacity prior to its incorporation into the TL11i chondrule. However, both oscillatory and normally zoned TL11i chondrule olivines, with the exception of relict grains, all plot in the same cluster on the three-O plot (Fig. 3.6; Table 3.3). Therefore, all TL11i chondrule olivines formed in the same oxygen reservoir. Yet, we find oscillations in the olivine composition, which tells us that parts of that oxygen reservoir underwent varying redox conditions. We consider this scenario is the most likely one for the formation of the oscillatory zoned olivine.

An alternative chondrule formation model, specifically for formation of porphyritic olivine chondrules (type I), is the inheritance of components from differentiated planetesimals of earlier generations (e.g. Libourel and Krot 2007). Such a model could explain the igneous textures, such as triple-junction, found among olivines in some chondrules (e.g. Vigarano, CV3). It is possible also that this oscillatory zoned olivine grain is an impact-ejected grain from a magmatic environment on a differentiated planetary body from an earlier generation (e.g., Libourel and Krot 2007). Such a scenario implies that this grain grew in a magma chamber on a partially molten planetesimal in a similar fashion to terrestrial magmatic oscillatory zoned grains. Then a collision with another asteroid body ejected the grain into a turbulent nebular environment in close proximity to a partially liquid TL11i chondrule with normally zoned olivine grains growing inside. Although this scenario could also explain the similarity in $\Delta^{17}O$ and

difference in zoning seen in olivines within one chondrule, it might be more challenging to explain an ejection of a single igneous grain than the nebular formation of the same grain.

Subsequently in both scenarios the oscillatory grain was incorporated into the chondrule while the mesostasis was still liquid and equilibrated with it similar to other zoned olivines. This is supported by the fact that the outer edge on all olivines in this chondrule has the same fayalitic composition. Once all olivines equilibrated with it, the mesostasis solidified and was later altered by a parent body processes to form sheet silicates.

3.5 CONCLUSIONS

We analyzed oxygen isotopes in olivines and pyroxenes *in-situ* in two chondrules from two Tagish Lake lithologies, TL5b and TL11i.

(1) The majority of olivines, with the exception of relict cores, and pyroxenes in both chondrules show similar oxygen variation to each other and to other anhydrous silicates in ferromagnesian chondrules from primitive chondrites. Therefore, these two chondrules from two mineralogically different Tagish Lake specimens formed in the same nebular environment.

(2) The relict cores are found only in TL11i complex type IIA chondrule. These show enrichment in ^{16}O relative to other olivines and formed in a reducing environment prior to their incorporation to the chondrule, whereas the rims formed later from a more oxidized melt..

(3) The oscillatory zoned olivine could be a product of changes in redox conditions from the same nebular environment as the normally zoned olvines. And alternative scenario it is an impact-ejected grain, which formed on an earlier generation of planetesimals in the same oxygen reservoir prior to its accretion into the TL11i chondrule.

(4) Overall, our results provides additional points onto the Tagish Lake oxygen isotope “field” that covers the range of oxygen variations observed in all other carbonaceous chondrites.

3.6 REFERENCES

Bindeman, I., Gurenko, A., Sigmarsson, O., and Chaussidon, M. 2008. Oxygen isotope heterogeneity and disequilibria of olivine crystals in large volume Holocene basalts from Iceland: Evidence for magmatic digestion and erosion of Pleistocene hyaloclastites. Geochimica et Cosmochimica Acta 72:4397-4420.

Blinova, A.I., Zega, T.J., Herd, C.D.K., and Stroud, R.M. (submitted). Testing variations within the Tagish Lake meteorite – I: Mineralogy and petrology of pristine samples. Meteoritics and Planetary Science.

Blinova, A., Herd, C.D.K., and Matveev, S. 2010. Chondrules in the Tagish Lake meteorite: Lithological variations. Meteoritics and Planetary Science 45:A17-A17.

Brearley, A. J. and Jones, R. 1998. Chondritic meteorites. In *Planetary materials* (ed. J. J. Papike) Mineralogical Society of America, Washington D.C., USA. pp. 3-1 - 3-398.

Brown, P. G., Hildebrand, A. R., Zolensky, M. E., Grady, M., Clayton, R. N., Mayeda, T. K., Tagliaferri, E., Spalding R., MacRae, N. D., Hoffman, E. L., Mittlefehldt, D. W., Wacker, J.F., Bird, J. A., Campbell, M. D., Carpenter, R., Gingerich, H., Glatiotis, M., Greiner, E., Mazur, M. J., and McCausland, P. J. A. 2000. The fall, recovery, orbit, and composition of the Tagish Lake Meteorite: A new type of carbonaceous chondrite. Science 290(5490):320.

Buening, D.K., and Buseck, P.R. 1973. Fe-Mg lattice diffusion in olivine. Journal of Geophysical Research 78:6852-6862.

Chakraborty, S. 1997. Rates and mechanisms of Fe-Mg interdiffusion in olivine at 980 degrees-1300 degrees C. Journal of Geophysical Research-Solid Earth 102:12317-12331.

Clayton, R.N. 1993. Oxygen isotopes in meteorites. Annual Review in Earth and Planetary Science 21:115-149.

Clayton, R. N. 2003. Oxygen isotopes in the solar system. Space Science Review

106(14):19-32.

Clayton, R. N., Grossman, L., and Mayeda, T. K. 1973. Component of primitive nuclear composition in carbonaceous meteorites. Science 182(4111):485-488.

Connolly, H. C., Weisberg, M. K., and Huss, G. R. 2003. On the nature and origins of FeO-rich chondrules in CR2 chondrites: a preliminary report (abstract #1770). 34th Lunar and Planetary Science Conference. CD-ROM.

Desch, S. J. and Connolly, H. C. 2002. A model of the thermal processing of particles in solar nebula shocks: Application to the cooling rates of chondrules. Meteoritics and Planetary Science 37(2):183-207.

Engrand, C., Gounelle, M., Duprat, J., and Zolensky, M.E. 2001. In-situ oxygen isotopic composition of individual minerals in Tagish Lake, a unique type 2 carboneceous chondrite (abstract #1568). 32nd Lunar and Planetary Science Conference. CD-ROM.

Hiyagon, H., and Hashimoto, A. 1999. 16O excesses in olivine inclusions in Yamato-86009 and Murchison chhondrites and their relation to CAIs. Science 283(5403):828-831.

Holten, T., Jamtveit, B. and Meakin, P. 2000. Noise and oscillatory zoning of minerals. Geochimica et Cosmochimica Acta 64:1893-1904.

Hua, X., Li, J. and Buseck, P.R. 2003. Oscillatory zoned fayalitic olivine from the Lewis Cliff 90500 CM2 meteorite. Geochimica et Cosmochimica Acta 67:2201-2211.

Izawa, M.R.M., Flemming, R.L., King, P.L., Peterson, R.C. and McCausland, P.J.A. 2010. Mineralogical and spectroscopic investigation of the Tagish Lake carbonaceous chondrite by X-ray diffraction and infrared reflectance spectroscopy. Meteoritics and Planetary Science 45:675 - 698.

Jarosewich, E. 2002. Smithsonian Microbeam Standards. Journal of Research National Institute of Standards and Technology 107:681-685.

Leshin, L.A., Farquhar, J., Guan, Y., Pizzarello, S., Jackson, T. and Thiemens, M.H. 2001. Oxygen isotopic anatomy of Tagish Lake: Relationship to primary and secondary minerals in CI and CM chondrites (abstract #1843). 32nd Lunar and Planetary Science Conference. CD-ROM.

Libourel, G. and Krot, A.N. 2007. Evidence for the presence of planetesimal material among the precursors of magnesian chondrules of nebular origin. Earth and Planetary Science Letters 254:1-8.

McSween, H.Y. 1977. Carbonaceous chondrites of the Ornans type: metamorphic sequence. Geochimica et Cosmochimica Acta 44:477-491.

Nakamura, A. and Schmalzried, H. 1984. On the Fe^{2+}-Mg^{2+}- interdiffusion in olivine. 2. Berichte Der Bunsen-Gesellschaft-Physical Chemistry 88:140-145.

Russell, S.D.J., Longstaffe, F.J., King, P.L. and Larson, T.E. 2010. The oxygen-isotope composition of chondrules and isolated forsterite and olivine grains from the Tagish Lake carbonaceous chondrite. Geochimica et Cosmochimica Acta 74:2484-2499.

Scott, E.R.D. and Krot, A.N. 2001. Oxygen isotopic compositions and origins of calcium-aluminum-rich inclusions and chondrules. Meteoritics and Planetary Science 36:1307-1319.

Shore, M. and Fowler, A.D. 1996. Oscillatory zoning in minerals: A common phenomenon.Canadian Mineralogist 34:1111-1126.

Steele, I.M. 1986. Compositions and textures of relic forsterite in carbonaceous and unequilibrated ordinary chondrites. Geochimica et Cosmochimica Acta 50:1379-1395.

Steele, I.M. 1989. Compositions of isolated forsterites in Ornans (C3O). Geochimica et Cosmochimica Acta 53:2069-2079.

Van Schmus, W.R. and Wood, J.A. 1967. A chemical-petrological classification for the chondritic meteorites. Geochimica et Cosmochimica Acta 33:747-765.

Yurimoto, H. and Kuramoto, K. 2004. Molecular cloud origin for the oxygen isotope heterogeneity in the solar system. Science 305:1763-1766.

Zolensky, M.E., Nakamura, K., Gounelle, M., Mikouchi, T., Kasama, T., Tachikawa, O. and Tonui, E. 2002. Mineralogy of Tagish Lake: An ungrouped type 2 carbonaceous chondrite. Meteoritics and Planetary Science 37:737-761.

FIGURE CAPTIONS CHAPTER 3:

Figure 3.1:
(a) Back-scattered electron image of the TL5b chondrule; (b) Mg X-ray map (olivines are in red, pyroxenes are in green); (c) Si X-ray map; and (d) Ca X-Ray map (Ca-rich pyroxene is prominent).

Figure 3.2:
Compositional diagrams showing (a) Mg-Fe-Ca pyroxene compositions and (b) the Mg-Fe range of olivines in the TL5b chondrule.

Figure 3.3:
(a) Back-scattered electron (BSE) image of TL11i chondrule. Box refers to figure 4; (b) BSE image with marked olivine grains that were measured by SIMS. The approximate pit locations based on (c) are outlined in yellow.

Figure 3.4: A back-scattered close-up image of the zoning in the grain "5" from the TL11i chondrule.

Figure 3.5:
Oxygen isotopic composition of olivine and pyroxene grains from TL5b and TL11i chondrules on $\delta^{17}O$ vs. $\delta^{18}O$. CCAM - Carbonaceous chondrite anhydrous mineral; Y&R - Young and Russell (1998) line; TFL – Terrestrial fractionation line. Error bars are 2σ. Numbers refer to grain numbers in Figure 3.3.

Figure 3.6:
A close-up of Fig. 3.5 showing oxygen isotopic composition of minerals in TL5b and TL11i chondrules.

Figure 3.7:
Composition of olivines (Mg#) versus $\Delta^{17}O$ in TL5b and TL11i chondrules. Error bars are 2σ.

Figure 3.8:

Comparison of oxygen isotopic composition of minerals (olivine and pyroxene) from Tagish Lake meteorite from this study and literature. Symbols for Tagish Lake samples from this study are the same as in Fig. 3.5. Blue field – Tagish Lake matrix (Engrand et al. 2001); Pink field – Tagish Lake bulk (Engrand et al. 2001); Green field – Tagish Lake carbonates (Engrand et al. 2001). CCAM - Carbonaceous chondrite anhydrous mineral; Y&R - Young and Russell (1998) line; TFL – Terrestrial fractionation line. Error bars are 2σ.

Figure 3.1

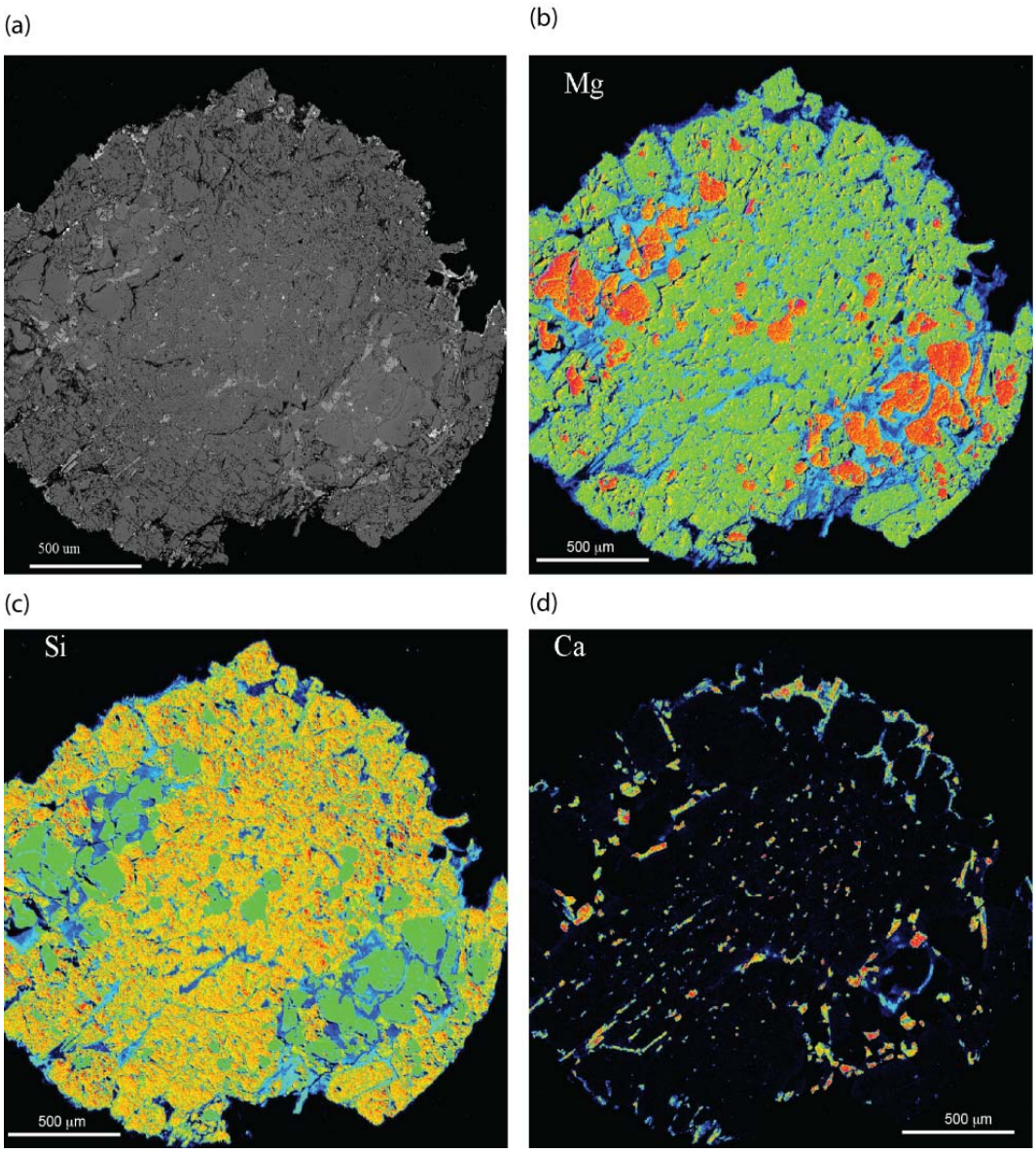

Figure 3.2

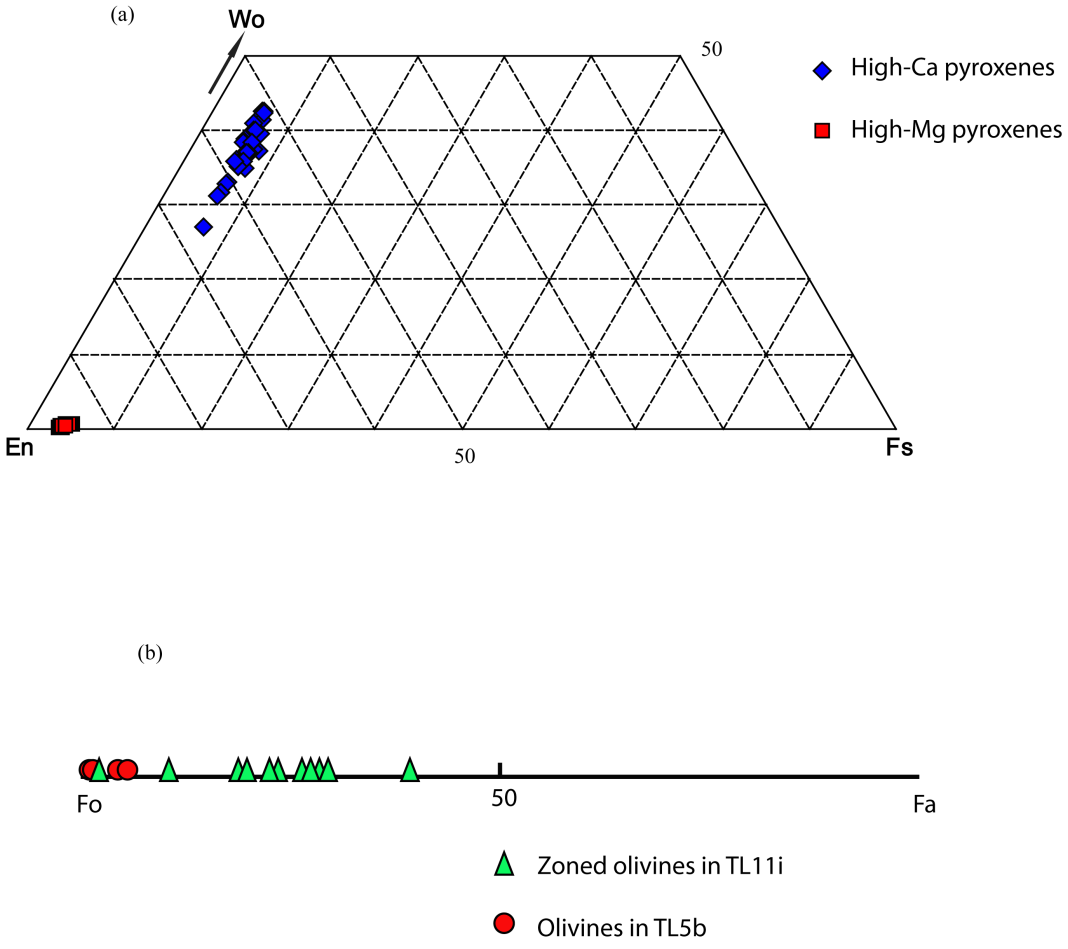
(a)
Wo
50
High-Ca pyroxenes
High-Mg pyroxenes
En
50
Fs
(b)
Fo
50
Fa
Zoned olivines in TL11i
Olivines in TL5b

Figure 3.3

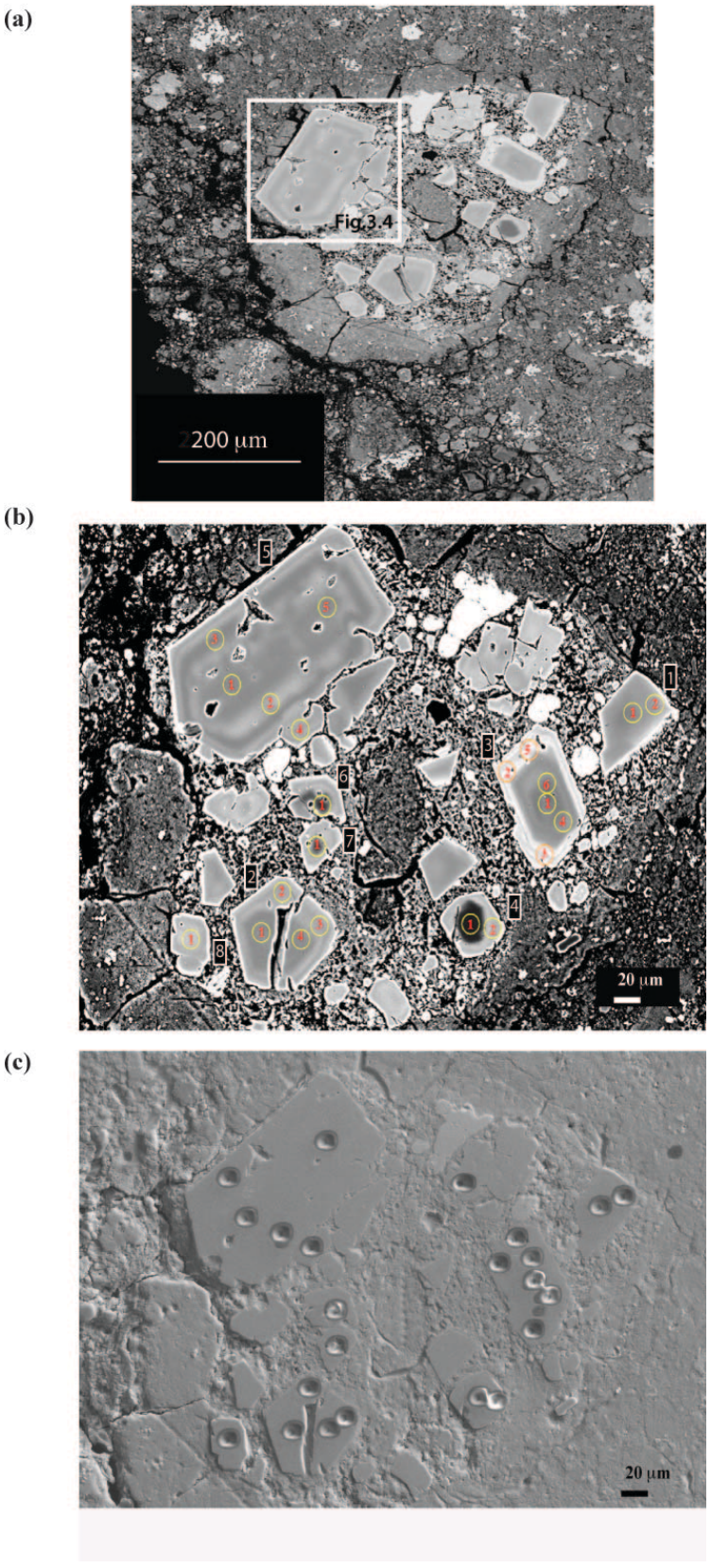

Figure 3.4

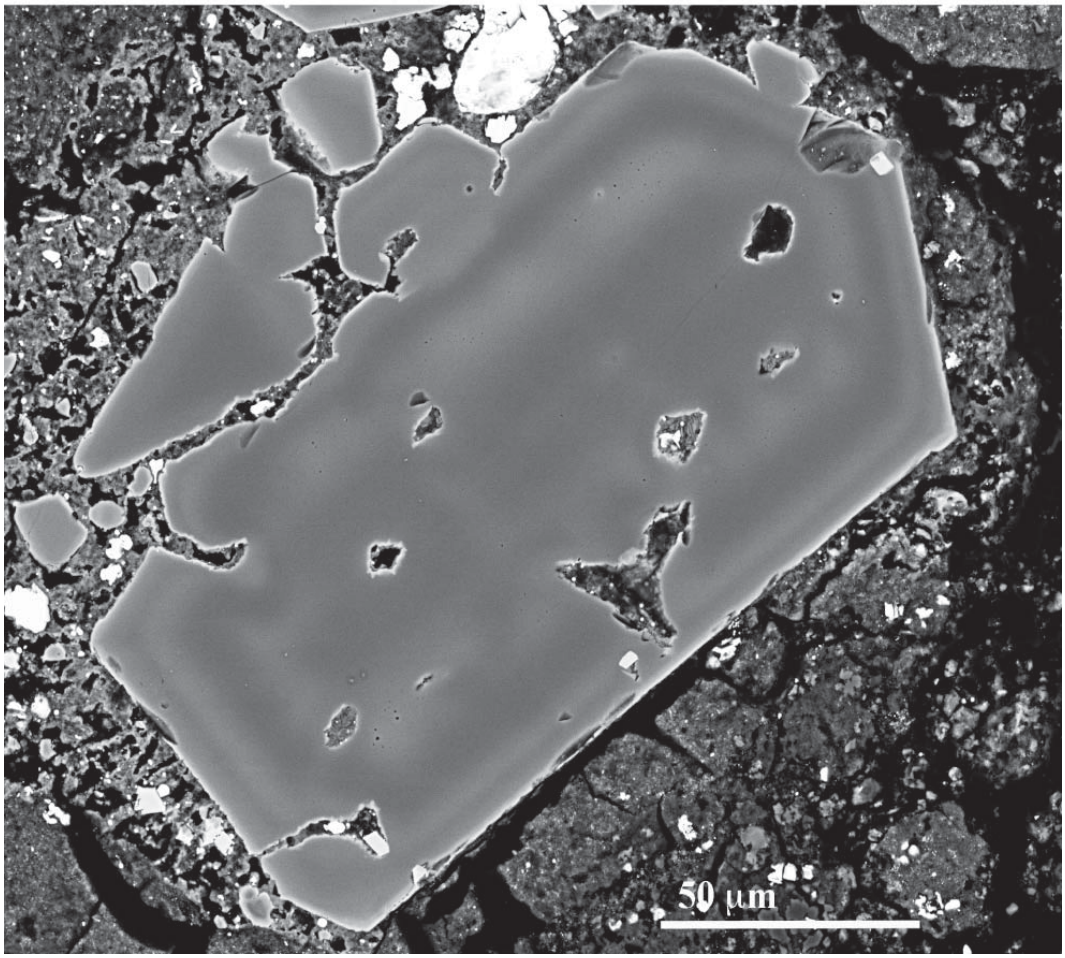

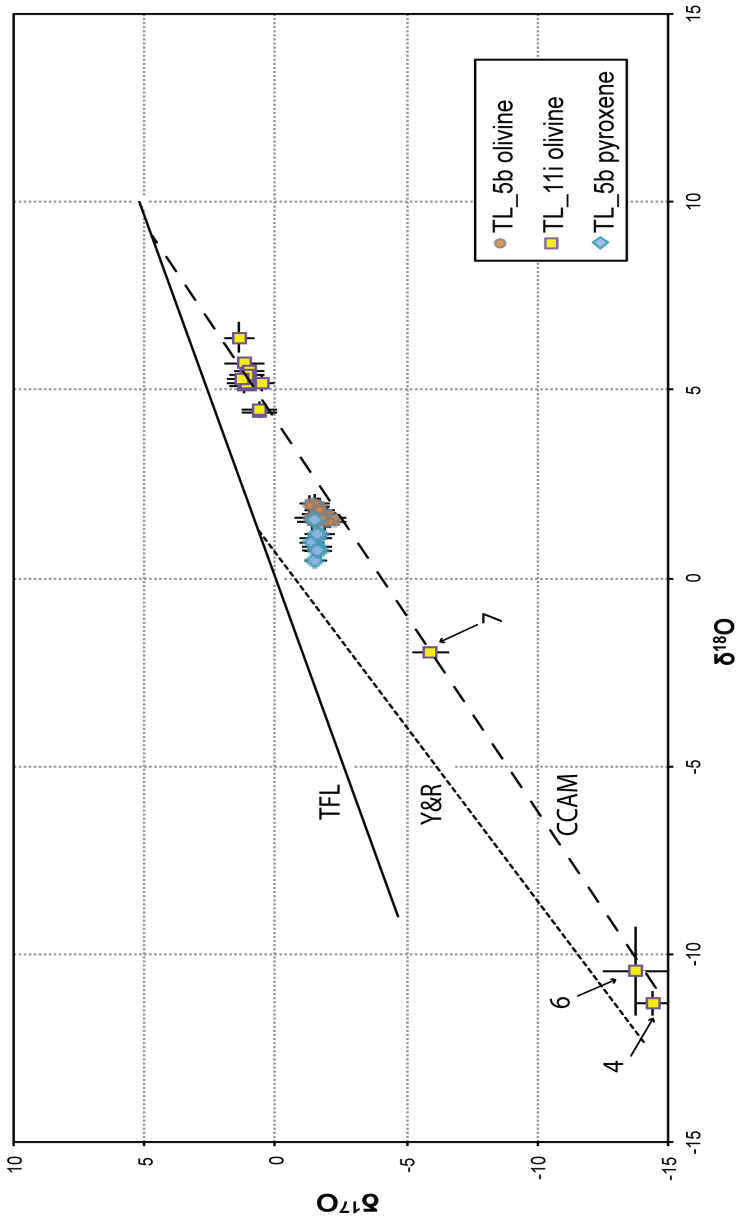
TL_5b olivine
TL_11i olivine
TL_5b pyroxene
TFL
Y&R
CCAM
7
6
4
δ17O
δ18O
10
5
0
-5
-10
-15
15
10
5
0
-5
-10
-15

Figure 3.5

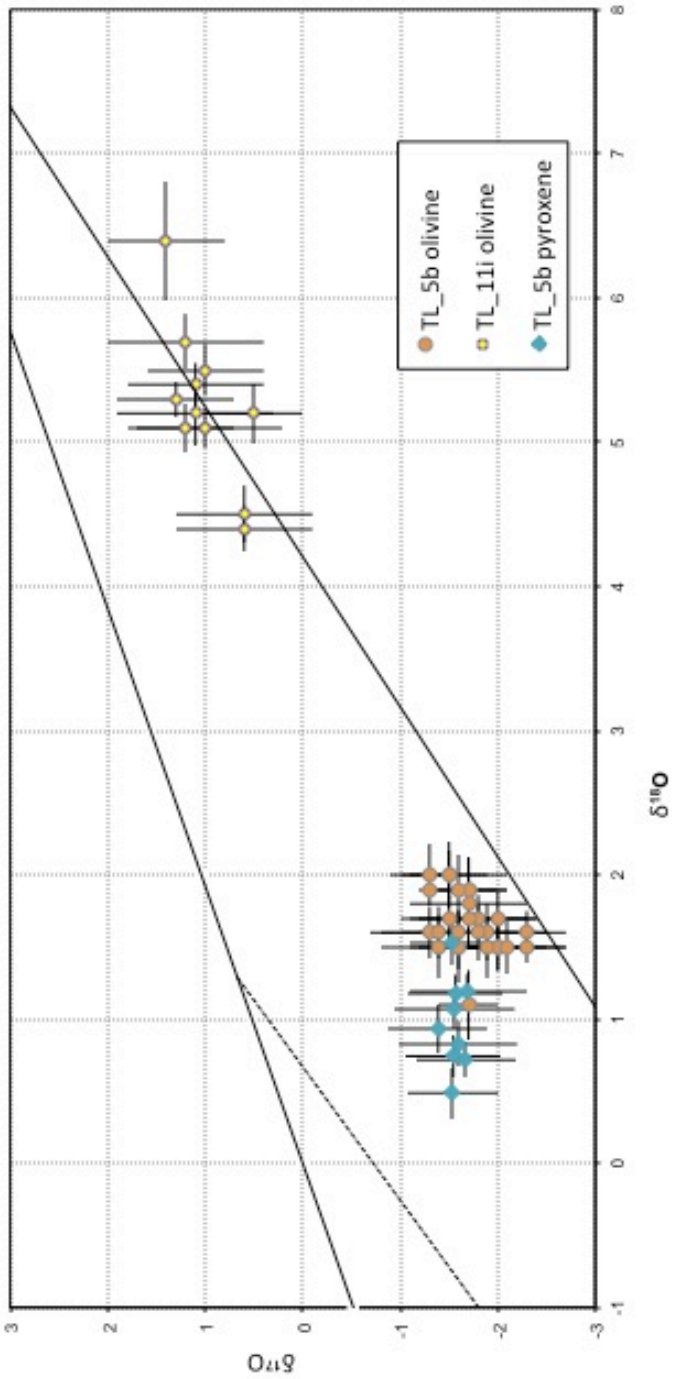

Figure 3.6

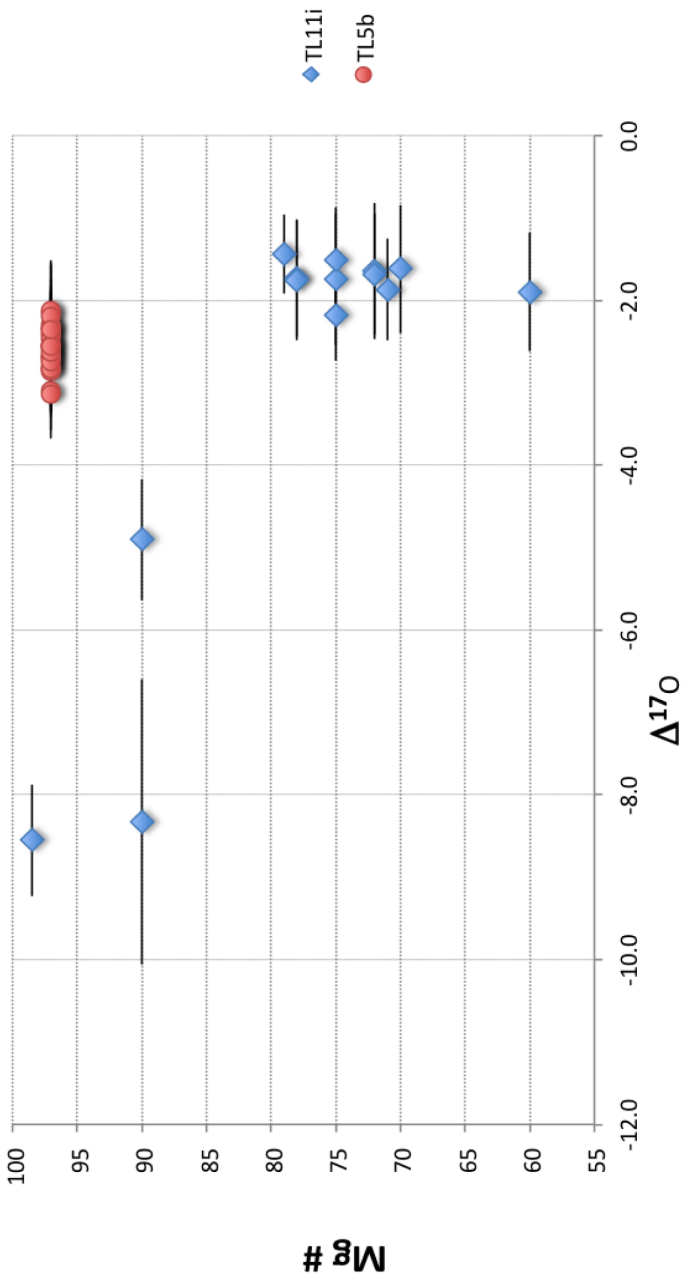
TL11i
TL5b
Mg #
100
95
90
85
80
75
70
65
60
55
-12.0
-10.0
-8.0
-6.0
-4.0
-2.0
0.0
Δ17O

Figure 3.7

Figure 3.8

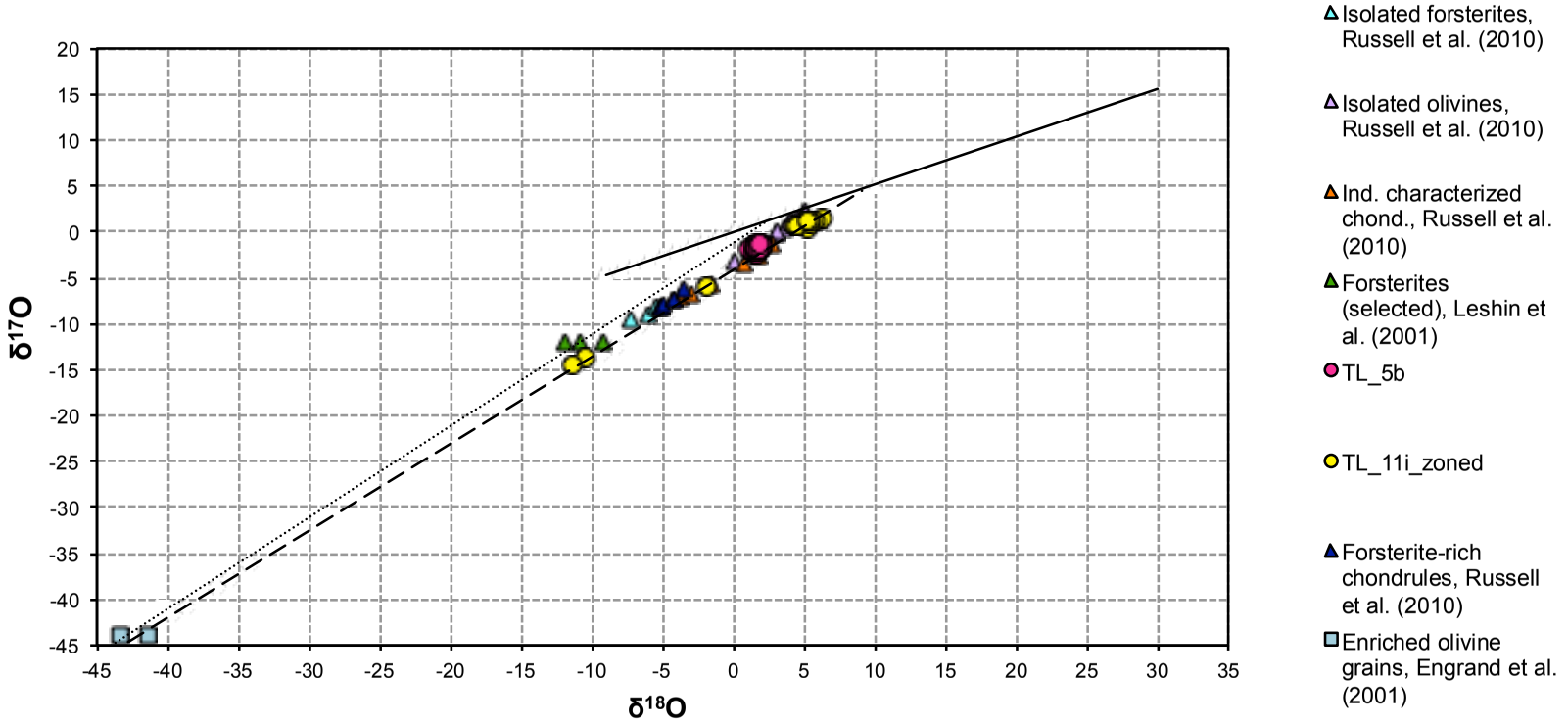
δ17O
δ18O
20
15
10
5
0
-5
-10
-15
-20
-25
-30
-35
-40
-45
-45
-40
-35
-30
-25
-20
-15
-10
-5
0
5
10
15
20
25
30
35
Isolated forsterites, Russell et al. (2010)
Isolated olivines, Russell et al. (2010)
Ind. characterized chond., Russell et al. (2010)
Forsterites (selected), Leshin et al. (2001)
TL_5b
TL_11i_zoned
Forsterite-rich chondrules, Russell et al. (2010)
Enriched olivine grains, Engrand et al. (2001)

Table 3.1:Average EPMA olivine and pyroxene composition from TL5b chondrule.

	OLIVINE		PYROXENE			
	Aveage	stdev	Average	stdev	Average	stdev
N	*25*		*40*		*35*	
Wt% oxides						
SiO_2	42.5	0.1	59.2	0.8	49.1	1.0
TiO_2	0.01	0.02	0.05	0.02	1.14	0.18
Al_2O_3	0.02	0.01	0.30	0.17	0.00	0.01
FeO	4.50	0.23	2.45	0.27	0.00	0.47
MnO	0.41	0.09	0.24	0.09	8.07	1.22
MgO	51.2	0.4	37.1	0.7	2.87	0.25
CaO	0.12	0.09	0.26	0.06	0.87	0.16
Na_2O	0.00	0.01	0.00	0.01	0.11	0.03
K_2O	0.01	0.00	0.00	0.01	18.4	1.6
P_2O_5	na	na	0.00	0.01	0.02	0.01
Cr_2O_3	0.69	0.06	0.70	0.11	2.58	0.49
NiO	0.01	0.02	0.00	0.01	17.0	1.3
Total	99.5		100.3		100.1	
Fo	97.5	2.1				
Fa	2.5	2.0				
En			95.6	0.4	56.3	3.4
Fs			3.9	0.3	6.4	0.6
Wo			0.5	0.1	37.3	3.5

Table 3.2: Average EPMA zoned olivine composition from TL11i chondrule.

	Grain 1		Grain 2		Grain 3		Grain 4		Grain 6*	Grain 7*
	Core	Rim	Core	Rim	Core	Rim	Core	Rim		
Wt% oxides										
SiO_2	38.57	36.27	38.36	35.97	38.63	34.91	41.84	36.26	39.42	39.64
TiO_2	0.01	0.00	0.00	0.01	0.02	0.01	0.04	0.01	0.01	0.02
Al_2O_3	0.06	0.06	0.07	0.07	0.06	0.08	0.11	0.06	0.05	0.03
FeO	17.51	23.22	19.56	26.95	17.18	33.52	1.21	26.20	10.00	10.38
MnO	0.17	0.22	0.21	0.26	0.19	0.35	0.19	0.26	0.27	0.21
MgO	42.59	37.87	41.38	35.69	42.81	30.05	56.44	36.08	36.48	48.95
CaO	0.19	0.23	0.18	0.31	0.20	0.60	0.26	0.36	0.33	0.25
Na_2O	0.02	0.01	0.02	0.03	0.01	0.05	0.01	0.03	0.23	0.02
K_2O	0.01	0.00	0.00	0.00	0.00	0.02	0.00	0.00	0.01	0.00
P_2O_5	0.03	0.07	0.03	0.11	0.07	0.29	0.01	0.09	0.05	0.03
Cr_2O_3	0.33	0.27	0.32	0.23	0.30	0.20	0.44	0.23	0.43	0.41
NiO	0.06	0.12	0.07	0.09	0.07	0.09	0.03	0.10	0.09	0.03
Total	99.55	98.33	100.20	99.72	99.54	100.14	100.58	99.68	99.51	99.95
Fo	81.25	74.41	78.53	70.25	81.63	60.65	98.63	71.66	89.11	89.37
Fa	18.75	25.59	21.47	29.75	18.37	39.35	1.37	28.34	10.89	10.63

	Grain 5 ^																		
	Rim								Core										Rim
Wt% oxides																			
SiO_2	37.32	37.98	37.56	37.76	37.77	37.54	37.68	37.61	37.83	37.93	37.86	37.75	37.83	37.72	37.45	37.15	36.95	37.17	36.25
TiO_2	0.00	0.00	0.01	0.01	0.02	0.00	0.02	0.01	0.00	0.00	0.00	0.01	0.00	0.03	0.00	0.02	0.00	0.00	0.00
Al_2O_3	0.04	0.04	0.07	0.03	0.10	0.03	0.11	0.09	0.06	0.04	0.04	0.08	0.05	0.10	0.06	0.03	0.08	0.05	0.10
FeO	24.46	20.40	22.47	20.32	19.75	22.15	20.13	21.57	19.84	19.23	19.17	19.42	19.41	19.86	20.76	22.37	23.76	21.06	25.43
MnO	0.24	0.22	0.26	0.22	0.23	0.21	0.23	0.22	0.22	0.23	0.22	0.23	0.22	0.18	0.24	0.23	0.23	0.21	0.29
MgO	37.28	40.25	38.62	40.29	40.62	39.07	40.19	38.98	40.37	40.59	40.94	40.47	40.76	40.49	40.01	38.44	37.27	39.48	35.59
CaO	0.26	0.19	0.24	0.18	0.18	0.19	0.21	0.18	0.19	0.21	0.19	0.19	0.20	0.19	0.19	0.20	0.24	0.18	0.34
Na_2O	0.03	0.04	0.00	0.02	0.02	0.01	0.05	0.04	0.05	0.00	0.01	0.02	0.05	0.03	0.02	0.04	0.00	0.02	0.04
K_2O	0.01	0.00	0.01	0.00	0.00	0.00	0.01	0.00	0.00	0.00	0.01	0.01	0.00	0.02	0.00	0.00	0.01	0.02	0.02
P_2O_5	0.05	0.04	0.04	0.02	0.24	0.04	0.17	0.05	0.06	0.06	0.04	0.07	0.00	0.06	0.06	0.05	0.04	0.06	0.11
Cr_2O_3	0.31	0.37	0.31	0.35	0.41	0.36	0.38	0.31	0.33	0.43	0.39	0.38	0.37	0.40	0.38	0.41	0.35	0.31	0.40
NiO	0.17	0.08	0.08	0.08	0.06	0.08	0.07	0.08	0.11	0.09	0.04	0.08	0.09	0.11	0.08	0.09	0.05	0.13	0.09
SO_2	0.01	0.06	0.01	0.06	0.00	0.00	0.04	0.01	0.00	0.05	0.00	0.00	0.05	0.01	0.03	0.02	0.00	0.00	0.00
Total	100.17	99.67	99.68	99.33	99.38	99.68	99.29	99.16	99.05	98.86	98.93	98.70	99.02	99.20	99.27	99.04	98.96	98.68	98.64
Mg#	73	78	75	78	79	76	78	76	78	79	79	79	79	78	77	75	74	77	71

Note: grain numbers reffer to Figure 3
* Core analyses only for grains 6 and 7
^ Grain 5 profile is from rim to rim along its shortest direction.

Table 3.3: Oxygen composition of olivines and enstatites in TL5b and TL11i chondrules.

	$\delta^{18}O$ (SMOW)(‰)	2σ (‰)	$\delta^{17}O$ (SMOW)(‰)	2σ (‰)	$\Delta^{17}O$ (‰)	2σ (‰)	Fo
TL5b olivines:							
TL5b_OL1@2	1.7	0.19	-1.5	0.5	-2.4	0.53	97
TL5b_OL2@1	1.5	0.15	-2.0	0.5	-2.8	0.57	97
TL5b_OL2@2	1.5	0.17	-2.3	0.5	-3.1	0.57	97
TL5b_OL1@3	1.6	0.11	-2.3	0.4	-3.1	0.44	97
TL5b_OL3@1	1.5	0.15	-1.6	0.4	-2.3	0.39	97
TL5b_OL3@2	1.7	0.15	-2.0	0.5	-2.9	0.47	97
TL5b_OL4@1	1.5	0.18	-2.0	0.4	-2.8	0.44	97
TL5b_OL4@2	1.5	0.15	-1.6	0.4	-2.4	0.40	97
TL5b_OL4@3	1.1	0.24	-1.7	0.4	-2.3	0.44	97
TL5b_OL4@4	1.5	0.24	-1.9	0.3	-2.7	0.42	97
TL5b_OL5@1	1.9	0.21	-1.7	0.4	-2.7	0.45	97
TL5b_OL5@2	1.9	0.22	-1.7	0.4	-2.7	0.46	97
TL5b_OL5@3	1.9	0.23	-1.6	0.4	-2.6	0.45	97
TL5b_OL6@1	2.0	0.24	-1.3	0.4	-2.3	0.44	97
TL5b_OL6@2	2.0	0.22	-1.5	0.3	-2.6	0.39	97
TL5b_OL6@3	2.0	0.23	-1.5	0.4	-2.5	0.45	97
TL5b_OL6@4	1.6	0.17	-1.6	0.6	-2.5	0.64	97
TL5b_OL7@1	1.5	0.16	-2.1	0.6	-2.8	0.59	97
TL5b_OL7@2	1.7	0.18	-1.8	0.6	-2.7	0.61	97
TL5b_OL7@3	1.6	0.16	-1.3	0.6	-2.1	0.62	97
TL5b_OL8@1	1.6	0.18	-1.9	0.6	-2.8	0.60	97
TL5b_OL8@2	1.5	0.20	-1.4	0.6	-2.1	0.61	97
TL5b_OL9@1	1.7	0.22	-1.7	0.6	-2.5	0.66	97
TL5b_OL10@1	1.6	0.20	-1.4	0.6	-2.2	0.62	97
TL5b_OL11@1	1.6	0.18	-1.8	0.6	-2.6	0.65	97
TL5b_OL11@2	1.8	0.19	-1.7	0.6	-2.6	0.60	97
TL5b_OL14@1	1.9	0.18	-1.3	0.6	-2.3	0.61	97
TL11i olivines:							
TL11i_8_1	5.1	0.14	1.0	0.8	-1.6	0.77	70
TL11i_2_4	5.1	0.17	1.2	0.5	-1.4	0.48	79
TL11i_3_4	5.2	0.21	0.5	0.5	-2.2	0.55	75
TL11i_3_5	6.4	0.41	1.4	0.6	-1.9	0.72	60
TL11i_3_6	5.7	0.19	1.2	0.8	-1.7	0.80	75
TL11i_4_2	5.5	0.18	1.0	0.6	-1.9	0.62	71
TL11i_5_1	4.4	0.16	0.6	0.7	-1.7	0.71	78
TL11i_5_2	5.2	0.23	1.1	0.8	-1.6	0.83	72
TL11i_5_3	4.5	0.20	0.6	0.7	-1.8	0.73	78
TL11i_5_4	5.4	0.15	1.1	0.7	-1.7	0.73	72
TL11i_5_5	5.3	0.12	1.3	0.6	-1.5	0.65	75
TL11i_7_1	-2.0	0.15	-5.9	0.7	-4.9	0.73	90
TL11i_4_1	-11.3	0.34	-14.4	0.6	-8.6	0.68	98.5
TL11i_6_1	-10.5	1.19	-13.8	1.3	-8.3	1.73	90
TL5b enstatites:							
TL5b_EN@1	0.8	0.16	-1.6	0.6	-2.0	0.62	na
TL5b_EN@2	1.2	0.12	-1.7	0.6	-2.3	0.62	na
TL5b_EN@3	0.7	0.13	-1.7	0.5	-2.0	0.53	na
TL5b_EN@4	1.1	0.14	-1.6	0.6	-2.1	0.63	na
TL5b_EN@5	0.5	0.18	-1.5	0.5	-1.8	0.50	na
TL5b_EN@6	0.9	0.17	-1.4	0.5	-1.9	0.53	na
TL5b_EN@9	1.2	0.13	-1.6	0.5	-2.2	0.50	na
TL5b_EN@10	1.5	0.16	-1.5	0.4	-2.3	0.46	na
TL5b_EN@12	0.7	0.15	-1.5	0.5	-1.9	0.51	na

na - not applicable

CONCLUSIONS

In this project I studied four specimens from the pristine Tagish Lake meteorite suite. The study encompassed the mineralogical and petrological investigations and whole-rock geochemistry of these samples, and oxygen isotope measurements of olivine and pyroxene grains in two chondrules from two samples.

Based on petrological and mineralogical observations we conclude that the Tagish Lake parent body was a heterogeneous mixture of anhydrous precursors of nebular origin, which were brecciated and aqueously altered. The degree to which the studied samples experienced aqueous alteration is in the order TL5b < TL11h < TL11i. Specimen TL11v, which consists of disaggregated material, is heterogeneous on the microscale and encompasses the petrologic characteristics of other three specimens as seen through EPMA observation. The presence of the abundant amorphous material in the TL5b argues that this sample experienced relatively milder parent-body alteration to preserve this indigenous nebular material and produce fine-grained sheet silicates. Other samples were subjected to a longer duration of hydrous alteration because they are dominated by coarse-grained sheets silicates. I observed two generations of sulfides in the studied samples. The first generation consists of exsolved pentlandite morphologies, which formed at higher temperature in the changing nebular conditions or metal diffusion from Ni-bearing MSS during cooling of the solar nebula below temperatures < 600 °C. The second generation includes non-exsolved pentlandite along grain boundaries, the 'bulls-eye' sulfide morphology, and rims around highly altered chondrules, which all formed by multiple precipitation episodes during low temperature aqueous alteration (≤ 100 °C) on the parent body.

The coronal, 'flower'-like microtexture consisting of core and radial arrays, observed in a lithic fragment from sample TL11i, shows both compositional changes from serpentine in the core to saponite-serpentine in the radial arrays and textural changes from fine-grained in the core to coarse-grained in the arrays. Our preferred model for production of this texture involves serpentine precipitation in the pore spaces around silicate grains to produce coarse-grained radial arrays, subsequent alteration of silicate grains to form fine-grained cores, and later introduction of Al-bearing fluid to precipitate the saponite in the already serpentinized cracks.

The total of 65 elements from the four specimens were obtained utilizing several methods such as ICP-MS, ICP-AES and INAA. In general, when comparing among samples, homogeneity of major and minor elements demonstrate that elemental mass

transfer occurred on a localized scale and alteration was isochemical, similar to other carbonaceous chondrites. Mobile trace elements, such as K and Br, on the other hand, have a positive correlation with alteration sequence, which is apparently controlled by an increase in phylloslicates from the least to the most altered sample. Three of the studied samples (TL5b, TL11h, TL11i) plot in a previously unoccupied area of the Zn/Mn vs. Sc/Mn space (Friedrich et al. 2002), a plot that is traditionally used for distinguishing between established carbonaceous groups (Kallemeyn and Wasson 1981). The location of specimen TL11v on this diagram is in the CM field, which is lower than other samples but is on the line connecting TL11h and TL11i, consistent with its nature as a physical mixture of other Tagish Lake samples.

I studied the oxygen isotopes in-situ in olivine and pyroxene grains in two chondrules from the two samples, TL5b and TL11i. The majority of olivine grains, with the exception of relict cores, and pyroxene grains in both chondrules show similar oxygen variation to each other and to other anhydrous silicates in ferromagnesian chondrules from primitive chondrites. I conclude that these two chondrules from two mineralogically different Tagish Lake specimens formed under the same redox conditions or in the same nebular environment prior to their agglomeration into the Tagish Lake parent body. The relict cores, which are found only in TL11i complex chondrule, show enrichment in ^{16}O relative to other olivine grains, suggesting that they formed in a reducing environment prior to incorporation into this chondrule; in contrast, the rims around these grains formed later in a more oxidizing environment. The oscillatory zoned olivine found in the complex TL11i chondrule formed in a nebular environment similar to the other zoned olivnies but under varying redox conditions. An alternative scenario is that this olivine is an impact-ejected grain, which formed on an earlier generation of planetesimals in the same oxygen reservoir prior to its accretion into the TL11i chondrule. Our results added additional points onto the Tagish Lake oxygen isotope "field" that covers the range of oxygen variations observed in all other carbonaceous chondrites.

Overall, through this project I was able to determine the mineralogical, petrological and whole-rock geochemical variations in the four Tagish Lake samples. As a result, I set up the sequence of alteration within these four samples. This sequence demonstrates that the four Tagish Lake samples and their parent body have undergone varying degrees of hydrothermal alteration and brecciation. The established sequence will serve as a foundation for any future mineralogical and geochemical work on this meteorite. For instance, it will assist in deciphering the question of the connection

between Tagish Lake meteorite and CM/CI chondrites. My mineralogical observations show that out of all four samples TL5b is more CM-like solely based on the abundance of chondrules. However, geochemistry demonstrates that the Tagish Lake meteorite is not a simple mixture of CI and CM material confirming the earlier observations (Friedrich et al. 2002). In addition, bulk oxygen isotopes show that the studied lithologies span a range that extends from CM into CI chondrites (Herd et al. 2012). Recent aqueous alteration models show that CM and CI chondrites are consistent with heterogeneous alteration in a single convecting parent body representing different regions of this body: surface CM- and interior CI-regions (Pulguda et al. 2010). Is it possible that Tagish Lake meteorite represents an intermediate region within such a heterogeneously convecting body? More work is required to answer such questions.

I conclude that future work should be focused on the understanding the formation and timing of various Tagish Lake components. For example, the oscillatory zoned olivine grain is unique not only in its setting in the complex TL11i chondrule, but as being a rare example of such compositional variations in meteorites. This grain should be studied in detail under TEM and SEM to verify the formation model proposed in this study. Another venue for future work should be concentrated on the study of origin of amorphous material, which is so abundant in the TL5b sample, in particular. It would be beneficial to determine the water content of the amorphous silicates to determine whether this material is the product of aqueous alteration or has a nebular origin. In addition to the water content, the measurements of presolar silicate abundance should be of high priority because it would help to verify the degree of hydration in these samples predicted by mineralogy. For example, based on mineralogy TL5b sample is less altered than other samples; therefore, should contain significantly higher quantities of primitive circumstellar silicates than do TL11h and TL11i. Additional work needs to be done on the carbonates in the Tagish Lake meteorite. The only carbonate from TL11h that I measured using Mn/Cr extinct radionuclide dating (Appendix 1) should be compared to carbonates from other samples. This will help to answer such questions as how the TL11h carbonate relates to the carbonates from the other lithologies in the Tagish Lake meteorite and CM/CI groups; and what it tells us about the duration of the aqueous alteration on its parent body.

REFERENCES

Friedrich, J.M., Wang, M.-S., and Lipschutz, M.E. 2002. Comparison of the trace element composition of Tagish Lake with other primitive carbonaceous chondrites. Meteoritics and Planetary Science 37:677-686.

Herd, C.D.K., Sharp, Z.D., Alexander, C.M.O'D., and Blinova, A. 2012. Oxygen isotopic composition of Tagish Lake Lithologies: insights into parent body alteration (abstract #1688). 43^{d} Lunar and Planetary Science Conference. CD-ROM.

Kallemeyn, G.W. and Wasson, J.T. 1981. The compositional classification of chondrites; I, The carbonaceous chondrite groups. Geochimica et Cosmochimica Acta 45:1217-1230.

Palguda, J., Schubert, G., and Travis, B.J. 2010. Fluid flow and chemical alteration in carbonaceous chondrite parent bodies. Earth and Planetary Science Letters 296:235_243.

APPENDIX 1

The following is the extended abstract from the 43d Lunar and Planetary Science Conference (2012) on the timing of the carbonate formation from the TL11h. I have been the principal initiator of this part of the project and also helped with the Mn/Cr measurements performed by Conel Alexander:

Mineralogy and Mn-Cr Extinct Radionuclide Dating of a Dolomite from the Pristine Tagish Lake Meteorite.

A. Blinova[1], C. M. O'D. Alexander[2], J. Wang[2], and C. D. K. Herd[1]. [1]Dept. Earth and Atmospheric Sciences, 1-26 Earth Sciences Building, University of Alberta, Edmonton, AB, T6G 2E3, Canada (blinova@ualberta.ca); [2]Dept. Terrestrial Magnetism, 5241 Broad Branch Road NW, Washington, DC, 20001.

Introduction: Tagish Lake has been identified as an ungrouped Type 2 carbonaceous chondrite (CC) with affinities to CIs and CMs [1,2]. Four pristine specimens (5b, 11h, 11i, 11v) identified by [3] encom-passing various degrees of alteration have been miner-alogically described in previous works [3-5]. In sum-mary, specimen 11h is an intermediate lithology be-tween the less altered 5b specimen, containing abun-dant chondrule-like objects, and the more altered 11i and 11v specimens. We identified a large (~100 x 200 μm) dolomite grain in specimen 11h. Its size and composition allowed us for the first time the oppor-tunity to use the 53Mn-53Cr chronometer (t1/2 = 3.7 Ma) to investigate the time scales of carbonate formation on the Tagish Lake meteorite parent body.

Methodology: Mineral analysis of the carbonate was carried out with a JOEL8900 EPMA at the Uni-versity of Alberta. The Mn-Cr measurements used a 10x10 μm rastered O- beam using Carnegie's Na-noSIMS 50L in multicollector mode. Each analysis took ~1 hr. As a standard for determining the relative Mn-Cr sensitivity factor, we used a Mn- and Cr-doped synthetic diopside. The 53Cr/52Cr isotopic ratios of the diopside and three matrix areas adjacent to the dolo-mite grain were also determined – the total variation was ~6 ‰.

Mineralogy: Specimen 11h has large quantities of chondrule-like objects similar to 5b (~ 20 vol%), but they are smaller in size and more altered than in sep-cimen 5b [3,4]. The

abundance of irregular lithic frag-ments (up to 10 vol %) is similar to that in specimen 11i [3,4]. Fine-grained magnetites are found both as isolated grains and in clusters (15 vol%). Fine-grained, porous to compact matrix that is rich in ribbon-like phyllosilicates [5] is similar in abundance to 11i (up to 40 vol%) [3]. On the TEMscale, sulfides are relatively abundant in the matrix [5]. Also, Ca-rich phosphate has been iden-tified in this specimen. Most of the carbonates are fine-grained with abundance up to 11 vol % [5].

Mineralogy of 11h dolomite grain. The carbonate grain is approx. 100 by 200 μm and set in a phyllosili-cate-rich matrix. It is surrounded by an irregular, fine grained rim of 30 to 100 μm in thickness. The compo-sition of the rim is dominated by Mg and Si with small random pockets of concentrated Mn and Ca, possibly phyllosilicates with sparse carbonates.

The average composition (Table 1) of this grain is dominated by Mg and Ca, but with up to 2 wt % of Mn. The chemical formula of the grain, based on 3 oxygens, is $(Mg_{1.3}Ca_{1.3}Fe_{0.3}Mn_{0.07})CO_3$.

	Average (wt %)	Standard deviation
MgO	19.5	1.3
CaO	26.8	1.2
MnO	1.8	0.8
FeO	7.8	0.8
CO_2 *	44.0	1.9

Table 1. Average chemical composition of 23 analyses of the dolomite grain from Tagish Lake specimen 11h.

The composition of each analysis (in mol %) is plotted on a ternary Ca-Mg-(Fe+Mn) diagram in Fig. 1, along with the approximate fields of CI and CM dolomites [6,7]. The composition of the 11h dolomite grain falls in the Ivuna field and slightly overlaps the fields of other CI and CM dolomites.

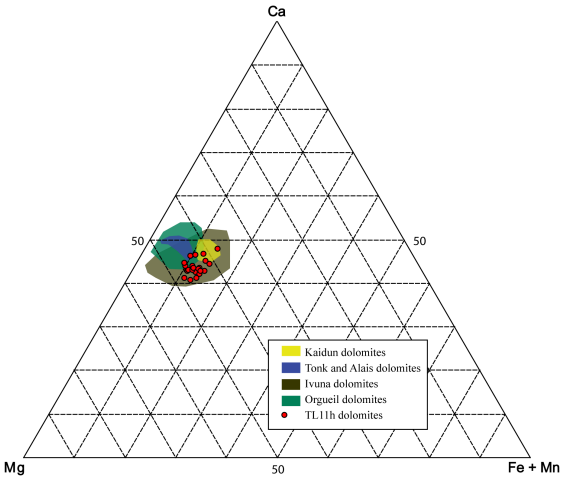

Figure 1. Ternary diagram showing the dolomite com-position from Tagish Lake specimen 11h, along with dolomites from CI [6] and CM [7] chondrites.

Mn-Cr results: We measured five points on the dolomite and all exhibited enrichments in ^{53}Cr, with $^{53}Cr/^{52}Cr$ ratios ranging from 0.154 ± 0.004 to 0.178 ± 0.007. The large uncertainties in these ratios reflect the low and variable Cr contents of this dolomite (Cr_2O_3 = 0.004 ± 0.004 wt%). The excesses in ^{53}Cr are linearly correlated with the respective $^{55}Mn/^{52}Cr$ ratios (Fig. 2), indicative of the in-situ decay of ^{53}Mn and demonstrat-ing that short-lived ^{53}Mn was present at the time of formation of this dolomite. This is the first reported presence of the 53Mn daughter product in the Tagish Lake meteorite. On the ^{53}Mn – ^{53}Cr evolution diagram (Fig. 2) the regression through five dolomite and three matrix points gives the correlation line with the corre-sponding $^{53}Mn/^{55}Mn$ slope of 3.13 x 10^{-6} calculated using Isoplot.

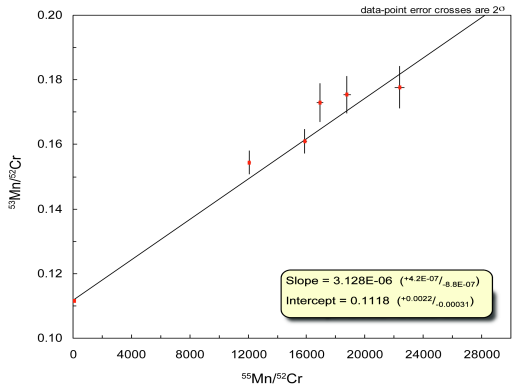

Figure 2. ^{53}Mn - ^{53}Cr evolution diagram for dolomite from the Tagish Lake specimen 11h.

Discussion and Conclusion: We calculate the ab-solute formation age of the 11h dolomite to be 4562.8± 0.94 Ma using the angrite LEW86010 as a time anchor. The absolute age of the 11h dolomite falls within the middle of the range of ages of Orgueil carbonates (Fig. 3) [8]. Carbonates from other CM1, CM2 and Kaidun [7,9,10] are >1 Ma older than the 11h dolomite, except for Y791198, which is similar within the error to the age of the oldest CAIs [11]

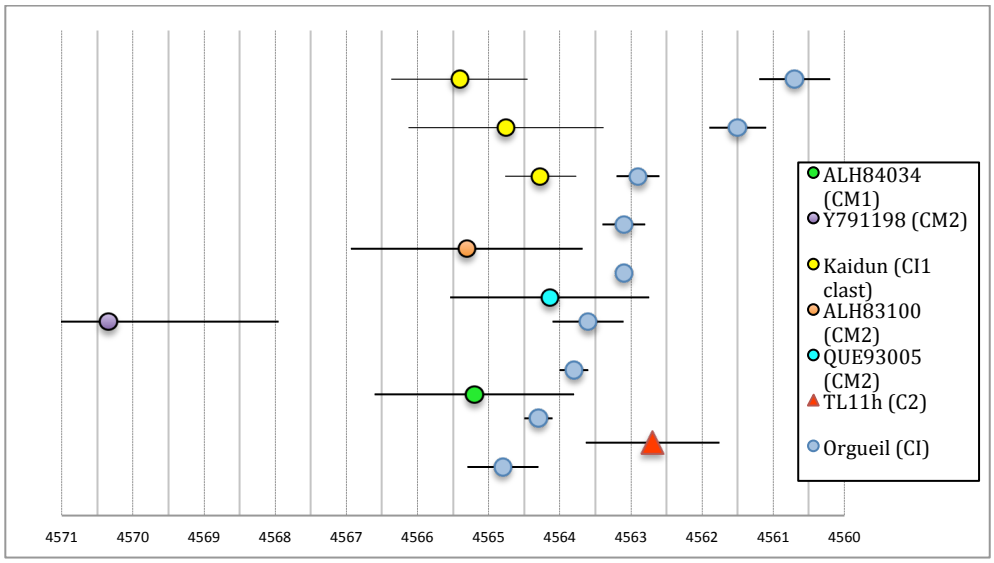

Figure 3. Absolute ages of carbonates in CI, CM1, CM2, Kaidun and Tagish Lake 11h (TL11h) based on Mn-Cr extinct radionuclide dating.

Assuming the solar system initial ^{53}Mn/^{55}Mn of ~3 x10^{-5} [12], the difference corresponds to a time interval of ~12 Ma between the formation of CAIs and the formation of the 11h dolomite. Such an extended time interval shows that this dolomite most likely grew on an asteroidal parent body during aqueous alteration in a similar setting and timescale to the CI parent body.

Several questions remain. Do carbonates from the other pristine Tagish Lake specimens (e.g., 5b, 11v, 11i) have a comparable initial ^{53}Mn/^{55}Mn ratio? How does this

dolomite relate to the carbonates from the carbonate-rich lithology described by [2]? And what does it tell us about the duration of the aqueous alteration on the Tagish Lake parent body?

References: [1] Brown P.G. et al. (2002) Meteor-itics and Planetary Science, 37(5), 661-675. [2] Zolen-sky et al. (2002) Meteoritics and Planetary Science, 37(5), 737-761. [3] Blinova et al. (2009) LPSC 40th, Abstract #2039. [4] Blinova et al. (2010) LPSC 41st, Abstract #2140. [5] Blinova et al. (2011) LPSC 42nd, Abstract #2517. [6] Endress and Bichoff (1996) Geo-chimica Cosmochimica Acta, 60(3), 489-507. [7] Peti-tat et al. (2011) Meteoritics and Planetary Science, 46(2), 275-283. [8] Hoppe et al. (2007) Meteoritics and Planetary Science, 42(7/8), 1309-1320. [9] Brear-ley and Hutcheon (2000) LPSC 31st, Abstract #1407. [10] deLeuw et al. (2009) Geochimica et Cosmochimi-ca Acta, 73, 7433-7442. [11] Bouvier and Wadhwa (2010) Nature, 3, 637-641. [12] Birck and Allegre (1985) Geophysical Research Letters, 12(11), 745-748.

APPENDIX 2:

Digestion procedure for ICP Analyses

We used the following digestion procedure for standards, blanks and samples. The mass of sample was noted prior to dissolution for calculation of dilution factor at the end of the procedure. A single drop of Millipore water was added before the addition of acid to moisten the samples against static.

1. Digestion:
    a. Weigh samples into Teflon Parr bomb beakers
    b. Add 1 mL of conc. HNO_3, leave for 5-10 minutes then add 5 mL of conc. HF to Teflon Parr bomb beakers
    c. Cap and put the beakers into the Teflon Parr bomb and into the oven at 170°C for ~ 3 days
    d. After 3 days take out the beakers, cool, open & evaporate almost to dryness on a hot plate (~85°C)
2. Flux:
    a. Add 2 mL of conc. HNO_3, cap, heat on a hot plate for 2-3 hours and then overnight at 120°C in oven in Parr bombs
    b. Remove Parr bombs, cool and open and evaporate almost to dryness on a hot plate
3. Conversion:
    a. Add 2 mL of conc. HNO_3, evaporate almost to dryness on a hot plate (repeat 3 times)
4. Dilution:
    a. Add 2 mL of conc. HNO_3, cap and put on a hot plate for 30 min – 1 hour. Then remove and cool. Once cooled examine for any un-dissolved material, if none transfer solution to a larger vial and dilute with Millipore H_2O to 20 g. If un-dissolved material present, repeat steps 2 to 4.
    b. Prior to ICP-MS runs, all samples are further diluted to 1:10 solution.